Phase Sensitive Amplification using Parametric Processes in Optical Fibers

Kang, Ning; Peucheret, Christophe; Rottwitt, Karsten; Seoane, Jorge

Publication date:
2012

Document Version
Publisher's PDF, also known as Version of record

Phase Sensitive Amplification using Parametric Processes in Optical Fibers

PhD Thesis

Supervisors:

Christophe Peucheret

Karsten Rottwitt

Jorge Seoane

Ning Kang

Nov. 2012

DTU Fotonik, Denmark

Joy in looking and comprehending is nature's most beautiful gift.

– *Albert Einstein*

Résumé

Faseføls om forstærkning baseret på parametriske processer i fibre kan potentielt give stor forstærkning over et bredt bølgelængdeområde med ganske lidt støj. Med det rette design kan denne type forstærker regenerer både amplitude og fasemodulerede signaler. Specifikt vil denne afhandling både undersøge design samt optimiserering af disse faseføls omme forstærkere (PSAs). Optimale operationspunkter for faseføls om forstærkning i stærkt ulineære fibre er blevet identificeret for både standard fibre samt for nyudviklede fibre med høj stimuleret Brillouin scattering (SBS) tærskel. Regenererings egenskaberne for PSAer i en optisk forbindelse baseret på fasemodulerede signaler er blevet optimeret. En følsomhedsprofil med flad top er blevet syntetiseret. Den kan simultant sammenpresse støj i både amplitude og fase med en forøget fasestøjsmargin sammenlignet med konventionelle design. Ydermere er faseføls om parametriske processer i silicium bølgeledere strukturer på nanometer skala blevet målt eksperimentelt for første gang nogensinde. Numerisk optimering viser at med et reduceret bølgeledertab samt reduceret carrier livstid kan give høje faseføls omhedsudslukningsforhold. Til slut er de indledende simuleringer som undersøger inline forstærkningsegenskaberne af disse PSAer samt deres mulige indflydelse på pulsformer præsenteret.

Abstract

Phase sensitive amplification using the parametric processes in fiber has the potential of delivering high gain and broadband operation with ultralow noise. It is able to regenerate both amplitude and phase modulated signals, simultaneously, with the appropriate design. This thesis concerns, in specific, the design and optimization of such phase sensitive amplifiers (PSAs). For phase sensitive amplification in highly nonlinear fibers, optima points of operation have been identified for both the standard and the novel high stimulated Brillouin scattering (SBS) threshold highly nonlinear fiber types. The regeneration capability of PSAs on phase encoded signal in an optical link has been optimized. Flat-top phase sensitive profile has been synthesized. It is able to provide simultaneous amplitude and phase noise squeezing, with enhanced phase noise margin compared to conventional designs. Further, phase sensitive parametric processes in a nano-engineered silicon waveguide have been measured experimentally for the first time. Numerical optimizations show that with reduced waveguide propagation loss and reduced carrier life time, larger signal phase sensitive extinction ratio is achievable. Finally, preliminary simulations were carried out to investigate the inline amplification properties of such PSAs, and their pulse shaping capabilities.

Acknowledgement

I am most grateful to my main supervisor Christophe Peucheret, my supervisors Karsten Rottwitt, and Jorge Seoane, for their focus and dedication in the investigation of parametric amplification in the earlier years, whose efforts has enabled grant for the project phase sensitive amplification using parametric processes in optical fibers. I am very thankful to the Danish council for independent research technology and production sciences (FTP), the Danish agency for science technology and innovation under the ministry of science technology and innovation for offering the economic support for this project. Many thanks to my former fellow colleague Toke Lund-Hansen who had worked on this project as a postdoc, who besides theoretical discussions, had been extremely helpful in helping setting up earlier experimental trials.

I want to address my gratitude to my coworkers in the ultra-high-speed optical communications (UHSOC) group. My most grateful gratitude and respect to Professor Palle Jeppesen, who established the group in the 1980s, who had a tremendous influence on the development of communication technology in Denmark since the 1970s. Thanks to the current group leader Leif K. Oxenløwe, who with his radiating enthusiasm positively encourages fellow postdocs and PhD students. Thanks to the senior stuffs at the group Anders Clausen, Michael Galili, Hans Christian Hansen Mulvad, Hao Hu, Hua Ji, and Evarist Palushani, for their experimental experience and helpfulness on a daily basis. Thanks to my fellow colleagues under the parametric amplification research Zohreh Lali-Dastjerdi, Francesco Da Ros, and Dragana Vukovic for their day-to-day interaction, discussions and helpfulness.

It is a great privilege to be part of the department of photonics engineering at the technical university of Denmark. During the period of my master and PhD studies in this institute, the vision of the department has become clearer to me. The diligent researchers at the institute deliver every year record breaking scientific achievements. Quite a plural of these inventions and innovative applications using current photonic technologies undergo active tech-transfer, to make scientific discoveries applicable, and to create business value that feeds back to the society. The successful transformation of photonic technology with its value created to serve practical demand, creates growth of the industry, and keeps a healthy circulation of resources among the different sectors. For my current research project and beyond, I would like to contribute my efforts in the practice of technological development and active high-tech business transfer.

Ning Kang

Nov. 2012

Preface

The potential of optical phase modulated signals for high capacity, high spectral efficiency and long-distance transmission is now well established thanks to a significant research effort over the past decade. Beyond pure transmission aspects, advanced network functionalities are expected to migrate towards the optical layer in the long term. Optical signal processing has therefore been a very active area of research within the field of optical communications. One particular issue that is currently being investigated is how signal processing techniques, which for years have been studied solely in conjunction with intensity modulated signals, can accommodate the phase dimension. This project addresses precisely those contemporary topics by studying how phase sensitive amplifiers can be optimally designed to allow signal processing of phase modulated signals.

Phase sensitive amplifiers are known to be appropriate candidate devices for simultaneous amplitude and phase noise processing of optical signals. Signal regeneration of phase shift signals by means of phase sensitive amplification has been proposed since the early 1990s [1,2]. It is capable to provide different gains to the two phase quadratures, and is useful to regenerate degraded phase modulated signals along transmission all optically. As known, phase modulated signals can be severely degraded due to linear phase noise added by the optical amplifiers, and nonlinear phase noise can be caused by the fiber nonlinearity effects.

In this project, the investigations of phase sensitive amplifiers will mainly be focused on a highly efficient degenerate four wave mixing regime, employing two pump waves in a highly nonlinear fiber symmetrically surrounds the signal in the center wavelength. After a brief description on data transmission in fiber in chapter 1, phase insensitive fiber optical parametric amplifiers are introduced in chapter 2. Some practical consideration concerning development of highly nonlinear fibers with respect to stimulated Brillouin scattering is covered in section 2.1. Numerical models solving the parametric four-wave mixing processes are briefly described in section 2.2. In chapter 3, optimization of the phase sensitive gain and extinction ratio of fiber-based PSAs configured in the dual-pump degenerate-idler regime are investigated. It's regeneration properties are further investigated in chapter 4, where a flat-top phase sensitive gain profile is designed which is able tolerate higher phase noise levels compared to conventional gain profiles. In chapter 5, it is demonstrated an experimental measurement of such dual-pump degenerate-idler configured PSA

implementation in a nano-engineered silicon waveguide. Distinctive phase sensitive extinctions are measured and matched numerically. Extended simulations taken into account of two photon absorption and free carrier effects have, through a numerical optimization, predicted the anticipated gain and extinction ratios achievable under various carrier lifetimes. This preliminary investigation can be served as guidelines for researchers to be taken into consideration when designing and fabricating the next volume of silicon waveguides targeted for nonlinear parametric oriented applications. In chapter 6, dispersion tolerance of phase sensitive amplifiers are assessed when PSAs are used as inline amplifiers in a multi-span transmission link. The eye opening penalty is characterized as a function of transmission length. Preliminary results of phase sensitive gain profile performance dependence on the signal quality at the input of PSAs are characterized. The pulse shaping capabilities as another interesting feature enabled by PSA is described in chapter 7.

Table of Contents

TABLE OF CONTENTS

1 Data transmission in optical fibers

Fiber optic communication systems are lightwave systems that employ optical fibers for information transmission. They have been deployed worldwide since the 1980s and have indeed revolutionized the technology behind telecommunications. They have consequently become the backbone of telecommunications infrastructures that support the internet. Light transmission in glass fibers was first explored in the 1960s, but the early fibers exhibited enormous propagation losses, so that the transmission distance was severely limited. Pioneering work was carried out on purifying the glass for making fibers to be able to reach the fundamental limit set by Rayleigh scattering due to the unavoidable density fluctuations in glass. And silica turned out to be a good candidate material. Corning company developed a silica fiber in the 1970s, with a propagation loss of 20 dB/km [3,4], which was a breakthrough as at that time the usual figures were on the scale of thousands of decibels. The development progressed rapidly, and nowadays standard single mode fiber has loss 100 times lower at only around 0.2 dB/km in the 1550 nm spectral region [5], which is close to the fundamental limit. Comparing to systems based on electrical cables, the approach of optical fiber communications has numerous advantages. Fiber optic cables are immune to problems that arise with electrical cables such as ground loops or electromagnetic interference. Optical communication systems use high carrier frequencies in the visible or near-infrared region of the electromagnetic spectrum and therefore it offer huge data transmission capacity. Data transmission using light offers ultrahigh data rates due to the high optical frequencies, which make it possible to utilize very broad optical bandwidths. In lightwave communications, wavelengths are designated into telecommunication windows described as in Table 1.

Band	Description	Wavelength range
O band	original	1260–1360 nm
E band	extended	1360–1460 nm
S band	short wavelengths	1460–1530 nm
C band	conventional (“erbium window”)	1530–1565 nm
L band	long wavelengths	1565–1625 nm
U band	ultralong wavelengths	1625–1675 nm

Table 1 – Telecommunication windows.

1.1 Optical loss

Losses for light propagating in fibers are very small. As mentioned, they are only about 0.2 dB/km for modern single mode silica fibers. The low loss allows transmission being bridged over tens of kilometers without deploying components for amplifying the signal. Hence optical fibers are ideal for use in long distance transmission of data information using light. Optical fiber based systems have largely replaced radio transmitter systems for long-haul optical data transmission. Attenuation in fibers enable different transmission windows. The loss spectrum of a typical standard single mode fiber can be seen from Figure 1. Over a broad wavelength window, the loss differs at various wavelengths range, and is the lowest around the 1550 nm range, known as the conventional C band. The S- and L- bands extending towards the lower and longer wavelength ranges experience slightly higher losses.

1.2 Optical amplification

Optical amplifiers, devices where light signals are periodically amplified along their transmission paths in a network, have revolutionized communications using optical fibers and have had a major impact on the information revolution and the building of the Internet. Even though optical fibers can be used to carry massive amounts of information, it is expected that the growth of data usage will result in capacity exhaustion in the coming decades if no breakthrough technology is introduced [6].

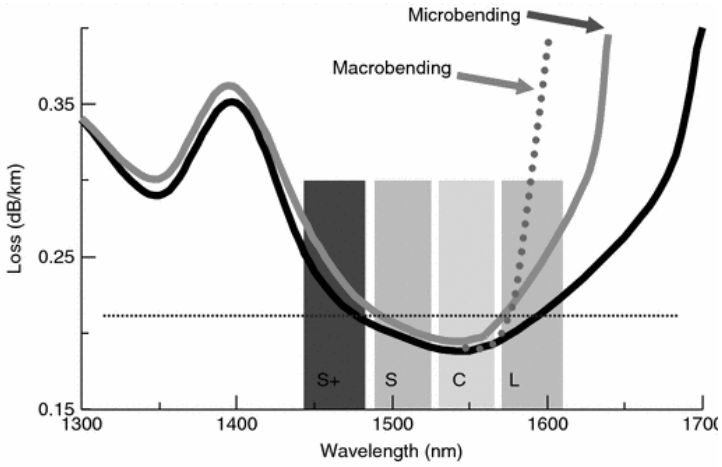

Figure 1 – Loss spectrum of standard single mode fiber [7].

Transmission over optical fibers is currently limited by the bandwidth of available amplification schemes, by the noise generated in optical amplifiers, and by signal distortion induced by the high intensity of the light propagating in the small dimension fibers, resulting in so-called nonlinear effects [8, 9].

In the C-band conventional erbium-window, erbium-doped fiber amplifiers (EDFAs) are by far the most important fiber amplifiers in the context of long-range optical fiber communications. They can efficiently amplify light in the 1550 nm wavelength region, where standard single mode fibers have their minimum loss. They can easily provide gain up to 15 dBm as standard commercial modules, and 33 dBm modules are available for high power amplification applications, for example, amplifying an optical signal to work as a pump for the consecutive stages' operation.

Raman fiber amplifiers (RFAs), optical amplifier based on Raman gain, result from the effect of stimulated Raman scattering. Provided a suitable pump source is used, Raman amplifiers can be operated in very different wavelength regions in the telecom window.

Amplifiers are one of the key components in the widely deployed lightwave communication systems. When it comes to multi-wavelength broadband operation, it is desirable to adopt amplifiers with uniform gain spectral profile in order to cope with the enormous transmission bandwidth offered by optical fibers. Various approaches have been carried out, and amongst which combining of available fiber amplifiers had been a straight forward engineering solution to offer.

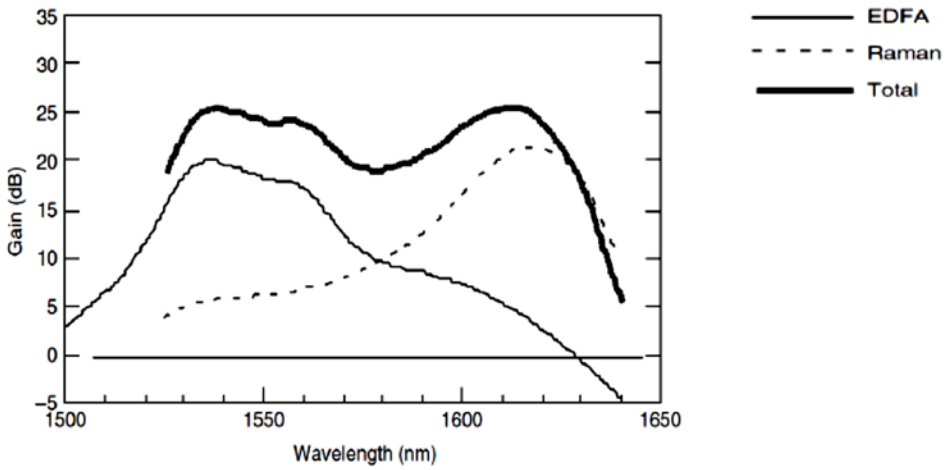

Figure 2 – Broadband flat gain profile obtained via hybrid EDFA/Raman amplifier [7].

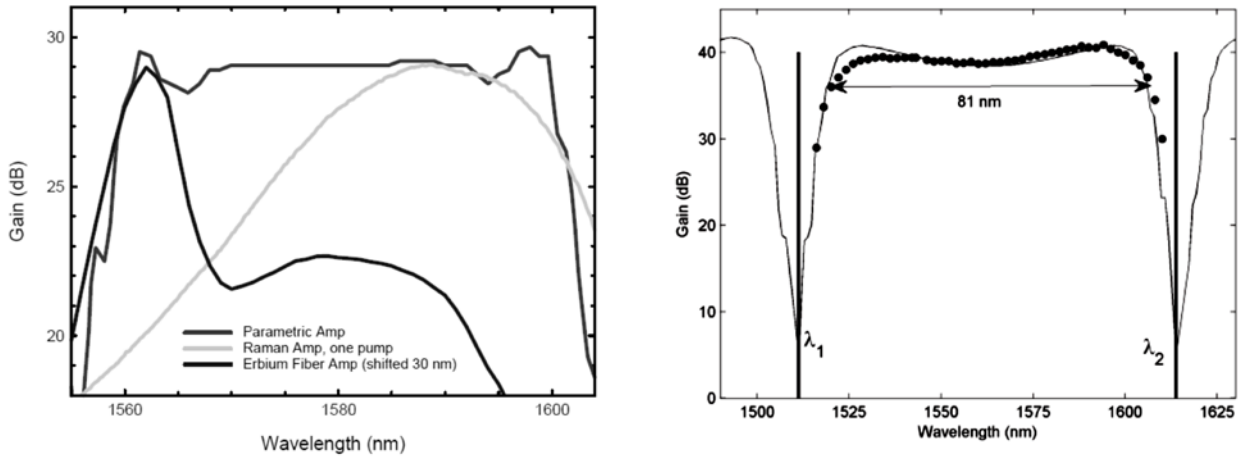

Figure 3 – Broadband flat gain profile obtained via FOPA, compared to the respective gain profile of EDFA and Raman fiber amplifiers (left) [10]; Calculated and measured (circles) gain spectra for HNLF FOPA with 3 dB bandwidth of 81 nm (right) [11].

One example could be the hybrid EDFA/Raman amplifier designed to have an almost uniform gain profile covering the C- and L-band wavelength regions. In this implementation, according to the design specification, two kinds of hybrid amplifier can be achieved, the so called narrowband hybrid amplifier, and the seamless wideband hybrid amplifier. The typical gain bandwidth achievable for the narrowband case is 30 to 40 nm, and for the wideband case up to 70 to 80 nm. Because the gain spectra of the EDFA and RFA have opposite gain slopes, and that the Raman amplifier is able to compensate for the gain decay at longer signal wavelengths uncovered by an EDFA, an almost flat gain profile can be obtained without using a gain equalizer, as shown in Figure 2. However this design involves cascading of two different types of fiber amplifier systems, and critical pumping requirements which involves employment of more components in the design, the noise accumulated would reduce the signal to noise ratio and degrade signal quality.

Fiber optical parametric amplifiers on the other hand, can be configured to offer very broad wavelength band flat top gain profiles in a single highly nonlinear fiber stage when pumped with two pumps. Figure 3 (left) shows the unequalized gain spectrum of a 41 nm bandwidth parametric gain profile [10] compared to scaled gain spectra provided by a single Raman pump and an erbium-doped fiber. Another record performance demonstrates a continuous-wave double-pump fiber optical parametric amplifier exhibiting 40 dB flat gain over 81 nm bandwidth [11]. Figure 3 (right) shows the broad flat gain profile experimentally measured and matching theoretical predictions. In this case, the bandwidth was not limited by fiber properties, but by the location of the pump wavelength relative to the zero dispersion of the highly nonlinear fiber. It is obvious that

the gain spectrum of parametric amplifiers can compare favorably to the currently deployed amplifiers. This is only a small glimpse into what FOPAs are able to deliver with it design performances. There are several other functionalities being demonstrated apart from amplification.

The availability of low-loss silica fibers led to the advent of the new field of nonlinear fiber optics. Optical Kerr effect describes when an optical beam is modifying the refractive index of the fiber either for the beam itself or for a beam at another wavelength. In the former case, the intensity dependence of the refractive index in nonlinear optical media occurs through self-phase modulation, a phenomenon that leads to spectral broadening of optical pulses. Four-wave mixing, the nonlinear effect arising from the third-order optical nonlinearity described with $\chi^{(3)}$ coefficient, occurs when at least two different frequency components propagate together in a nonlinear medium such as an optical fiber. In this case, the beam with strong intensity modifies the fiber refractive index for a signal beam at another wavelength. Four-wave mixing is a parametric process.

1.3 Optical regeneration

A fiber optical amplifier is only one of the crucial key components that are needed in a lightwave communications transmission link. Other functionalities like optical regenerators are needed to restore the signal quality along the transmission line to combat undesired transmission impairments. Impairments such as dispersion, nonlinearity and noise degrade the signal quality in optical communications links. To meet the system demand for signal transmission at higher modulation rates and over broader wavelength ranges, broadband and high speed regeneration devices are desirable. Regeneration schemes are usually described in terms of the 3-R regeneration, where the 3-R stands for re-amplification, re-shaping, and re-timing. FOPAs under appropriate configuration could serve as excellent candidates for amplitude-regeneration. And since parametric processes like four-wave mixing is an intrinsic phase sensitive process, with proper design, FOPAs are capable of providing simultaneous phase sensitive amplitude and phase regeneration.

Current systems based on conventional binary modulation formats such as NRZ or RZ, use conventional fiber amplifiers, which produce signal gain that is independent of the phase of the signal, and are classified as phase insensitive amplifiers (PIAs). A class of optical amplifiers, known

as phase sensitive amplifiers (PSAs), provides low-noise operation and can be used for phase regeneration. Even though their principle of operation has been theoretically predicted for many years, practical limitations have hindered their successful implementation as in-line amplifiers. Beyond amplification, PSAs offer the possibility to selectively process the in-phase and quadrature components of a signal. Such a feature is eminently attractive since one major trend in optical communication is the introduction of advanced modulation formats that mimic those that have made the breakthrough of digital wireless communication a reality.

Advanced optical modulation formats, which have been a hot topic in optical communication research for the past decade, make use of the phase of the electric field. However, the interaction between amplifier noise and optical fiber nonlinearities along the transmission link is known to result in nonlinear phase noise [12], which ultimately limits the range and capacity of future systems. Phase sensitive amplification offers the potential to periodically regenerate the phase of the transmitted signal.

Being able to process both the amplitude and phase of the signal all-optically will open the way to new functionalities, including the periodic regeneration of the phase of high bit rate (>40 Gbit/s) signals. It has been realized recently that a number of nonlinear processes in optical fibers could be used to realize phase sensitive amplification while overcoming some of its inherent practical limitations [13-19].

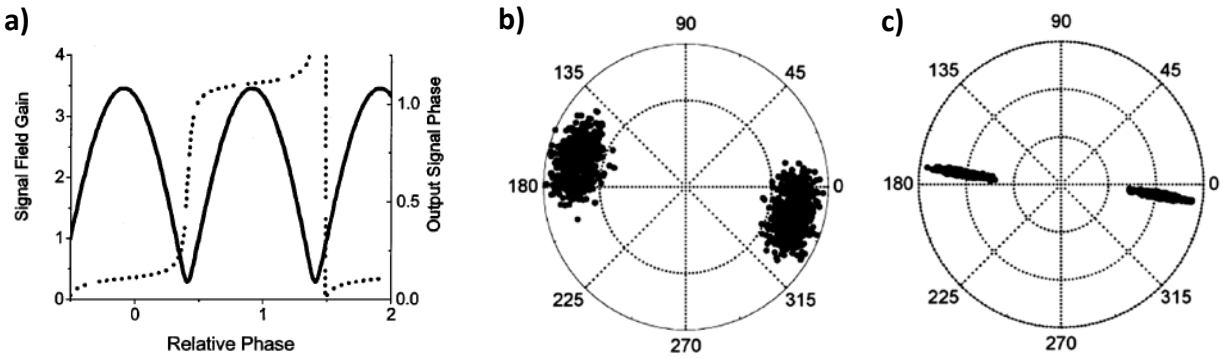

Figure 4 – (a) Normalized gain and phase profile of the HNLF based PSA as a function of relative phase. Constellation diagrams of (b) DPSK data after 500 km transmission, and (c) output constellation of the HNLF based PSA with phase-only regeneration [13].

For phase-shift keying (PSK) modulation formats, information is carried in the optical phase while the pulse amplitudes remain constant. The simplest PSK format is differential phase-shift keying (DPSK), where information is carried by phase changes of 0 or π radius between pulses in adjacent time slots. DPSK implemented in combination with balanced detection provides nearly a 3 dB improvement in receiver sensitivity compared to on-off keying [20, 21]. The constant amplitude also increases the tolerance to fiber nonlinearities to a certain degree. DPSK emerged as a leading modulation format for long-haul networks and has prompted the development of new optical signal processing technologies in order to meet the requirements imposed on PSK signal processing. Regeneration of DPSK signal can be ultimately accomplished by using phase-sensitive amplifiers. In DPSK systems, a fourth dimension is required on top of the usual 3-R regeneration determined for amplitude-modulated systems, namely re-phasing in terms of phase-regeneration.

Phase sensitive amplifiers can be configured to squeeze the phase of a signal. As an example, Figure 4 shows an early demonstration in 2004, where all-optical regeneration was performed for DPSK signals based on phase sensitive amplification [13]. The phase regeneration performance is represented using constellation diagrams to provide a visual representation of how the phase and amplitude noise are affected. From the constellation diagram of DPSK data, it can be seen how the phase level is squeezed into two discrete levels from a broad phase noise ranging over 50°. Figure 4 (left) shows the normalized gain and phase profile of the PSA versus input signal phase.

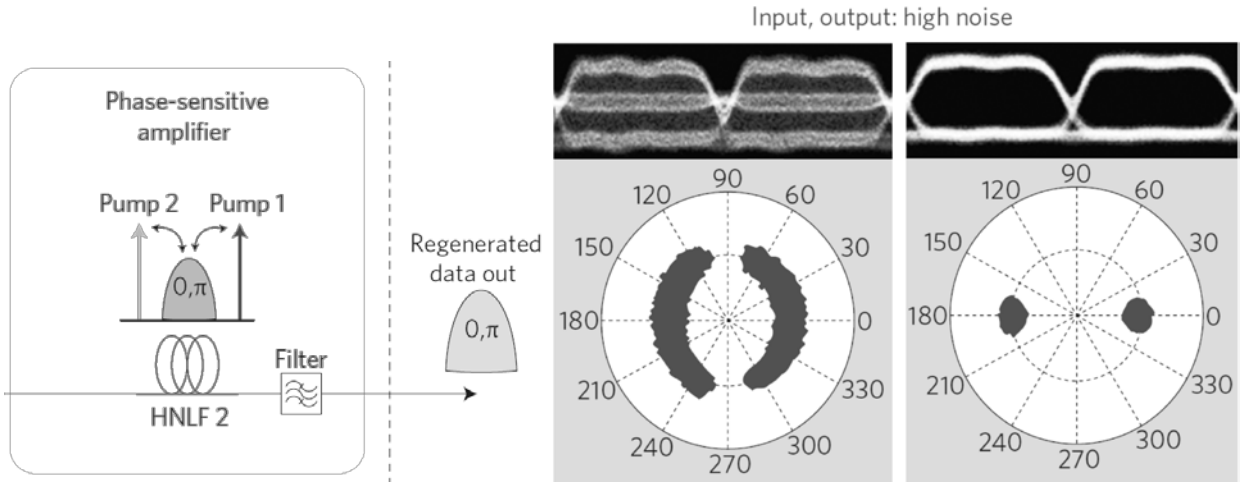

Figure 5 – Demodulated eye diagrams after balanced detection and differential constellation diagrams (showing bit-to-bit phase changes) measured at 10 Gbit/s. Diagrams measured at the input/output of the regenerator with phase noise added [22, 23].

Figure 5 shows a recent demonstration of an all-optical phase and amplitude regenerator [22, 23]. This Nature Photonics publication reports the development of the first practical 'black-box' all-optical regenerator capable of removing both phase and amplitude noise from binary phase-encoded optical signals. The regenerator is bit rate transparent, and switching between operating bit rate does not require any change in configuration. The results show that the phase noise was squeezed by the regenerator to the original back-to-back level without degrading the signal amplitude even for an extreme differential phase distortion with peak-to-peak value of $\pm 80°$. Furthermore, with suitable configuration, it is possible to control the number of phase levels allowed at the regenerator output. Therefore, PSA systems can be a basic building block adjustable to operate for different advanced modulation formats, such as phase and amplitude regeneration of quadrature phase shift keyed (QPSK) signals [24, 25].

Phase sensitive amplifiers with phase squeezing property and simultaneous regeneration of signal phase and amplitude represent a powerful signal processing tool for multilevel phase-encoded signals. PSAs deliver the regeneration capabilities demanded by the next-generation telecommunications systems.

2 Fiber optical parametric amplifier

The fundamental principles of parametric amplification in optical fibers have been studied since the 1980s. Recent breakthroughs have enabled parametric amplifiers to provide outstanding performances compared to those of conventional optical fiber amplifiers. Some of the major technological breakthroughs include the development of highly nonlinear fibers (HNLFs), and methods for efficient suppression of stimulated Brillouin scattering (SBS).

In optical fibers, parametric amplification is obtained by exploiting the $\chi^{(3)}$ nonlinearity relying on the nonlinear process of four-wave mixing (FWM). A schematic illustration of degenerate-pump FWM in fiber is shown in Figure 6. Consider the signal is input together with a pump into the $\chi^{(3)}$ medium, along propagation, nonlinear interactions between the waves will result in the pump being depleted, the signal being amplified and an idler being generated. The signal and idler frequencies are symmetrically placed with respect to the pump frequency. The idler photons retain their polarization relation with respect to the signal and the pump. Phase matching condition is a critical issue in FWM. Significant FWM would only occur when the phase mismatch is nearly vanished.

Fiber optical parametric amplifiers (FOPAs) provide outstanding performances in comparison to those of the conventional optical amplifiers such as erbium doped fiber amplifiers (EDFAs), semiconductor optical amplifiers (SOAs) and Raman fiber amplifiers (RFAs). The gain region(s) of a FOPA can be centered about any arbitrary wavelength provided a zero-dispersion wavelength (ZDWL) closely below that wavelength center. It is relatively easy to obtain large gain. The gain bandwidth scales with pump power, fiber nonlinearity and fiber dispersion properties. The gain profile can be tailored depending on the wavelength configuration of the interacting waves. A dual-pump FOPA can provide a flatter gain profile over a wider wavelength range compared to the single-pump case. Like EDFAs, FOPAs can in principle have a noise figure (NF) approaching 3 dB, and even 0 dB when operating in a phase-sensitive mode. However, as parametric processes are sensitive to the phase of the optical waves involved, phase-matching must be arranged in the wavelength range of interest to ensure efficient conversion between the interacting waves. As the nonlinear response in optical fibers is inherently instantaneous, it enables FOPAs to have numerous potential applications in the field of ultrafast optical signal processing, such as wavelength conversion [26, 27], optical sampling [28, 29] and signal regeneration [30-32], etc.

Figure 6 – Degenerate pump FWM in a $\chi^{(3)}$ medium.

Nevertheless, injecting intensive pump power into a fiber will cause stimulated Brillouin scattering (SBS), a back scattering effect of light one must circumvent to achieve power efficiency for the parametric processes. Extensive efforts have been dedicated to the development of SBS suppression schemes, and most recently, the development of novel highly nonlinear fibers with increased SBS threshold level.

2.1 Development of highly nonlinear fibers

The parametric processes in optical fibers rely on the third order susceptibility $\chi^{(3)}$. Though this nonlinearity in silica fibers is relatively weak, the invention of highly nonlinear fibers (HNLFs) has elevated the research interest in optical fiber based parametric amplification in the recent years. Highly nonlinear fibers were first developed in the 1990s. They are defined as fibers with an increased nonlinear parameter (γ) and an engineered dispersion close to zero. Many nonlinear effects inside optical fibers depend on the parameter.

$$\gamma = \frac{2\pi n_2}{\lambda A_{eff}} \qquad \text{Equation 1}$$

The nonlinear index coefficient n_2 is usually expressed in unit of m^2/W. the A_{eff} parameter is known as the effective core area, which is evaluated using the modal distribution for the fundamental fiber mode. It depends on the core radius and the core-cladding index difference. c is the speed of light in vacuum, and ω_0 is the carrier frequency. Fiber based OPA can be implemented in various fiber types. Among them are the conventional dispersion shifted fibers (DSFs), highly-nonlinear fibers (HNLFs), micro-structured fibers (MSFs) which are also called photonic-crystal fibers (PCFs), bismuth-doped fibers (BiDFs), and chalcogenide fibers (CHFs). As the nonlinear coefficient plays an important role in determining the parametric gain, fibers with a higher nonlinear parameter are desired. A list of typical nonlinear coefficient for those fibers is shown in Table 2.

Type of fiber		Nonlinear coefficient γ [$W^{-1}km^{-1}$]
Dispersion-shifted fiber	(DSF)	2.1
Highly-nonlinear fiber	(HNLF)	10
Micro-structured fiber Photonic-crystal fiber	(MSF) (PCF)	10-100
Bismuth-doped fiber	(BiDF)	100-1000
Chalcogenide fiber	(CHF)	>1000

Table 2 – Nonlinear parameter for various types of fibers.

Conventional silica based HNLF have the advantage of precise dispersion control, and easy splicing to standard single mode fibers. A typical value of these nonlinear parameter is on the level of 10 $\mathrm{W}^{-1}\mathrm{km}^{-1}$. They have been widely used for applications like wavelength conversion, four wave mixing, supercontinuum generation, phase (in)sensitive parametric amplification, and optical regeneration.

2.1.1 Stimulated Brillouin scattering in fibers

Research in molecular scattering was intensively studied in the 1920s. Scattering from optical phonons (quantized states of the lattice vibration) known as the Raman process, is the inelastic scattering processes of light with vibrational properties of matter. Interaction of light with acoustic phonons is the process of scattering of light from thermally excited acoustic waves, and is known as Brillouin scattering [33].

Stimulated Brillouin scattering (SBS) is a nonlinear process, whose efficiency depends on the input power. The input signal power at which the Stokes wave power increases rapidly and may even be comparable with the input power is called the threshold power, denoted as the SBS threshold. The threshold power is given by:

$$P_{th} \propto \frac{A_{eff}}{g_B L_{eff}} \frac{\Delta\nu_p + \Delta\nu_B}{\Delta\nu_B} \qquad \text{Equation 2}$$

where g_B is the Brillouin gain coefficient, $\Delta\nu_p$ is the linewidth of the pump, and $\Delta\nu_B$ is the linewidth of the Brillouin gain spectra. A widely used, simple and effective way to increase the SBS threshold is using phase dithering to broaden the linewidth of the pump. A widely used method for pump dithering is combining multi-tune radiofrequency to broaden the pump spectrum to increase the SBS threshold through phase modulation [34-37].

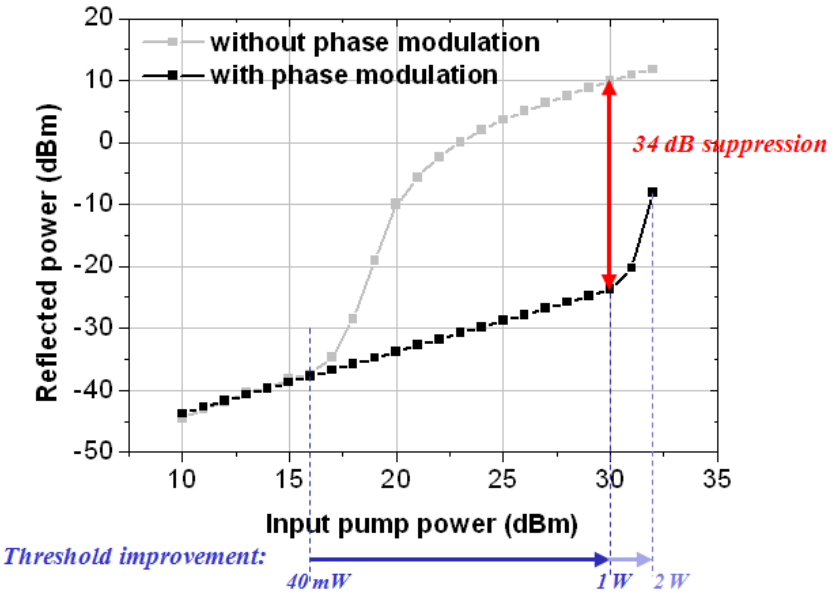

Figure 7 – Experimental measurement of SBS suppression obtained with 40 GHz single tone pump phase modulation.

Figure 7 shows the impact of phase dithering of a pump using 40 GHz single-tone phase modulation for SBS suppression. The experimentally measured results show an effective suppression of the back reflected power of 34 dB. This in turn improves the SBS threshold by almost 15 dB.

However, for several applications, pump broadening is not a suitable solution to be used, due to the extra phase noise it introduces. Other techniques for increasing the SBS threshold include applying linear or stepwise temperature gradient, or linear or stepwise strain gradient along the fiber [38, 39]. The temperature or strain changes the SBS frequency shift, and therefore broadens the effective Brillouin linewidth, which leads to a higher threshold level. Up to 8 dB improvement in SBS threshold has been demonstrated with this method [40]. However, changes in temperature or strain not only modify the SBS properties, but also alter the dispersion profile, and increase the polarization mode dispersion of HNLFs. Furthermore, a large strain may reduce the fiber lifetime too. Under these circumstances, doping of the HNLF core turns out to be an efficient method to increase the SBS threshold. With this technique, aluminum is used to dope the core of HNLF instead of germanium. The core doping with aluminum raises the refractive index and lowers the acoustic index. It creates a guiding structure for the optical field and an anti-guiding structure for the acoustic field. The decrease of the effective overlap between the optical and acoustic fields leads to an increased SBS threshold.

2.1.2 Al-doped HNLF with increased SBS threshold

SBS is generated by electrostrictive density fluctuations or sound waves that exhibit a transverse distribution proportional to the optical intensity distribution. It limits the amount of power that can be launched into a fiber. It limits the maximum nonlinearity achievable from a highly nonlinear fiber, which is often referred to as the figure of merit of SBS limited HNLFs, and scales as:

$$\gamma L_{eff} P_{th} \propto \frac{n_2}{g_B} \qquad \text{Equation 3}$$

Recently, a novel type of HNLF, the aluminum doped Al-HNLF-strained type [41], which provides high SBS threshold has become a highlight that has attracted researchers' interest. The Al-HNLF was reported with 8.8 dB improvement in figure of merit for SBS limited highly nonlinear fibers. With the utilization of HNLF with high SBS threshold, an additional SBS suppression stage is no longer necessary and it would hence simplify the design setup of FOPAs, and further reduce its cost.

Figure 8 (a) shows an experimental characterization of this strained Al-HNLF of length 130 m and a comparison to conventional germanium-doped standard highly nonlinear fiber (Std-HNLF) of length 500 m. Figure 8 (b) shows the analytical prediction of SBS threshold level with respect to fiber length, according to $P_{th} = 21\, A_{eff}/(g_B L_{eff})$.

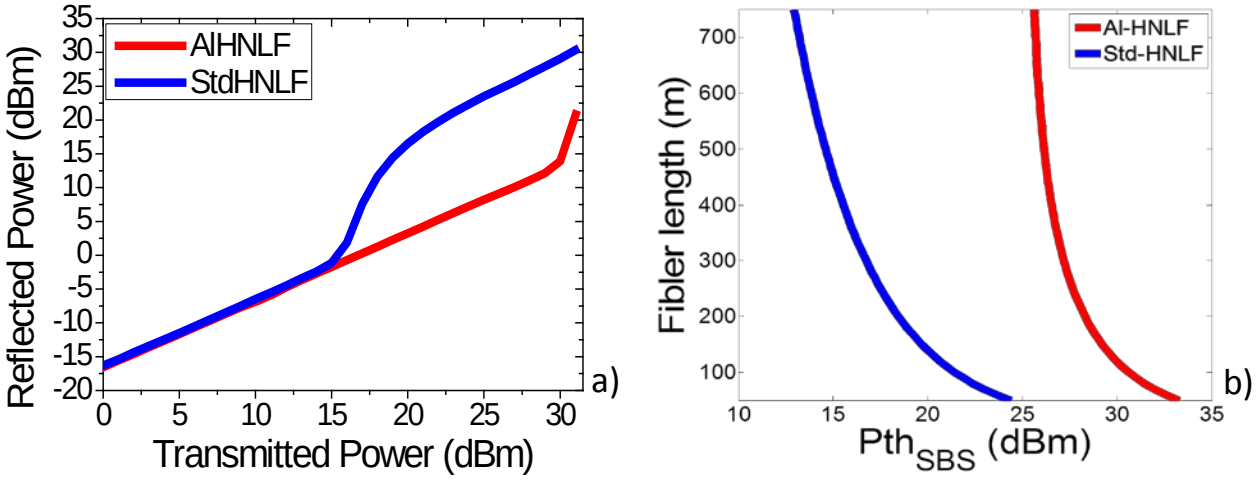

Figure 8 – SBS characterization for Al- and Std-HNLF of (a) experimentally measured backscattered light as a function of transmitted power, (b) analytical solution of SBS threshold vs. fiber length

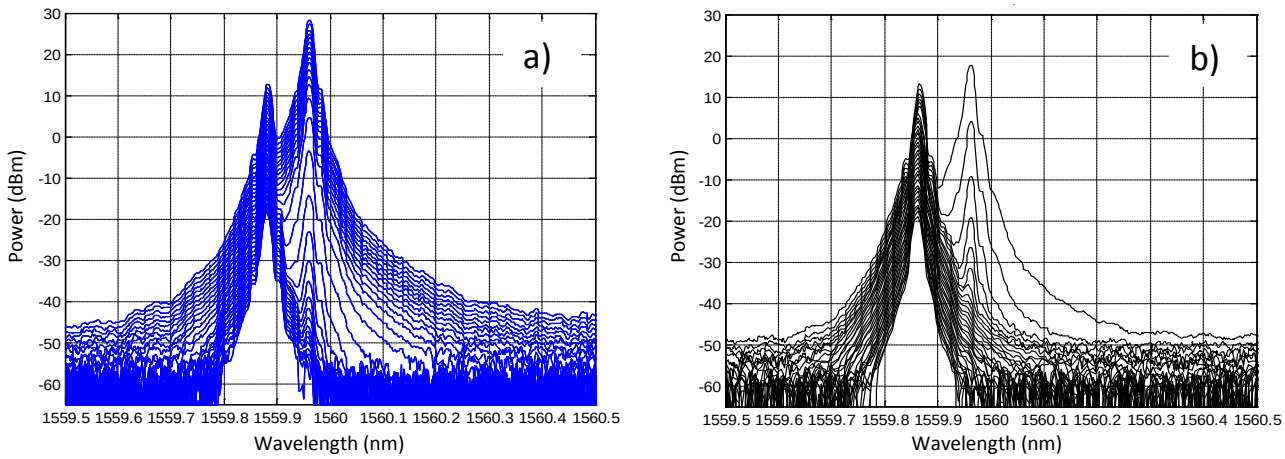

Figure 9 – Characterization of the SBS spectra for (a) Std-HNLF, (b) Al-HNLF.

Figure 9 (a) and (b) shows the spectra measured for the 500 m Std-HNLF and the 130 m Al-HNLF, respectively. In each of the plot, the power levels used are equivalent to the x axis of figure 8 (a). It can be clearly seen that the Stokes-shifted peak builds up much more slowly in the case of Al-HNLF than for Std-HNLF. That is because the core doping of aluminum reduces the acoustic index N, which is defined as the sound speed ratio between the fiber cladding and the core V_0/V_c. Aluminum doping increases the sound speed relative to that of the cladding and lead to a reduced acoustic index ratio. This acoustic anti-guiding structure refracts the electrostrictive density fluctuations away from the core and thereby reduces the interaction with the optical mode. Taking a closer look at the experimentally measured spectra, a slight SBS frequency shift of 2.1 GHz is observed, as shown in Figure 10. This is an implication of successfully obtaining a negative acoustic index step for the aluminum doped core.

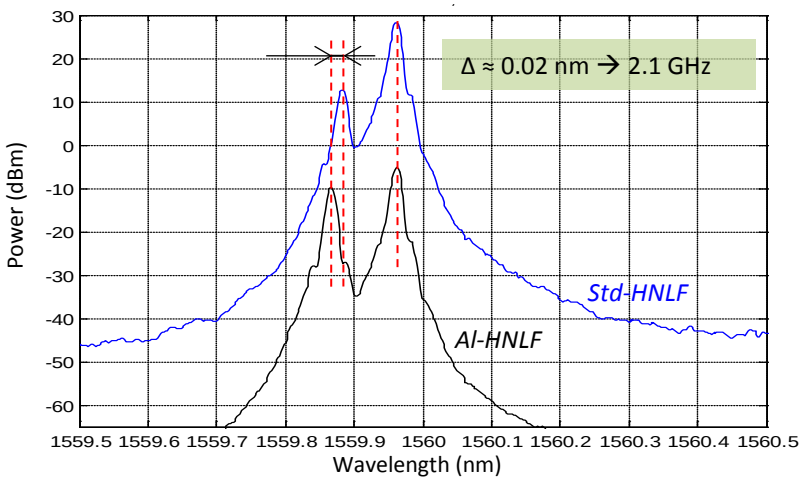

Figure 10 – Spectral comparison between the Al- and Std-HNLF, aluminum doping for the Al-HNLF leads to a 2.1 GHz shift of the Stokes spectrum compared to the case of the Std-HNLF.

From Figure 8 (a) it can be seen that the novel Al-HNLF has a SBS threshold higher than 30 dBm. However, the allowance of higher power into the fiber via Al doping does not necessarily lead to a higher nonlinear FOM factor. The aluminum ions doped into the fiber core introduce a high fiber transmission loss. Compared to the conventional germanium doped Std-HNLF with a fiber loss of ~ 0.9 dB/km, the loss of the Al-HNLF is as high as 15 dB/km. The nonlinear parameter, deduced from the measurement of nonlinear coefficient n_2 and fiber effective area, is reduced too, as can be read from Table 3.

Despite the fact that Al-doping leads to a lower FOM factor, the Al-HNLF has been adopted in various FOPA demonstrations showing superior performance [42]. The SBS threshold improvement suppresses the need for pump phase dithering, and Al-HNLFs are therefore a preferred nonlinear media for PSA applications. There is continuous development for advancing Al-HNLF performance. A new Al-HNLF has recently been reported with the fiber attenuation reduced down to 6 dB/km from 15 dB/km [43].

In chapter 3 we show the numerical prediction of the achievable PSA gain and extinction ratio performance if SBS was not setting a performance limit on the HNLFs. Following the rapid development of high SBS threshold HNLFs, there are reasons to believe that the predicted convincing performance of PSAs can be realistically demonstrated in the near future.

Fiber type	Unit	Ge-HNLF	Al-HNLF
Length	Km	0.5	0.13
Attenuation	dB/km	0.83	15
Effective length	km	0.477	0.105
SBS threshold	dBm	15	30
	mW	31.6	1000
Effective area	μm^2	11.6	13.5
γ	$(W \cdot km)^{-1}$	11	7.4
FOM ($P_{th} \cdot \gamma \cdot L_{eff}$)		0.166	0.775

Table 3 - Comparison of nonlinear figure of merit of the 500 m Std-HNLF and the 130 m Al-HNLF.

2.2 Parametric processes in HNLFs

The optical parametric amplification (OPA) can be configured in either two-pump case or one-pump case, featuring non-degenerate FWM and frequency degenerate pump FWM, respectively. The two-pump case OPA offers a number of advantages over conventional one-pump OPA designs, such as flexibility in tailoring the wideband gain profile. The single pump case is a special case where the pump spacing goes to zero. The wavelength configurations of dual-pump and single pump FOPAs are displayed in Figure 11.

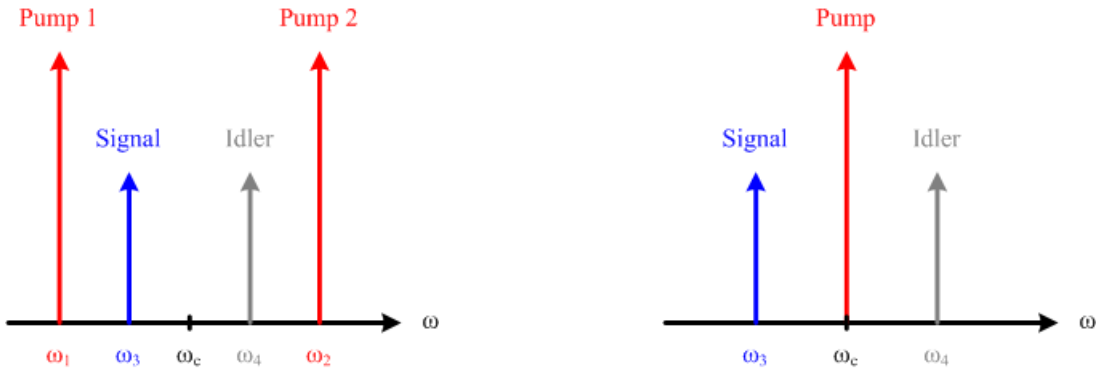

Figure 11 – General configuration of FOPAs, in the two-pump (left) and one-pump (right) cases.

Four-wave mixing (FWM) is a parametric process in which a signal is amplified along with generation of an idler wave. In the single-pump case, signal and idler are at frequencies on opposite sides of a strong pump wave. When an optical field is applied to an optical fiber, the polarization induced in the medium is not linear but contains nonlinear terms whose magnitude is governed by the nonlinear susceptibilities. In an isotropic medium like optical fiber, the third-order susceptibility $\chi^{(3)}$ is responsible for the wave mixing process. The third-order polarization term is defined as:

$$P_{NL} = \varepsilon_0 \chi^{(3)} : EEE \qquad \text{Equation 4}$$

where E is the electric field, P_{NL} is the induced nonlinear polarization, and ε_0 is the vacuum permittivity.

The total electric field for four waves oscillating at frequencies $\omega_1, \omega_2, \omega_3, and\ \omega_4$ linearly polarized along the same axis x has the form

$$E = \frac{1}{2}\hat{x}\sum_{j=1}^{4} E_j\, exp\left[i\left(k_j z - \omega_j t\right)\right] + c.c. \qquad \text{Equation 5}$$

k_j is the propagation constant equal to $k_j = n_j\omega_j/c$. Herein, n_j is the refractive index, and all four waves are assumed to be propagating in the same direction. Expressing the nonlinear polarization P_{NL} in the same form as E:

$$P_{NL} = \frac{1}{2}\hat{x}\sum_{j=1}^{4} P_j\, exp\left[i\left(k_j z - \omega_j t\right)\right] + c.c. \qquad \text{Equation 6}$$

Here we have P_j (j = 1 to 4) consisting of a large number of terms involving the products of three electric fields. Among those P_4 can be expressed as:

$$P_4 = \frac{3\varepsilon_0}{4}\chi^{(3)}_{xxxx}[\underline{|E_4|^2E_4} + \underline{2(|E_1|^2 + |E_2|^2 + |E_3|^2)E_4} + \underline{2E_1E_2E_3\exp(i\theta_+) + 2E_1E_2E_3\exp(i\theta_-)} + \cdots]$$

Self-phase modulation; Cross-phase modulation; Four-wave mixing

Equation 7

where the underlined terms are responsible for the effects of self-phase modulation, cross-phase modulation, and four-wave mixing, respectively. Four-wave mixing in fibers is related to self-phase modulation and cross-phase modulation. All these effects originate from the same Kerr nonlinearity and differ only in terms of degeneracy of the waves involved. The effectiveness of FWM processes in producing a parametric coupling depends on the phase mismatch between E_4 and P_4 governed by θ_+, θ_-, or a similar quantity,

$$\theta_+ = (k_1 + k_2 + k_3 - k_4)z - (\omega_1 + \omega_2 + \omega_3 - \omega_4)t$$
$$\theta_- = (k_1 + k_2 - k_3 - k_4)z - (\omega_1 + \omega_2 - \omega_3 - \omega_4)t \qquad \text{Equation 8}$$

Significant FWM requires complete phase matching, which requires matching of the frequencies as well as of the wave vectors. Satisfying the phase-matching condition requires a specific choice of the frequencies and the refractive indices for parametric processes to occur. The type of FWM

term containing θ_+ corresponds to three photons transferring their energy to a single photon at the frequency $\omega_4 = \omega_1 + \omega_2 + \omega_3$. Such processes are difficult to occur in optical fibers.

In the wave mixing term θ_-, two photons at frequencies ω_1 and ω_2 are annihilated with simultaneous creation of two photons at frequencies ω_3 and ω_4, such that $\omega_3 + \omega_4 = \omega_1 + \omega_2$. In this case, the relation $\omega_4 = \omega_1 + \omega_2 - \omega_3$ holds for energy conversation, and the phase matching condition $k_4 = k_1 + k_2 - k_3$ holds for momentum conservation.

The parametric gain responsible for FWM peaks when the phase mismatch $\kappa = 0$. The net phase mismatch is given by:

$$\kappa = \Delta\beta + \Delta k_{NL} \qquad \text{Equation 9}$$

The linear Phase mismatch, Δβ, is the wave-vector mismatch related to dispersion parameters.

$$\Delta\beta = \beta_3 + \beta_4 - \beta_1 - \beta_2 \qquad \text{Equation 10}$$

By properly choosing the pump wavelengths, it is possible to use this term for compensating the nonlinear phase mismatch, Δk_{NL}, stemming from self-phase modulation and cross-phase modulation.

$$\Delta k_{NL} = \gamma(P_1 + P_2) \qquad \text{Equation 11}$$

As a result, the total phase mismatch can be maintained close to zero over quite a wide spectral range, after the first term is made small by carefully balancing different orders of fiber dispersion.

The parametric gain g depends on the pump power. In the undepleted pump case it is defined as

$$g = \sqrt{(\gamma P_0 r)^2 - (\kappa/2)^2} \qquad \text{Equation 12}$$

Where $r = \frac{2\sqrt{P_1 P_2}}{P_0}$ and $P_0 = P_1 + P_2$. Under pump depletion, the effect can be included by numerically solving the four wave equations. The FWM conversion efficiency is defined as:

$$\eta_c = \frac{P_4(L)}{P_3(0)} = (\gamma P_0 r/g)^2 \sinh^2(gL) \qquad \text{Equation 13}$$

2.2.1 Nonlinear Schrödinger equation (NLSE)

The nonlinear Schrödinger equation (NLSE) can be used to describe pulse propagation in optical fibers. For continuous-wave operation, the NLSE takes its simple form as:

$$\frac{\partial A}{\partial z} + \beta_1 \frac{\partial A}{\partial t} + \frac{i\beta_2}{2}\frac{\partial^2 A}{\partial t^2} + \frac{\alpha}{2}A = i\gamma|A|^2 A \qquad \text{Equation 14}$$

The pulse amplitude is described by its slowly varying envelope A(z,t), and is assumed to be normalized such that $|A|^2$ represents the optical power. Chromatic dispersion is governed through the β_1 and β_2 terms, where the pulse envelope moves at the group velocity $v_g = 1/\beta_1$ and the effects of group-velocity dispersion (GVD) are governed by the β_2 term. Fiber loss is described through the α term. Third order nonlinearity is described through the term on the right hand side of the equation. Here γ is the nonlinear parameter defined in Equation 1.

For ultrashort optical pulses whose duration is shorter than 1 ps, therefore preserving a wide spectrum, one may need to include extra terms. The NLSE should therefore take a more generalized form:

$$\frac{\partial A}{\partial z} + \frac{\alpha}{2}A + \frac{i\beta_2}{2}\frac{\partial^2 A}{\partial T^2} - \frac{\beta_3}{6}\frac{\partial^3 A}{\partial T^3} = i\gamma\left(|A|^2 A + \frac{i}{\omega_0}\frac{\partial(|A|^2 A)}{\partial T} - T_R A\frac{\partial|A|^2}{\partial T}\right) \qquad \text{Equation 15}$$

with a retarded frame defined as $T = t - \frac{z}{v_g} \equiv t - \beta_1 z$.

Higher order nonlinear effects appear in this expression. Third-order dispersion (TOD) is described through the β_3 term. The term ${\omega_0}^{-1}$ result from including the first derivative of P_{NL}, it governs self-steepening [44] and shock formation effects. The T_R term originates from the delayed Raman response, and is responsible for the self-frequency shift induced by intrapulse Raman scattering.

2.2.2 Propagation regimes

To classify different propagation regimes in a fiber, two length scales associated with group-velocity dispersion and self-phase modulation are expressed as:

$$L_D = \frac{{T_0}^2}{|\beta_2|}, \qquad L_{NL} = \frac{1}{\gamma P_0} \qquad \text{Equation 16}$$

β_2 is the group velocity dispersion parameter related to the dispersion parameter D. γ is the nonlinear parameter, and $\mathrm{P_0}$ is the peak power of the incident pulse. The dispersion length $\mathrm{L_D}$ and the nonlinear length $\mathrm{L_{NL}}$ give a length scale over which dispersive or nonlinear effects become important for pulse evolution. For a certain type of fiber with known β_2 and γ, one can estimate the initial pulse width $\mathrm{T_0}$ and peak power $\mathrm{P_0}$ to tailor the desired propagation behavior. Depending on the relative magnitudes of $\mathrm{L_D}$ and $\mathrm{L_{NL}}$, and the fiber length L, the propagation behavior can be classified into four categories: 1) Transporter: when the fiber length L is less than both $\mathrm{L_D}$ and $\mathrm{L_{NL}}$, neither dispersive nor nonlinear effect play a significant role during pulse propagation. 2) Dispersion dominant regime: when the fiber length L is less than $\mathrm{L_{NL}}$ but equivalent to $\mathrm{L_D}$, with fiber and pulse parameters satisfy $\mathrm{L_D/L_{NL}} = \gamma \mathrm{P_0 {T_0}^2}/|\beta_2| \ll 1$, the nonlinear effects are negligible and the pulse evolution is governed by GVD. 3) Nonlinearity-dominant regime: when the fiber length L is less than $\mathrm{L_D}$ but is equivalent to $\mathrm{L_{NL}}$, such that fiber and pulse parameters satisfies $\mathrm{L_D/L_{NL}} = \gamma \mathrm{P_0 {T_0}^2}/|\beta_2| \gg 1$, dispersion is negligible and the pulse evolution is governed by SPM, which induces spectral broadening of the pulse. 4) Interplay between GVD and SPM: with fiber length L longer or comparable to both $\mathrm{L_D}$ and $\mathrm{L_{NL}}$, the pulse propagation experiences interplay between GVD and SPM effects. The propagation behavior is qualitatively different compared with that expected from either GVD or SPM alone.

A parameter N is introduced to govern the relative importance of the SPM and GVD effects on pule evolution along the fiber. In the context of optical solitons, N is referred to as soliton order. The parameter N takes the form:

$$N = \sqrt{\frac{L_D}{L_{NL}}} \equiv T_0 \sqrt{\frac{\gamma P_0}{|\beta_2|}} \qquad \text{Equation 17}$$

Dispersion dominates for $\mathrm{N} \ll 1$, whereas SPM dominates for $\mathrm{N} \gg 1$. Both SPM and GVD play an equally important role during pulse evolution for $\mathrm{N} \approx 1$.

2.2.3 Split-step Fourier method for numerically solving NLSE

The split-step Fourier method (SSFM) is used to numerically solve the NLSE. The SSFM consists in solving the linear part and the nonlinear part of the NLSE separately. The NLSE is hence written in the following form with the denotation of the linear operator $\widehat{\mathrm{D}}$ and the nonlinear operator $\widehat{\mathrm{N}}$.

$$\frac{\partial A}{\partial z} = [\hat{D} + \hat{N}]A \qquad \text{Equation 18}$$

The linear operator $\widehat{\mathrm{D}}$ is a differential operator that accounts for dispersion and absorption in a linear medium. The nonlinear operator $\widehat{\mathrm{N}}$ governs the effects of fiber nonlinearities on pulse propagation, such as SPM, XPM, FWM, and the earlier mentioned self-steepening effect and intrapulse Raman scattering, etc.

With respect to the generalized NLSE, the linear operator including fiber loss, 2nd and 3rd order dispersion effects takes the form:

$$\hat{D} = -\frac{i\beta_2}{2}\frac{\partial^2}{\partial T^2} + \frac{\beta_3}{6}\frac{\partial^3}{\partial T^3} - \frac{\alpha}{2} \qquad \text{Equation 19}$$

The nonlinear operator governing Kerr effect but neglecting self-steeping and intrapulse scattering has the simple form:

$$\hat{N} = i\gamma|A|^2 \qquad \text{Equation 20}$$

Along propagation, dispersion and nonlinearity act together along the length of the fiber. The stepping scheme for the split-step Fourier method obtains an approximate solution by assuming that in propagating the optical field over a small distance h, the dispersive and nonlinear effects can be pretended to act independently.

The use of FFT algorithm makes numerical evaluation relatively fast. The SSFM can be faster by up to two orders of magnitude compared with most finite-difference schemes [45, 46].

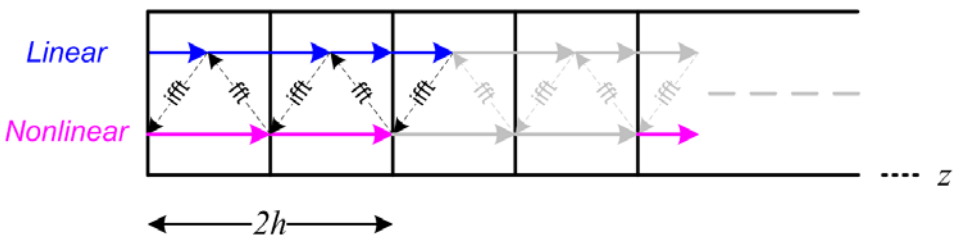

Figure 12 – Schematic illustration of a split-stepping Fourier scheme.

The optical field is first propagated for a distance $\mathrm{h}/2$ with dispersion only in the Fourier domain. At the midplane $\mathrm{z}+\mathrm{h}/2$, the field is inverse Fourier transformed and multiplied by a nonlinear term that represents the effect of nonlinearity over the whole segment length h. The stepping scheme is illustrated in Figure 12.

The segment length can be adaptive and need not to be spaced equally. The optimum choice of step sizes depends on the complexity of the problem.

2.2.3.1 Dispersion dominant: GVD

Pulses are propagating under the dispersion-dominant (linear) regime, when the fiber length is less than the nonlinear length but equivalent to the dispersion length. In this case, the GVD effects are studied alone by treating the fiber as a linear optical medium. Dispersion induced pulse broadening is discussed for Gaussian shaped pulses. The effects of a Gaussian pulse with initial frequency chirp are also described.

An un-chirped Gaussian pulse maintains its Gaussian shape on propagation whilst its width T_1 increases width distance z as

$$T_1(z) = T_0\sqrt{1+(z/L_D)^2} \qquad \text{Equation 21}$$

The magnitude of such a pulse decreases along the distance, the extent of this decrease is defined by the ratio z/L_D. Here L_D is the dispersion length defined in Equation 16. T_0 is the half-width at $1/e$ intensity point, which is related to the full-width at half-maximum (FWHM) of the pulse as

$$T_{FWHM} = 2(\ln 2)^{½}T_0 \approx 1.665T_0 \qquad \text{Equation 22}$$

As L_D is directly proportional to the initial pulse width and inversely proportional to the GVD parameter β_2, a narrower initial value of T_0 will lead to a shorter L_D. Same way, a smaller β_2 will lead to a longer L_D, indicating less efficient broadening of the pulse. The value $|\beta_2|$ gives a measure of the dispersion, therefore broadening of a pulse does not depend on the sign of β_2.

A linearly chirped Gaussian pulse has the form

$$U(0,T) = \exp\left(-\frac{1+iC}{2}\frac{T^2}{{T_0}^2}\right) \qquad \text{Equation 23}$$

Here, C is the chirp parameter that governs the frequency chirp imposed on the pulse. It can be estimated from the spectral width of the Gaussian pulse

$$\Delta\omega = \frac{\sqrt{1+C^2}}{T_0} \qquad \text{Equation 24}$$

$\Delta\omega$ is the spectral half-width at $1/e$ intensity point. The spectral width is transform limited such that $\Delta\omega T_0 = 1$ for $C = 0$. In the presence of linear chirp, the width of the spectrum is enhanced by the factor $\sqrt{1+C^2}$. A chirped Gaussian pulse maintains its Gaussian shape on propagation while its pulse width increases width distance z as

$$T_1(z) = T_0\sqrt{\left(1+\frac{C\beta_2 z}{T_0^2}\right)^2 + \left(\frac{\beta_2 z}{T_0^2}\right)^2} \qquad \text{Equation 25}$$

The broadening factor can be obtained by taking the ratio between T_1 and the initial widthT_0. For chirped Gaussian pulse, the broadening depends on the relative sign of β_2 and C. Their relative behavior is shown in Figure 13. When β_2 and$C$ are having identical signs ($\beta_2 C > 0$), the Gaussian pulse broadens monotonically with distance. And when they are having opposite signs ($\beta_2 C < 0$), the pulse goes through an initial narrowing stage before it starts to broaden.

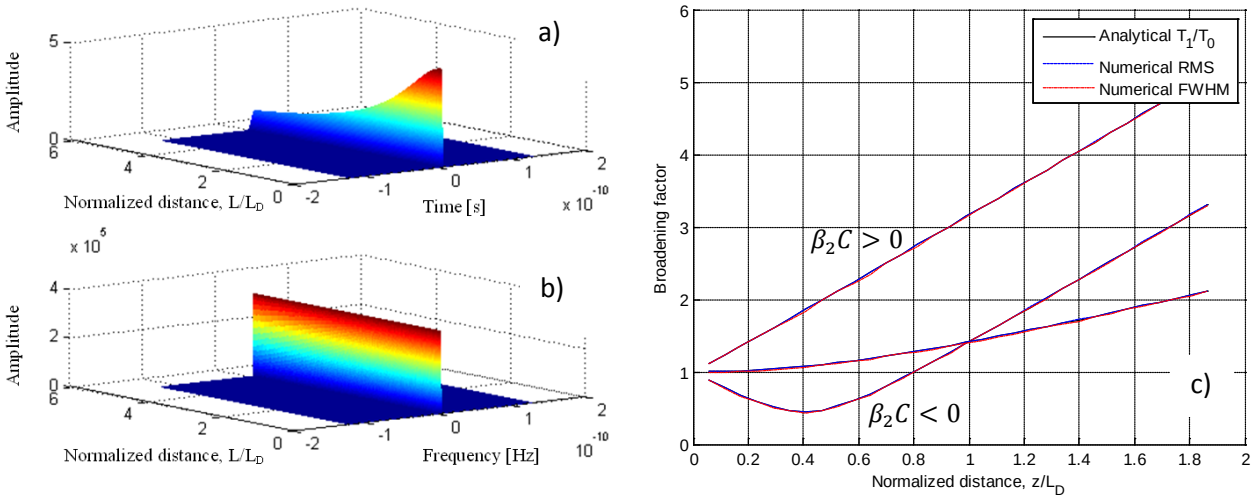

Figure 13 – Pulse evolution along fiber length under the dispersion-dominant (linear) regime, where the fiber length is less than the nonlinear length but equivalent to the dispersion length. (a) Time domain evolution (b) Frequency domain evolution (c) Pulse width evolution.

2.2.3.2 Dispersion dominant: GVD + TOD

When the pulse wavelength nearly coincides with the zero-dispersion wavelength (ZDWL), $\beta_2 \approx 0$. The β_3 term then provides the dominant contribution to the GVD effects. And for ultrashort pulses it is necessary to include the β_3 term even when $\beta_2 \neq 0$ [45]. In this case, the pulse evolution along the fiber depends on the relative magnitudes of β_2 and β_3. The dispersion length associated with the TOD term is then introduced to compare the relative importance of the β_2 and β_3 terms. It has the form:

$$L_D' = \frac{{T_0}^3}{|\beta_3|} \qquad \text{Equation 26}$$

Comparing the third order dispersion length to the second order dispersion length L_D that governs the GVD effect, the TOD effects play a significant role only when $L_D' \leq L_D$ or $T_0|\beta_2/\beta_3| \leq 1$.

A Gaussian pulse remains Gaussian when only the β_2 term contributes to the pulse propagation. For ultrashort pulses, TOD distorts the pulse such that it becomes asymmetric with an oscillatory structure near one of its edges [44]. In the case of positive β_3, oscillations appear near the trailing edge of the pulse. The oscillations are developed on the leading edge of the pulse when β_3 is negative. Oscillations are deep when $\beta_2 = 0$, and are damped significantly for even small value of β_2.

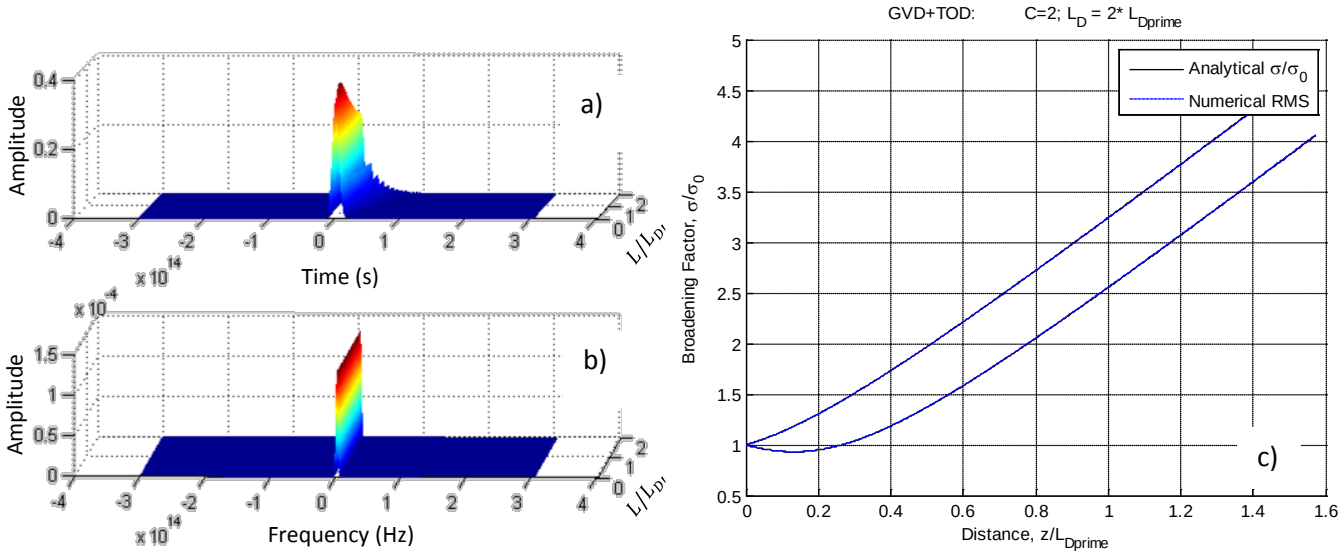

Figure 14 – Pulse evolution along fiber length under dispersion-dominant (linear) regime with third order dispersion. (a) Time domain evolution (b) Frequency domain evolution (c) Pulse width evolution.

2.2.3.3 Interplay between dispersion and nonlinearity

When injecting a pulse into an optical fiber, the Kerr effect leads to a time dependent phase shift that is proportional to the time dependent pulse intensity. The self-phase modulation (SPM) phenomenon can be understood as the nonlinear phase modulation of a pulse due to its own intensity via the Kerr effect. The SPM induced nonlinear phase shift φ_{NL} is intensity dependent and proportional to the relative ratio between the effective length $\mathrm{L_{eff}}$ and the nonlinear length $\mathrm{L_{NL}}$. It has the form

$$\varphi_{NL}(L,T) = |U(0,T)|^2 \frac{L_{eff}}{L_{NL}} \qquad \text{Equation 27}$$

$$L_{eff} = \frac{1 - e^{-\alpha L}}{\alpha} \qquad \text{Equation 28}$$

The effective length $\mathrm{L_{eff}}$ is less than the length L due to fiber loss. It equals to L when fiber loss goes to zero. The relative ratio between $\mathrm{L_{eff}}$ and $\mathrm{L_{NL}}$ is defined as the maximum phase shift φ_{max} that occurs at the pulse center

$$\varphi_{max} = \frac{L_{eff}}{L_{NL}} = \gamma P_0 L_{eff} \qquad \text{Equation 29}$$

When the pulse becomes so short that the dispersion length becomes comparable to the fiber length, it is necessary to consider the combined effects of GVD and SPM. Figure 15 shows a third-order soliton evolution over two soliton period ($\mathrm{z_0}$) lengths along a fiber. Recall that the soliton order N is proportional to T_0, and the ratio $\mathrm{L_D/L_{NL}}$, which is proportional to the ratio $\gamma \mathrm{P_0}/|\beta_2|$, as specified in Equation 17. Under this propagation regime ($\mathrm{N} = 3$), the input soliton pulse is reproduced at each of the soliton period lengths. The soliton period length is defined as

$$z_0 = \frac{\pi}{2} L_D \qquad \text{Equation 30}$$

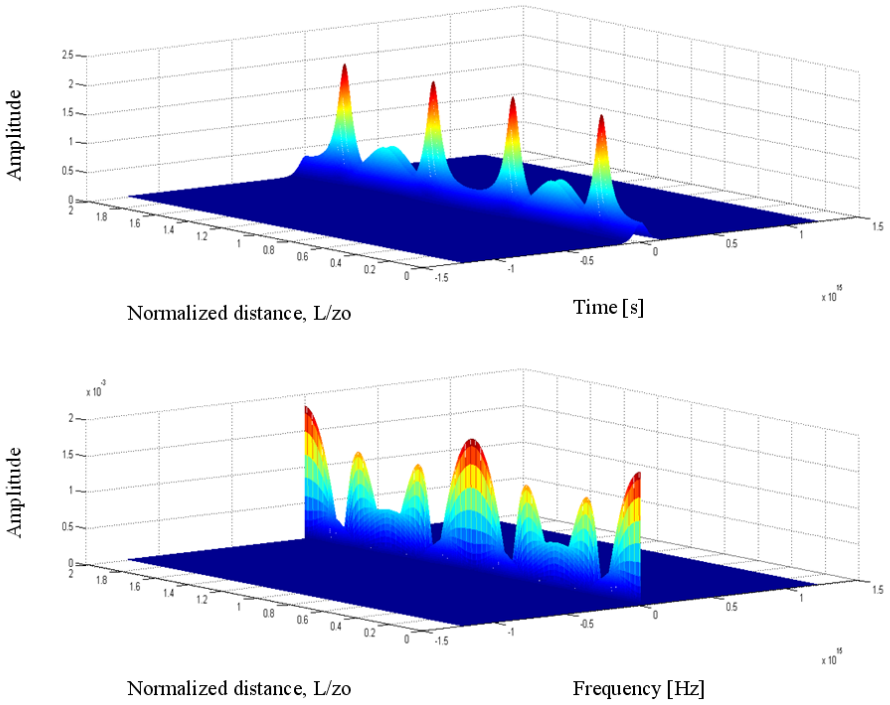

Figure 15 – Third order soliton evolution over two soliton period (z_0) lengths in a fiber. The input soliton pulse is reproduced at each of the soliton period lengths.

2.2.4 Single-pump phase insensitive parametric amplification

FOPAs have important characteristics, which make them potentially interesting for a variety of applications. The gain bandwidth of a FOPA increases with pump power. It supports arbitrary center wavelength, but requires the fiber to have its zero-dispersion wavelength (ZDWL) close to the center wavelength. It is relatively easy to obtain large gain. One can design FOPAs to work as wavelength converter, due to the FWM properties, namely the generation of an idler at a new wavelength.

Four-wave mixing in optical fibers has been studied extensively because it can be an efficient way for generating new waves (idlers). The four-wave mixing conversion efficiency is measured as the power ratio from the generated idler to the injected signal power. From the expression in Equation 13, the conversion efficiency is proportional to the nonlinearity γ, the total pump power P_0, the fiber length L, the wavelength displacement between the interacting waves, and the pump wavelength with respect to the fiber zero dispersion wavelength. Maximum conversion efficiency can be achieved when the phase mismatch κ goes to zero.

2.2.4.1 Gain bandwidth evolution

The pump wavelength displacement with respect to the zero-dispersion wavelength has significant impact on the four wave mixing conversion bandwidth. For relatively short fiber length, the conversion is flat but with no gain over a certain wavelength range. Figure 16 shows the conversion spectra obtained numerically for two types of commercially available highly nonlinear fibers. The dispersion flattened highly nonlinear fiber (DF-HNLF) has a dispersion slope one order of magnitude lower than that of a standard highly nonlinear fiber (Std-HNLF) [47]. In this case, the decrease in dispersion slope almost tripled the conversion bandwidth as can be seen in Figure 16. Broad bandwidth conversion in four wave mixing parametric conversion is best achieved when the pump is placed at wavelengths slightly above the ZDWL of a HNLF. In this simulation, the ZDWL for both fiber types are at 1550.39 nm. For Figure 16 a) and b), the pump wavelength is placed 4 nm above the ZDWL at 1554.39 nm. However, the bandwidth will be reduced when the displacement is increased i.e. from 4 nm to 10 nm, as shown in Figure 16 c) and d). The injected signal power was -10 dBm, and the used pump power was 24 dBm.

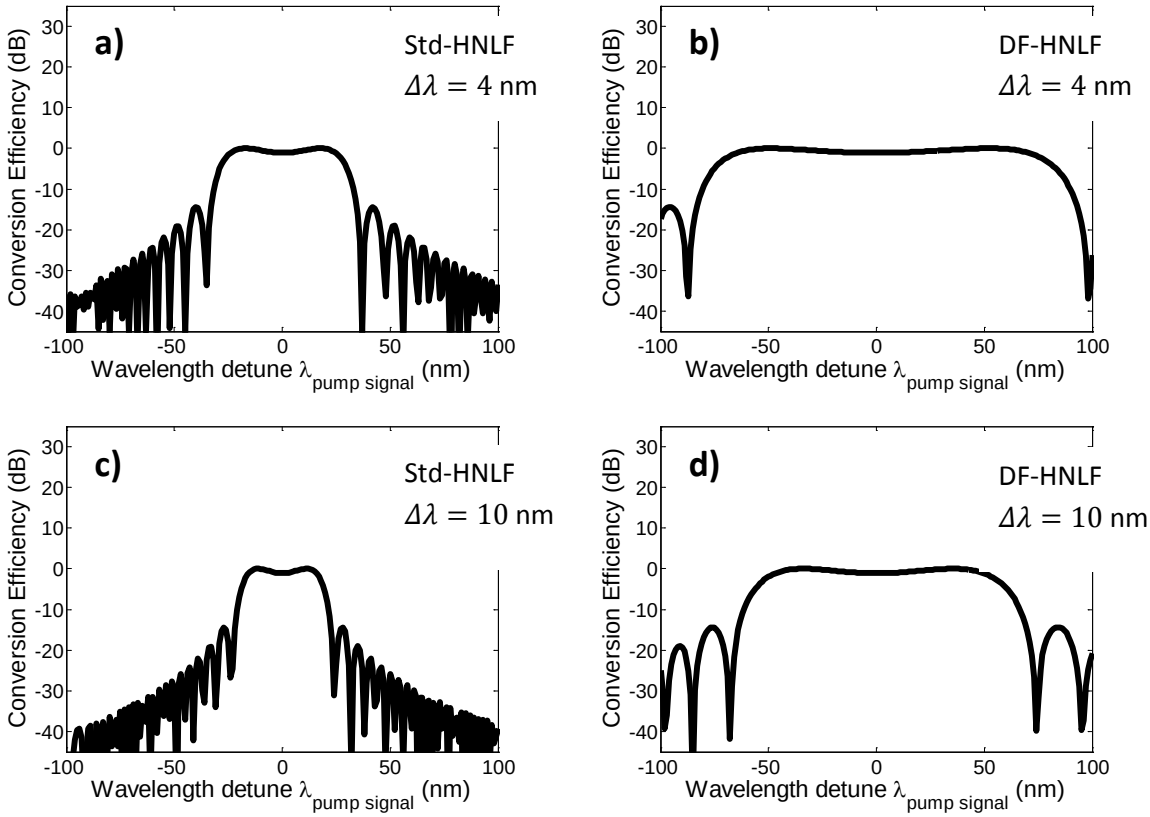

Figure 16 – Impact of fiber dispersion and pump detuning with respect to the ZDWL on a 100 m long FOPA. (a) and (c) are gain spectra of Std-HNLF, and (b) and (d) for DF-HNLF, at pump to signal detuning equals to 4 and 10 nm, respectively.

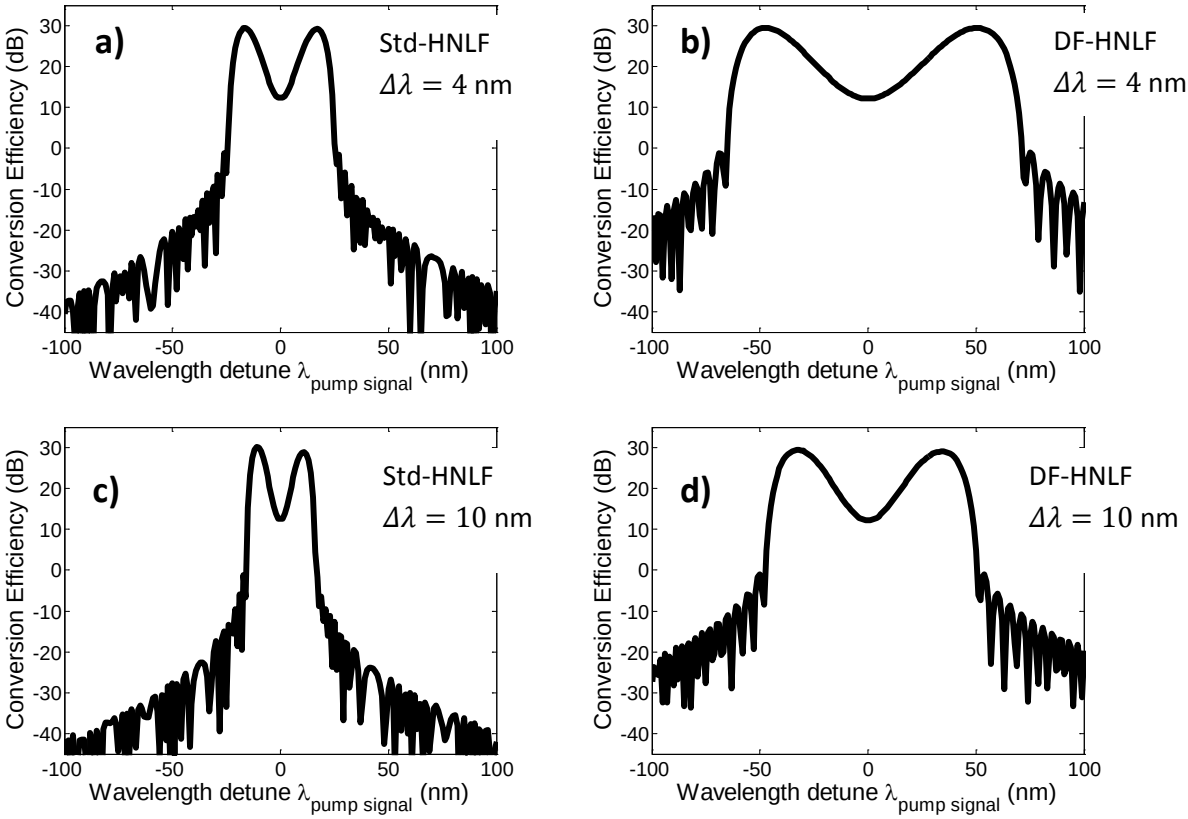

Figure 17 – Impact of fiber dispersion and pump detuning with respect to the ZDWL on a 500 m long FOPA. (a) and (c) are gain spectra of Std-HNLF, and (b) and (d) for DF-HNLF, at pump to signal detuning equals to 4 and 10 nm, respectively.

As the parametric gain is proportional to the product $\gamma P_0 L_{eff}$, positive conversion efficiency can be achieved when the fiber length is increased from 100 m to 500 m. This can be seen from Figure 17. Each of the sub-plots is equivalent to that in Figure 16 only scaled up in fiber length. Up to 30 dB positive gain is obtained for the converted idler, when the pump wavelength is placed slightly above the zero dispersion wavelength of the highly nonlinear fiber. The gain bandwidth reduces when the pump wavelength is further displaced above the fiber ZDWL.

Figure 18 compares the conversion gain and bandwidth in two cases: when the pump wavelength is 4 nm above the fiber ZDWL, and when the pump wavelength is below fiber ZDWL. The pump power used here is 21 dBm. Comparing with the curves in Figure 19, which have the same two pump wavelength displacements from ZDWL, but at a higher pump power 30 dBm, it can be seen that, for both cases, when the pump wavelength is above the fiber ZDWL, increasing the pump power leads to larger gain and broader gain bandwidth. In contrast, when the pump wavelength is below the fiber ZDWL, no parametric gain is obtainable, and an increase in pump power reduces the available conversion bandwidth.

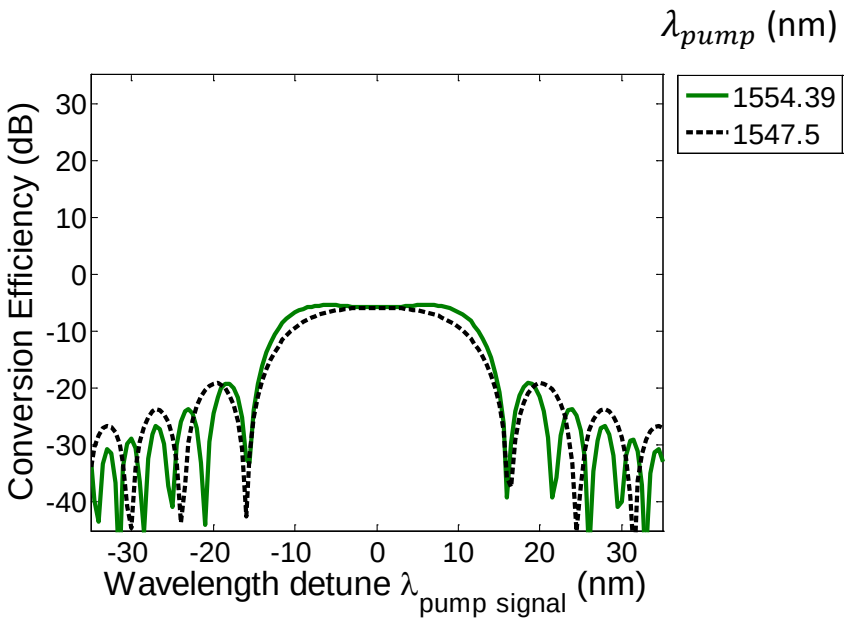

Figure 18 – Conversion efficiency of the idler for pump placed below and above the zero-dispersion wavelength. Pump power = 21 dBm.

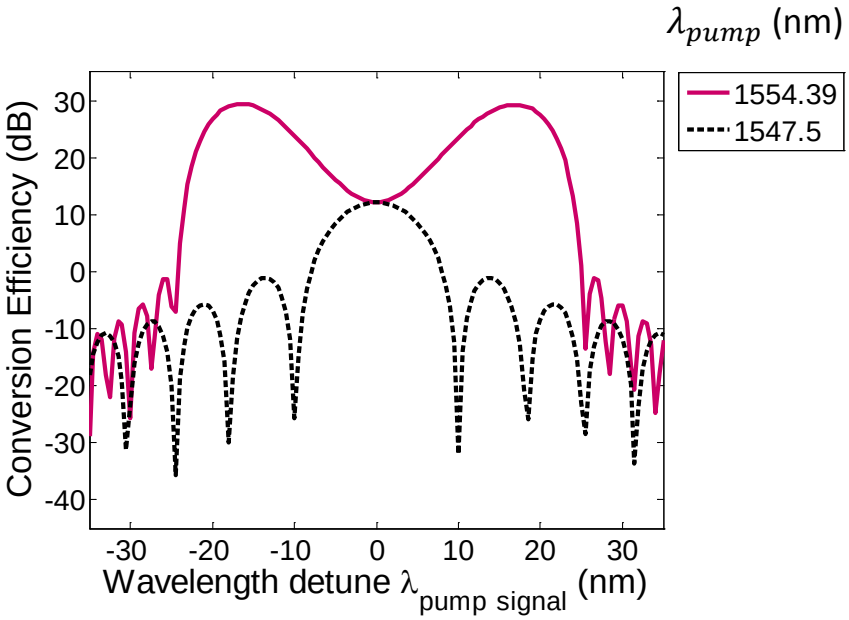

Figure 19 – Conversion efficiency of the idler for pump placed below and above the zero-dispersion wavelength. Pump power = 30 dBm.

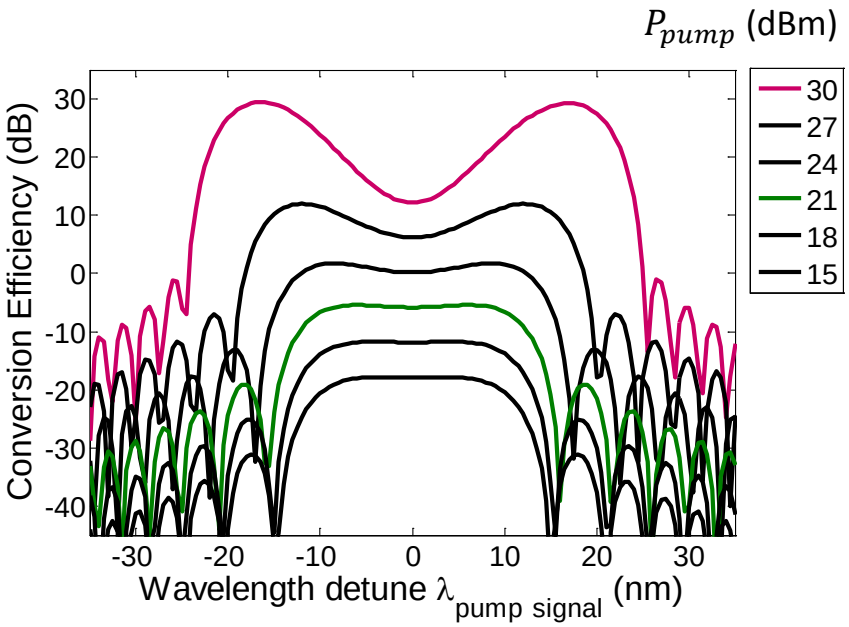

Figure 20 – Evolution of the conversion efficiency of the idler as a function of pump power.

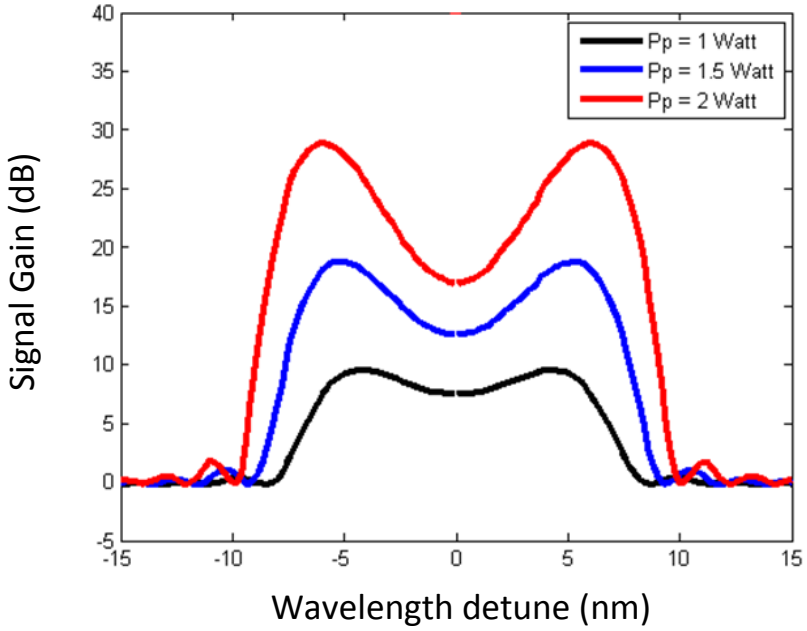

Figure 21 – Evolution of the signal gain and gain bandwidth as a function of pump power.

For single pump phase insensitive fiber optical parametric amplification, when the pump wavelength is placed slightly above the zero dispersion wavelength of the highly nonlinear fiber, and with high pump power, a significant parametric gain can be achieved for both signal and idler. It is observed in the single pump case, where two wavelength regions experience significant amplification. In Figure 19, this is seen as the positive conversion gain lobes at the two wavelength regions symmetrically around the pump which is placed at the wavelength center. In single pump parametric processes, the net phase mismatch has the form

$$\kappa \equiv \Delta\beta + 2\gamma P_1 \qquad \text{Equation 31}$$

In the perfect phase-matching case, where $\kappa = 0$, the signal and idler experience exponential growth in power, and the two peak gain regions in the conversion curves represent exponential gain attained via phase matching.

$$G_{exp} \approx \frac{1}{4}\exp[2\gamma P_1 L_{eff}] \qquad \text{Equation 32}$$

When the signal and pump overlap, such as in the case when the pump to signal wavelength detuning equals 0, the gain depends quadratically on the nonlinear phase-shift, and the signal and idler experiences quadratic gain.

$$G_{quad} \approx (2\gamma P_1 L_{eff})^2 \qquad \text{Equation 33}$$

Figure 20 shows how the conversion efficiency and the gain bandwidth of the idler increases with increasing pump power, whereas Figure 21 shows the pump power dependence of the signal gain. It can be seen that the gain on conversion bandwidth increases when the pump power increases. The higher the pump power is, the more distinct the two gain peak regions become. This shows the manifestations of phase matching acting on the gain. The dispersion dependent linear phase mismatch term better compensates the power induced nonlinear phase mismatch. At the two peak gain regions, exponential gain is obtained when the phase mismatch is close to zero.

The fiber dispersion properties play an important role in order to satisfy the phase matching condition, and hence impact the shape of the frequency dependent FOPA gain spectrum. Figure 22 shows the gain spectrum variation with respect to the sign and magnitude of fiber dispersion parameter.

Figure 23 shows the gain spectrum evolution as a function of highly nonlinear fiber length. At the two high gain regions symmetrically surrounding the pump, the signal gain builds up exponentially along propagation as described in Equation 32, whereas in the low gain region where the signal wavelength coincides with the pump wavelength, the gain increases slowly along propagation in a quadratic manner, as in Equation 33.

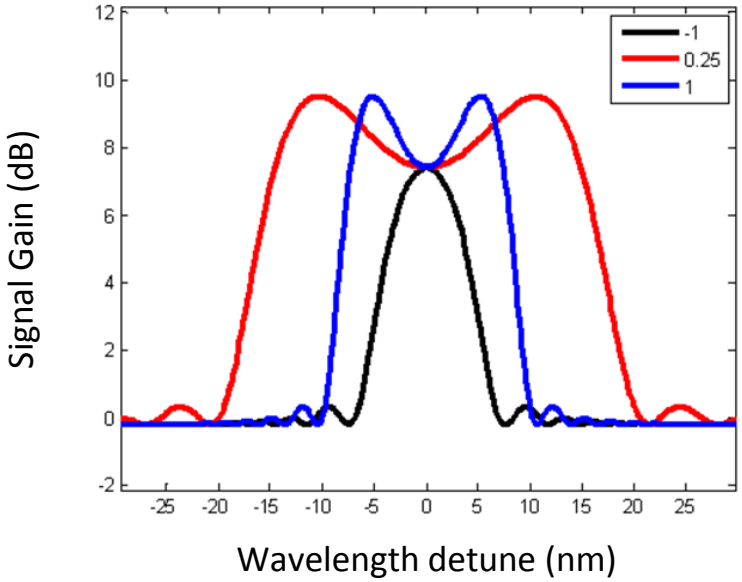

Figure 22 – Signal gain spectra as a function of signal to pump wavelength detuning of a single pump FOPA, for three different fiber dispersion values. Unit for the legend is in ps/(nm·km).

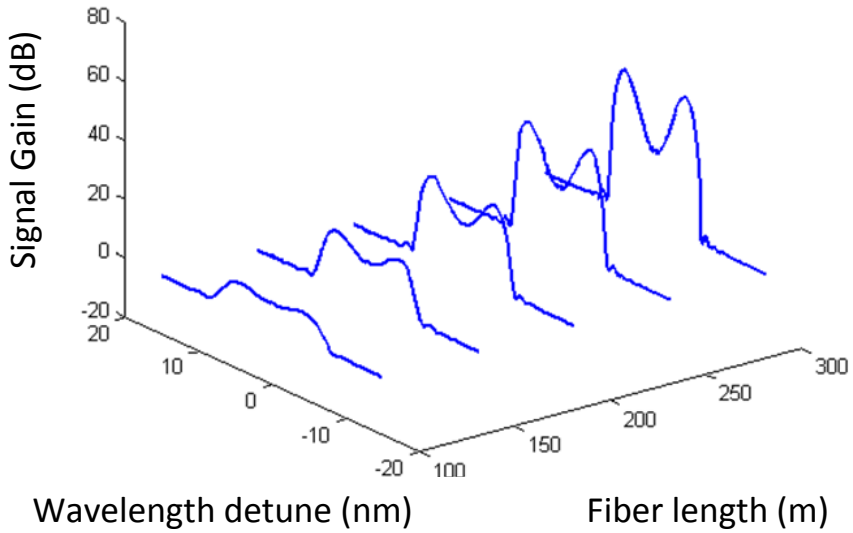

Figure 23 – Signal gain spectral evolution along the single pump OFPA HNLF length.

2.2.5 Dual-pump phase sensitive parametric amplification

As FWM is inherently sensitive to the phase of the interacting waves, FOPAs with correct configuration would offer not only phase-insensitive amplification (PIA) but also the important feature of phase-sensitive parametric amplification (PSA). This is one of the advantages OPAs have over conventional amplifiers that operate in the PIA regime, which includes erbium-doped fiber amplifiers (EDFAs), semiconductor optical amplifiers (SOAs), and Raman fiber amplifiers (RFAs). Ideally, PSA provides 6 dB more gain than PIA does [48]. And when implementing in phase sensitive mode, where an idler wave is also present at the amplifier input along with the signal and pump waves, the quantum-limited noise figure (NF) is 0 dB [49, 50]. This is a unique feature for PSA, as standard PIAs have a quantum limited noise figure of 3 dB.

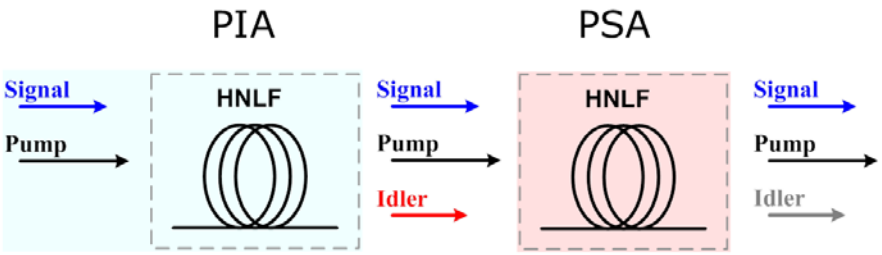

Figure 24 – Schematic of a PSA built with a two-stage structure. Coherent waves are generated from HNLF based PIA stage, which enables the phase sensitive interaction in the 2nd HNLF stage.

Four-wave mixing is a convenient way for phase coherent signal and idler generation. When phase coherent waves are provided at the input of the highly nonlinear fiber stage, phase sensitive amplification can be achieved. Figure 24 illustrates how such a phase sensitive amplifier can be built by deploying highly nonlinear fiber in a two-stage setup.

The relative phase among the interacting waves can be expressed as:

$$\varphi_{rel} = \varphi_{p1} + \varphi_{p2} - \varphi_s - \varphi_i \qquad \text{Equation 34}$$

In the single-pump case, φ_{rel} reduces to $2\varphi_{\mathrm{p}} - \varphi_{\mathrm{s}} - \varphi_{\mathrm{i}}$. However, the three frequency components can also be reconfigured by filtering and amplification, to form dual-pump degenerate-idler wavelength configuration, such as Figure 26 illustrates.

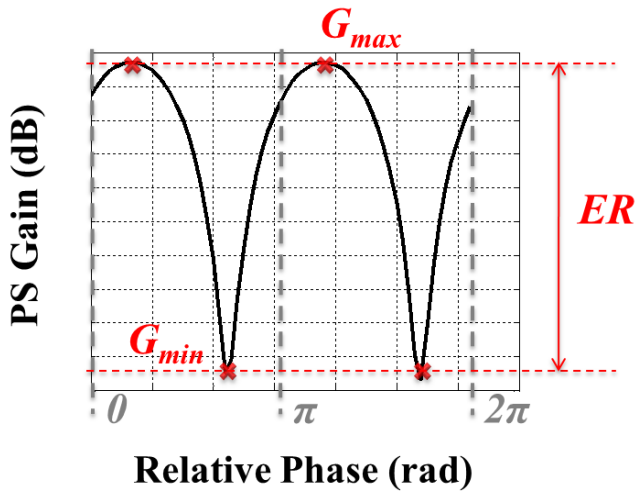

Figure 25 –Illustration of phase sensitive gain of the signal as a function of relative phase.

In the dual-pump case, the idler is degenerate in frequency with the signal, and the two pumps are placed symmetrically around the degenerate signal and idler. The interacting waves are phase coherent at the input of the highly nonlinear fiber based phase sensitive amplifier stage. Their relative phase relation is expressed as in Equation 34. If the relative phase is altered by i.e. sweeping the input signal phase, the signal output power varies accordingly in a sinusoidal fashion [51, 52], as shown in Figure 25. In this conceptual illustration, over a relative phase period of 2π, the signal experiences maximum amplification (G_{max}) when it is in phase with the pumps, and attenuation (G_{min}) when out of phase. The difference between maximum and minimum gain is defined as the phase sensitive extinction ratio.

In the design of a PSA for either amplification, regeneration or any signal processing purposes, it is important to have design guidelines targeting for maximum achievable performance. In what follows, numerical optimizations are carried out to explore optima in terms of phase sensitive gain and extinction ratio values.

3 Optimization of phase sensitive gain and extinction

Phase sensitive amplifiers (PSAs) among fiber-optic parametric amplifiers (FOPAs) rely on the nonlinear four-wave mixing (FWM) process to provide optical gain to one quadrature of the light signal while deamplifying the other. The ultrafast nature of PSAs enables various signal processing applications, including simultaneous phase- and amplitude-regeneration [22-25] and ultra-low noise amplification [48]. To achieve the performance feature for most of the PSA applications, it is desirable to design PSAs that could provide a high phase sensitive gain and a large phase sensitive extinction ratio.

Even though a number of impressive demonstrations of PSAs using a dual-pump degenerate-idler configuration have been reported over the past few years [13-19], a systematic optimization of the operating point of such amplifiers is still missing. Proper countermeasures against practical limitation such as stimulated Brillouin scattering (SBS) are instrumental for sustaining pump power efficiency and for achieving phase sensitive amplification. Since artificial linewidth broadening of the pumps through phase dithering is counter-productive, the best work-around so far is to use high-SBS threshold highly nonlinear fibers (HNLFs) [41]. In this investigation, performance optimization of PSAs based on widely used standard HNLFs (Std-HNLFs), and on novel high-SBS threshold aluminum-doped HNLFs (Al-HNLFs) are carried out. In particular, the PSA performance with respect to pump power and fiber length are explored, the existence of optimum points of operation are discovered, and the origin of their existence are discussed.

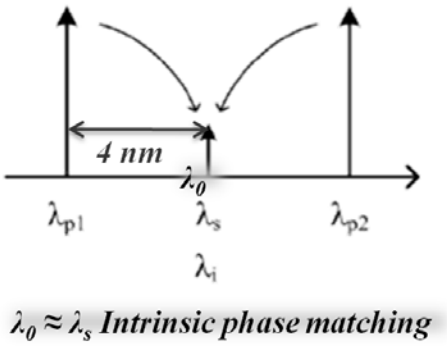

Figure 26 – Wavelength configuration of a PSA in a dual-pump degenerate idler configuration.

3.1 Investigation of dual-pump degenerate idler PSA

The wavelength configuration of the dual-pump degenerate-idler PSAs considered in this work is shown schematically in Figure 26. Here the frequency of the idler coincides with that of the signal, which is surrounded symmetrically by the two pumps.

Provided a pair of phase-coherent pumps, in this case generated via four-wave mixing in an earlier stage, the phase-coherent signal will experience maximum amplification (G_{max}) or deamplification (G_{min}) depending on its phase relation $\varphi_{rel} = \varphi_{p1} + \varphi_{p2} - 2\varphi_s$ with the pumps, as shown in Figure 25 (right). The phase sensitive (PS) extinction ratio is defined as $ER = G_{max}/G_{min}$. In what follows the phase sensitive maximum gain and extinction ratio are optimized numerically with respect to pump power and HNLF length.

3.2 Simulation verification of the existence of optima

The propagation of continuous wave pumps and signals in the HNLF is numerically simulated by solving the nonlinear Schrödinger equation using the split-step Fourier method. Fiber parameters are briefly listed in Table 4. The dispersion slope (S), nonlinear coefficient (γ) and fiber loss (α) are 0.011 $ps/(nm^2km)$, 7.4 $W^{-1}km^{-1}$ and 15 dB/km for the Al-HNLF, and 0.0185 $ps/(nm^2km)$, 10.8 $W^{-1}km^{-1}$ and 0.8 dB/km for the Std-HNLF [41]. The zero-dispersion wavelength (ZDWL, λ_0) of the two considered HNLFs is identical at 1559.9 nm. The wavelength of the signal (λ_s) and the two pumps (λ_{p1} and λ_{p2}) are 1560, 1556, and 1564 nm, respectively. λ_s is placed close to λ_0 to benefit from intrinsic phase-matching near the fiber ZDWL. The pump wavelength detuning from the signal is 4 nm, and this small wavelength spacing can keep the linear phase mismatch to be relatively low. The input signal power is set to a value of -7 dBm in order to operate in the unsaturated regime.

		Std-HNLF	Al-HNLF
Dispersion slope (S)	$ps/(nm^2 \cdot km)$	0.0185	0.011
Nonlinear coefficient (γ)	$W^{-1} \cdot km^{-1}$	10.8	7.4
Fiber loss	dB/km	0.8	15
A_{eff}	μm^2	11.6	13.5

Table 4 – Overview of fiber parameters used in the simulations.

Summaries of how the phase sensitive signal gain and extinction evolve as a function of fiber length (L) and total pump power level (P_0) are shown in Figure 27, for both types of HNLFs. The white curves across the left plots in Figure 27 (a) and (c), indicate the power margin set by the SBS threshold, which limits the amount of power that can be launched into the fiber according to the widely used definition $P_{th} = 21\,A_{eff}/g_B L_{eff}$ [45], where $L_{eff} = (1 - e^{-\alpha L})/\alpha$ is the fiber effective length, α is the fiber loss, A_{eff} is the effective area and g_B is the Brillouin gain coefficient. The A_{eff} values were 13.5 and 11.6 μm^2 for the Al- and Std-HNLF, respectively, while g_B was 2.3×10^{-11} m/W for the Std-HNLF [53] and 7 dB lower for the Al-HNLF [41]. For the Std-HNLF the fiber lengths and pump powers that provide gain are actually above the SBS threshold and the threshold curve consequently does not appear in Figure 27 (b) and (d).

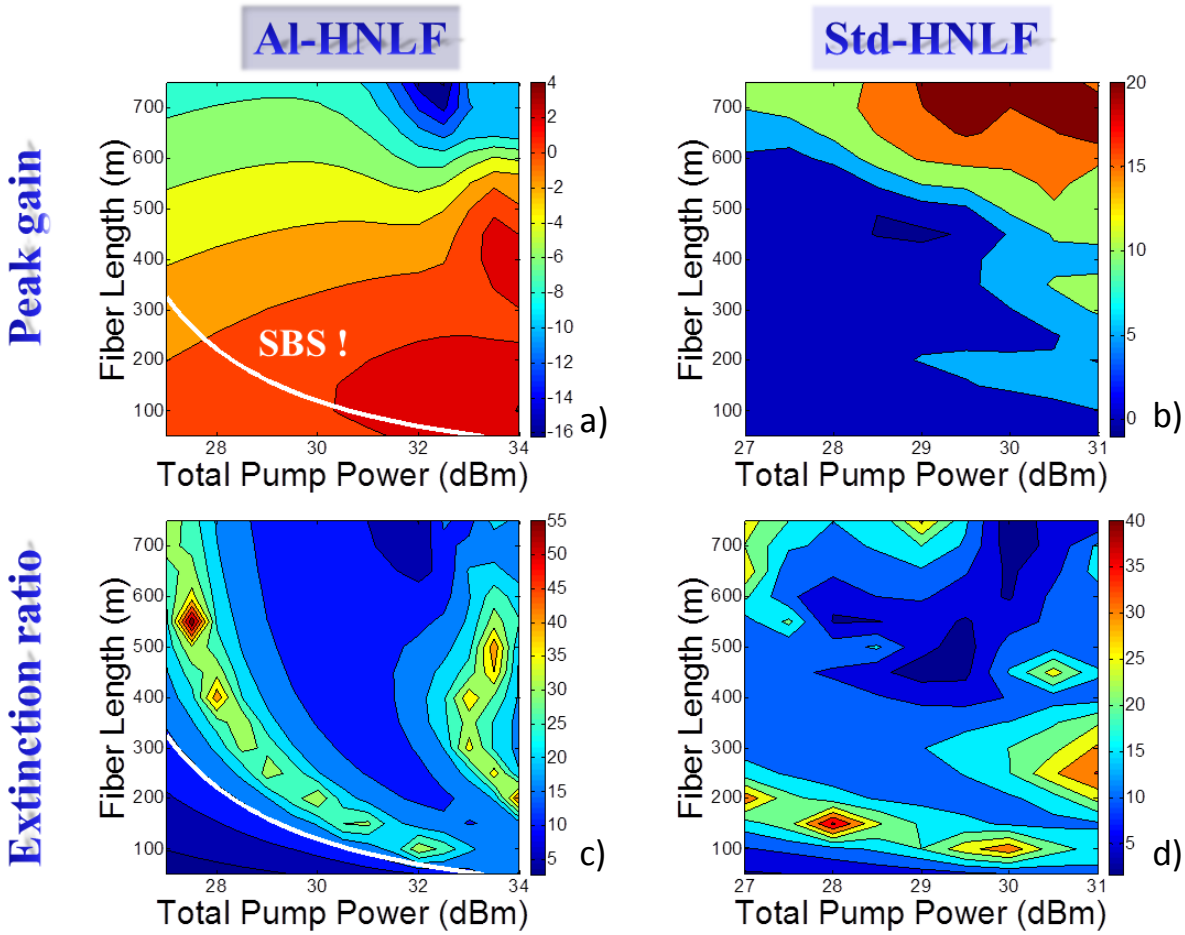

Figure 27 – Maximum phase-sensitive gain (in dB) of a) Al-HNLF and b) Std-HNLF, as well as phase-sensitive extinction ratio of c) Al-HNLF and d) Std-HNLF as a function of fiber length and total pump power. The white line indicates the SBS threshold limit. Color bar unit is in dB.

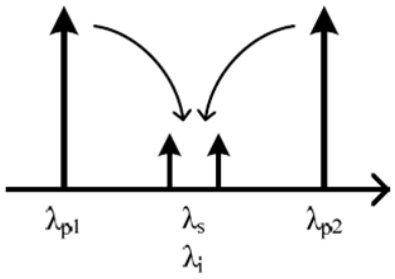

Figure 28 – Wavelength configuration of the dual-pump PSA with lifted degeneracy between signal and idler.

It can be seen in Figure 27 that the Std-HNLF can provide higher PS gain than the Al-HNLF (G_{max} of 20 dB compared to 4 dB in the best cases), mainly due to its higher γ and lower loss. However, the gain region is only reached beyond the SBS threshold for the Std-HNLF. Increasing L in the case of Al-HNLF does not result in higher PS gain due to its high loss. On the other hand, the Al-HNLF is able to provide 15 dB more PS extinction than the Std-HNLF at the optimum points of operation. However, an important conclusion of our work is that the optimum extinction areas are still located beyond the SBS threshold curve for the Al-HNLF. Further improvement in tailoring the SBS properties of the HNLFs would be required in order to exploit the areas of maximum extinction.

In order to understand the existence of PS extinction optima, implying minima of G_{min}, we have lifted the degeneracy between signal and idler by tuning the signal 0.5 nm away from the mid-pump frequency as illustrated in Figure 28.

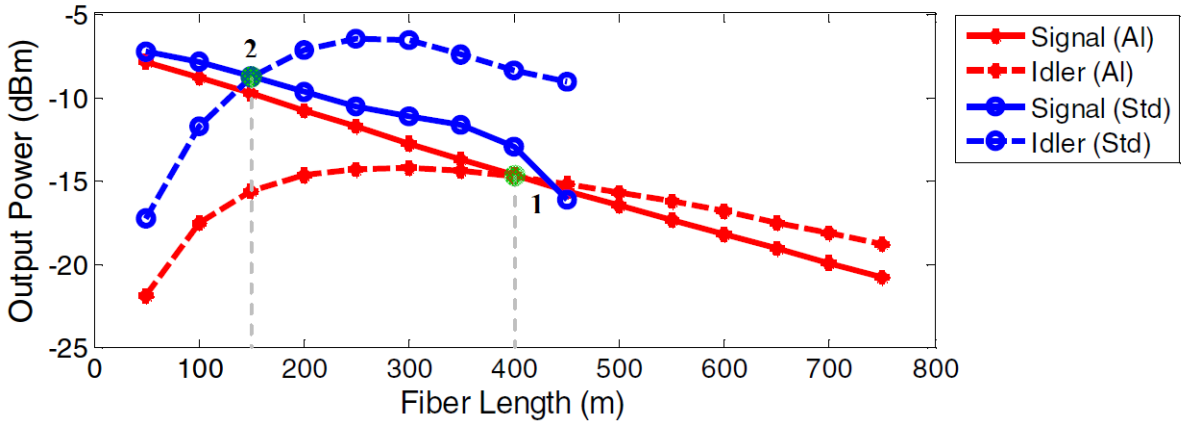

Figure 29 – Evolution of signal and idler power along the fiber length for a total pump power of 28 dBm for Al- and Std-HNLFs.

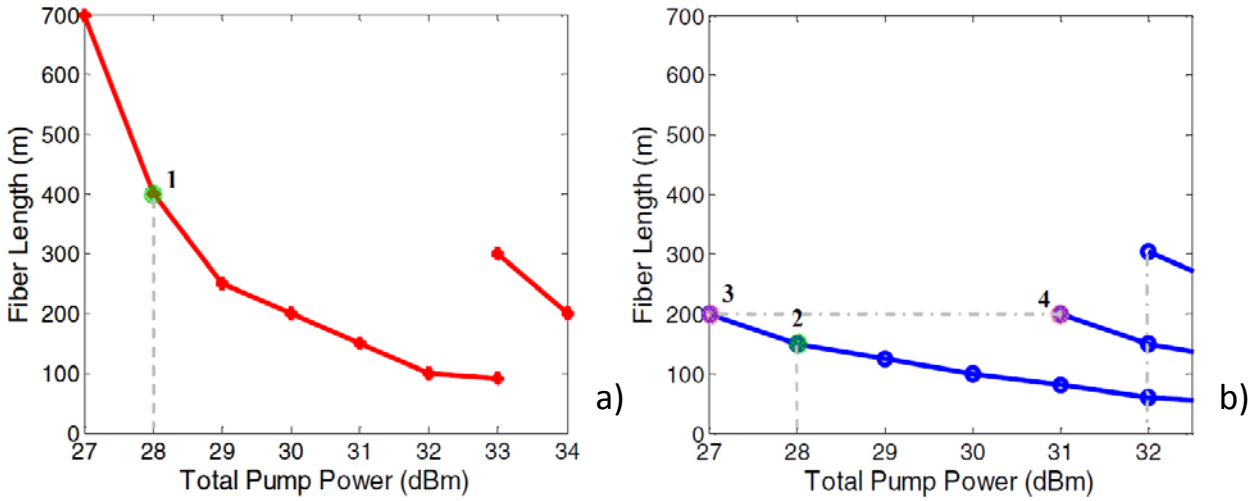

Figure 30 – Fiber length at which the signal and idler power are equal for a) Al-HNLF, and b) Std-HNLF.

Figure 29 shows how the power of the signal and the idler evolve along propagation at a specific P_0 level for both types of HNLFs. The fiber lengths corresponding to cross-over points between the signal and idler power have been extracted from graphs like Figure 29 for different P_0 and represented in Figure 30. It is clear that the curves in Figure 30 match the areas of optimum PS extinction in Figure 27. A comparison of the two sets of results is plotted on top of each other and is shown in Figure 32. If furthermore the phases of the signal and idler are examined, it can be shown that the phase differences between signal and idler along the curves in Figure 30 are equal to π, which accounts for the destructive interference leading to a low value of G_{min} and consequently a high PS extinction ratio.

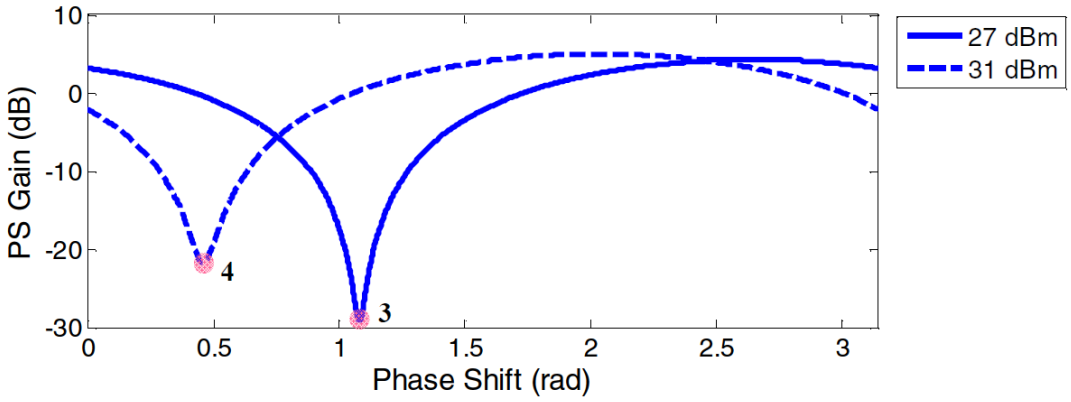

Figure 31 – Phase-sensitive gain in the case of Std-HNLF for a fixed fiber length of 200 m and total pump power of 27 and 31 dBm.

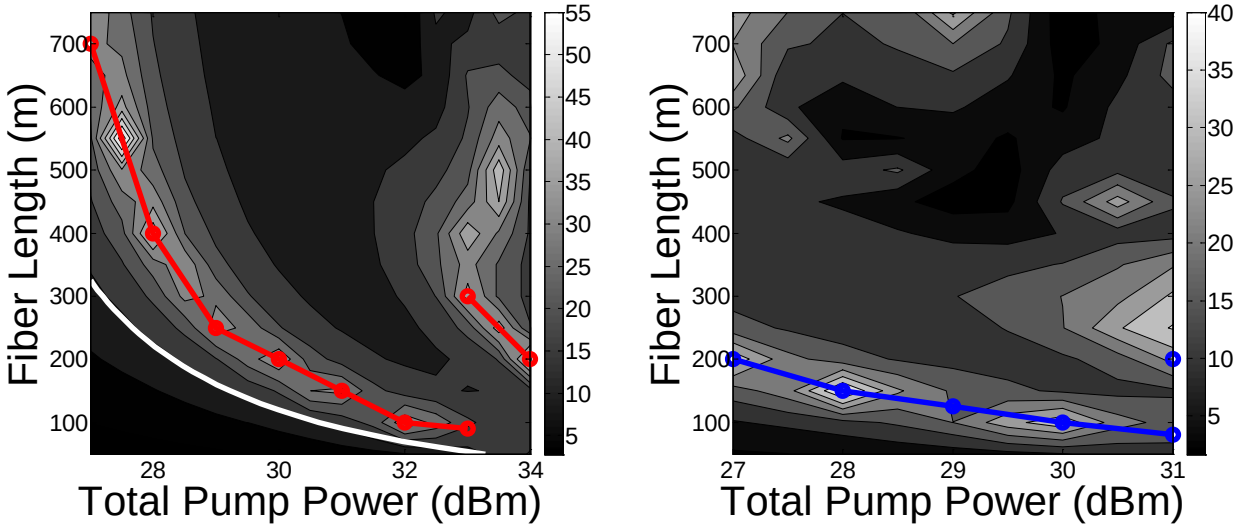

Figure 32 – The optimum phase-sensitive extinction ratio points obtained when the signal idler degeneracy is lifted shown to be in good agreement with the absolute degenerate case. The impact of interference when the signal and idler power become comparative is the cause for optimum extinction ratio to exist.

It can also be observed from Figure 30 that maximum PS extinction can occur for different combinations of fiber length and pump power. This point is illustrated in *Figure 31* where PS gain curves are represented for two P_0 values for a fiber length of 200 m, corresponding to the points labeled 3) and 4) in the optimum PS curves of Figure 30 (b). Moving from one optimum curve to the other would result in significant nonlinearity induced phase shift. Consequently a joint control and tracking of the pump power and phase shift would be necessary in practice to ensure operation at the optimum extinction point.

3.3 Summary – optima achievable once SBS is circumvented

In summary, we have performed a systematic optimization of the PS gain and extinction ratio of dual-pump degenerate-idler PSAs making use of both Std-HNLFs and Al-HNLFs. The existence of desirable extinction ratio optima can be accounted for by considering the interference between the signal and the degenerate idler. Lifting the degeneracy enables to predict the position of these optima in the pump power-fiber length space.

4 Regeneration of phase encoded signal in an optical link

In an optical transmission system, in order to achieve high spectral efficiency to fully utilize the available optical bandwidth, advanced modulation formats, such as phase shift keying are commonly adopted. In contrast to the intensity modulated on-off keying signals, phase shift keying signals carry information on the optical phase. In a typical all-optical communications link, link impairments lead to degradation of signal quality along propagation. All-optical regeneration of phase-shift keying (PSK) signals is desired and can be achieved by exploiting the phase squeezing capability of phase sensitive amplifiers (PSAs) utilizing parametric processes in optical fibers [13].

Due to the inherent phase sensitive nature of the gain, the phase regeneration of such signals is often performed at the expense of phase-to-intensity (PM-to-IM) noise conversion, which also degrades the signal and makes it more prone to nonlinear phase noise further along the link. Combining a phase-regenerator with a phase-transparent intensity regenerator, could solve the problem, at the expense of increased complexity of the regenerator. Alternatively, simultaneous amplitude and phase regeneration has been suggested and demonstrated by operating PSAs in the saturated regime [2, 22, 54,]. However, such simultaneous regeneration puts some stringent requirements on the amount of phase noise that can be tolerated. Engineering a flat-top gain response while maintaining the desired two-level phase output of the PSA would relieve such a limitation.

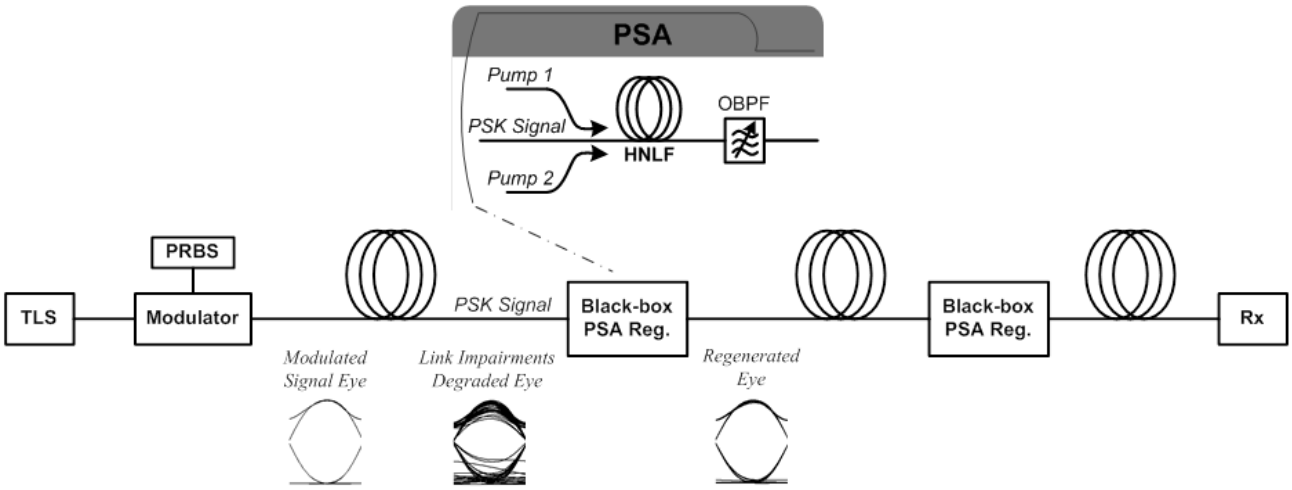

Figure 33 – Illustration of an all-optical communication link employing a phase sensitive regenerator for PSK signal regeneration.

In this investigation, we report a systematic numerical optimization of the gain and phase responses of dual-pump degenerate-idler PSAs with emphasis on the design of flat-top gain profiles that allow phase-regeneration without inducing excessive PM-to-IM noise conversion. We show that the design target can be reached by operating the PSA in moderate saturation together with proper dispersion engineering. The synthesized PSA response is further shown to result in enhanced phase noise tolerance compared to conventional designs.

4.1 Design of dual-pump PSA for phase regeneration

The dual-pump degenerate-idler PSAs investigated in this work are made from a standard HNLF up to 500 m long with zero dispersion wavelength chosen at 1550.39 nm and dispersion slope, nonlinear coefficient, and loss equal to 0.0185 $\mathrm{ps/(nm^2 \cdot km)}$, 10.8 $\mathrm{W^{-1} \cdot km^{-1}}$ and 0.9 $\mathrm{dB/km}$. The total pump power used is 31.5 dBm and the signal is set to 1560 nm with -10 dBm power. The propagation in the HNLF is numerically simulated by solving the nonlinear Schrödinger equation using the split-step Fourier method.

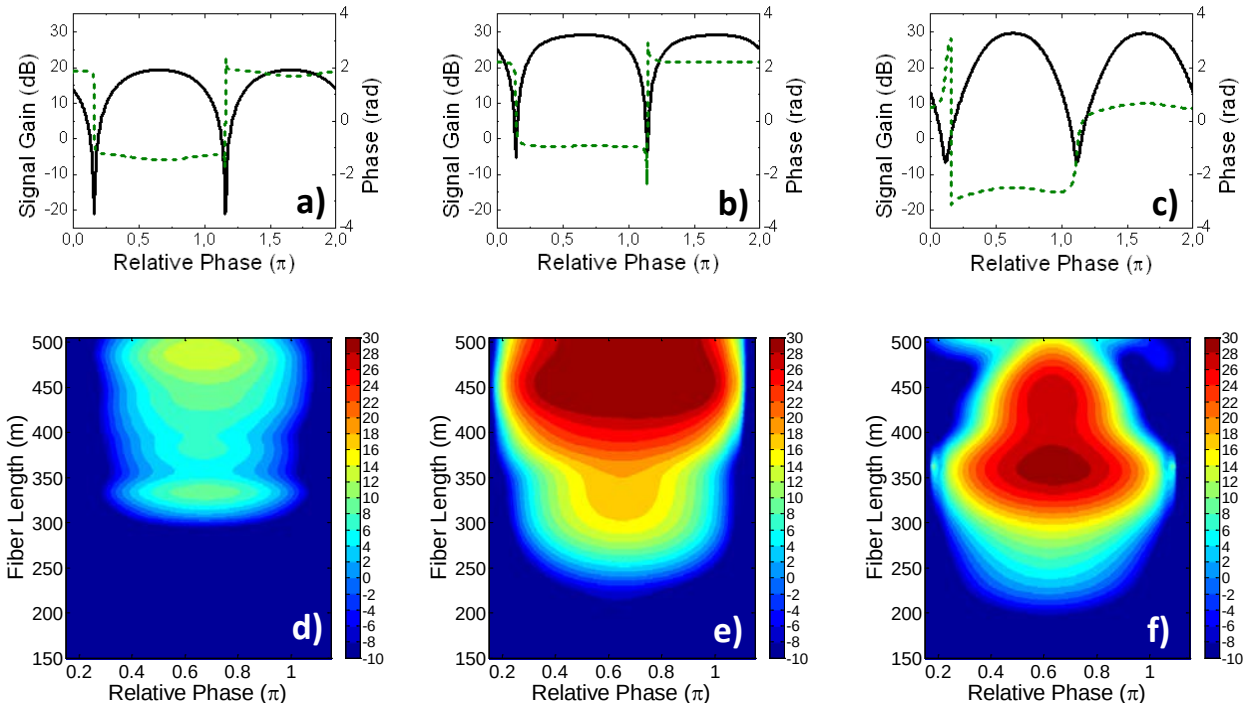

Figure 34 – Top: phase-sensitive gain and phase responses for 400 m HNLF; Bottom: phase sensitive gain (in dB) evolution as a function of fiber length for pump to signal wavelength detunings of 3 nm (a,d), 4.5 nm (b,e) and 5 nm (c,f).

It can be seen in Figure 34 (d-f) that, when the wavelength detuning between the pumps and the signal is set to 3, 4 and 4.5 nm, respectively, dramatic changes in the shape of the gain profile and its evolution as a function of distance in the HNLF occur. In particular, in the case of a wavelength detuning of 4.5 nm, a flat-top gain covering more than 0.7π is obtained, which is furthermore almost invariant with fiber length between 400 and 500 m. The desired two-level phase response is also obtained in this case, as shown for 400 m long HNLF in *Figure 34* (b). In contrast, results reported to date exhibit a narrow-top response such as the one obtained for 3 nm detuning.

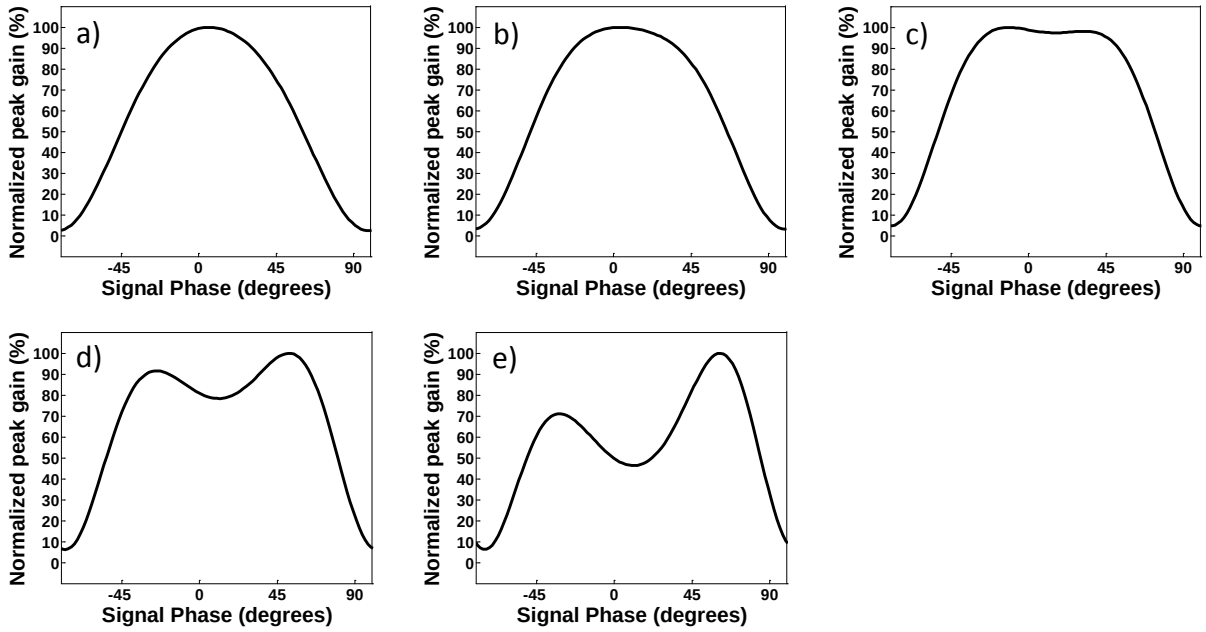

Figure 35 – Oscillatory peaks of the phase sensitive gain profile caused by saturation induced by increasing of signal power level in 2 dB steps from a) to e).

It should be pointed out that any deeper saturation would cause the gain curve to acquire a dip in its center portion [55] as shown in Figure 35 and at the same time distort the two-level phase function. Such distortions are responsible for insufficient amplitude and phase squeezing performances, and should be avoided in practical implementations for optimum regeneration.

The optimum wavelength detuning for achieving flat-top gain can be shown to increase as the fiber dispersion slope decreases. Consequently, our flat-top design relies on the exploitation of moderate saturation together with proper dispersion engineering, the latter being a new degree of freedom to be considered for the design of phase sensitive regenerators with low phase-to-intensity noise conversion.

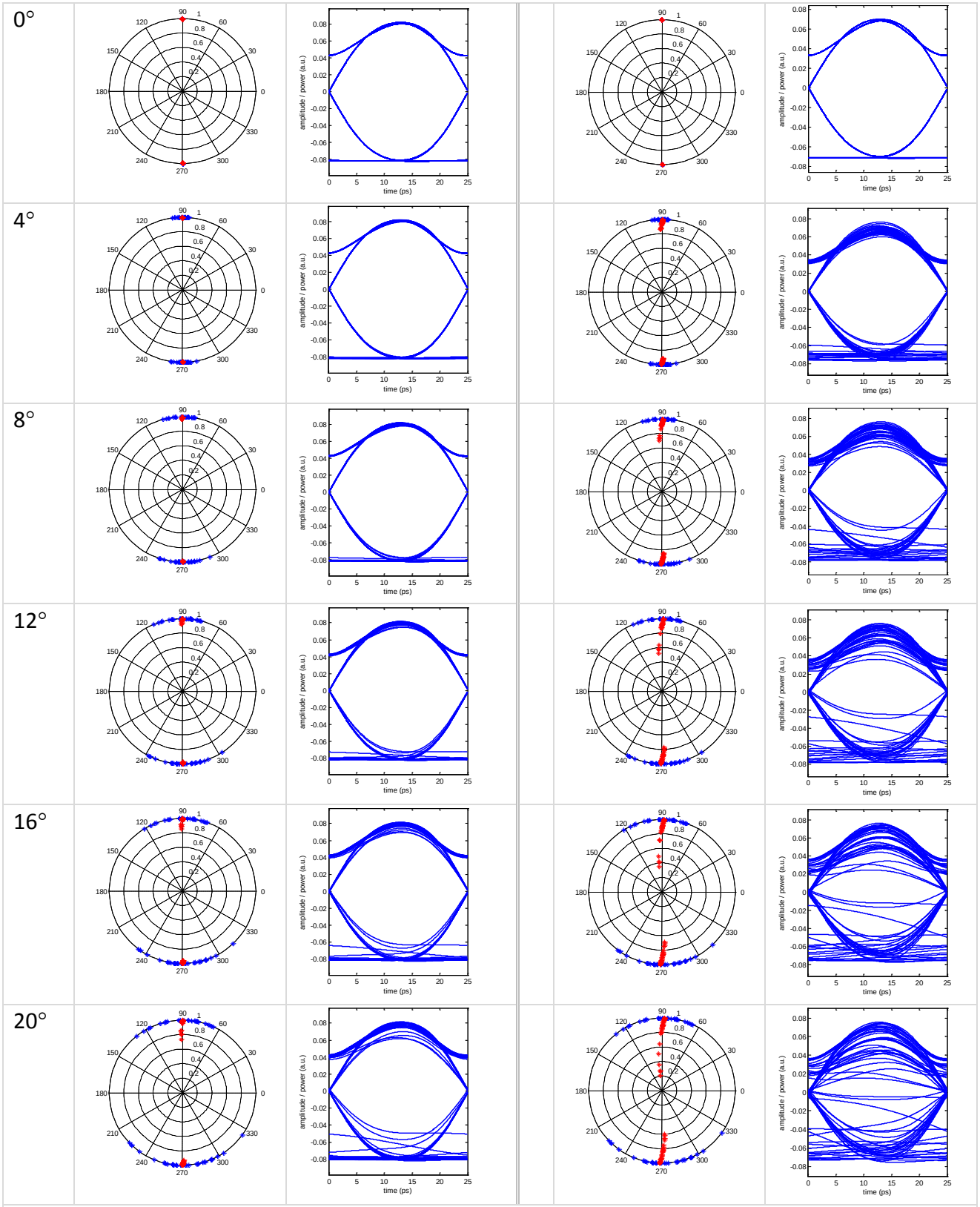

Figure 36 – Constellation- and eye-diagrams before and after (left) phase regeneration by a narrow-top, and (right) simultaneous amplitude and phase regeneration by the flat-top PSA for various phase noise standard deviation values.

4.2 Flat-top PSA designed with flat gain and phase profile

The regeneration properties of the 400 m long flat-top and narrow-top PSAs are then examined in a system context by simulating their impact on a 40 Gbit/s differential PSK signal. For this purpose white Gaussian phase noise (PN) is imposed to the signal prior to the PSA. Figure 36 shows how the constellation- and eye-diagrams evolve as a function of phase noise standard deviation. From the constellation diagrams, it can be seen that the phase-squeezing property of both narrow- and flat-top PSAs is achievable. However, regeneration carried out by narrow-top PSAs lead to significant phase noise to amplitude noise conversion. This can be observed in the eye diagrams as the multiple intensity levels superimposed on the graphs that leads to closed eyes at high phase noise standard deviation values.

Taking a closer look at the constellation diagram of Figure 37 (a) it can be seen that the regenerated outputs by a narrow-top PSA (circles) are phase-squeezed however at the expense of significant conversion to amplitude noise. In this example, the PN has a standard deviation of 10°. For the same PN amount, the flat-top PSA, on the contrary, shows simultaneous regeneration of both amplitude and phase noise without conversion to intensity noise, as shown in Figure 37 (b).

The optical signal-to-noise ratio (OSNR) penalty has also been assessed at different PN levels for a bit error ratio of 3.3×10^{-3}. As Figure 38 shows, the narrow-top PSA introduces a lot more OSNR penalty than the flat-top PSA at high PN levels, and the flat-top PSA improves the phase noise tolerance by a large range without introducing OSNR penalty, confirming the significantly enhanced phase noise margin of the flat-top PSA.

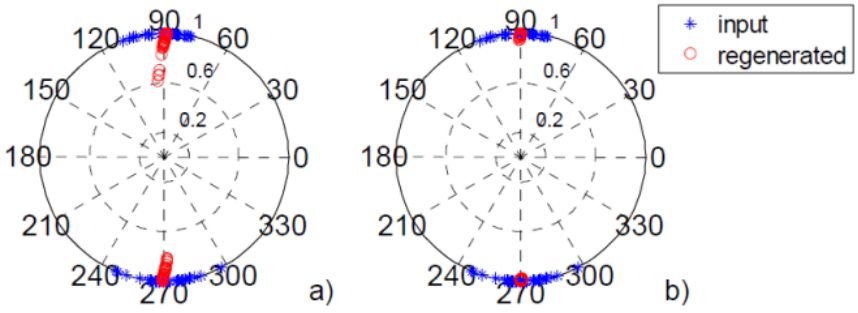

Figure 37 – Constellation diagrams before and after a) phase regeneration by a narrow-top, and b) simultaneous amplitude and phase regeneration by the flat-top PSA. The phase noise standard deviation is 10°.

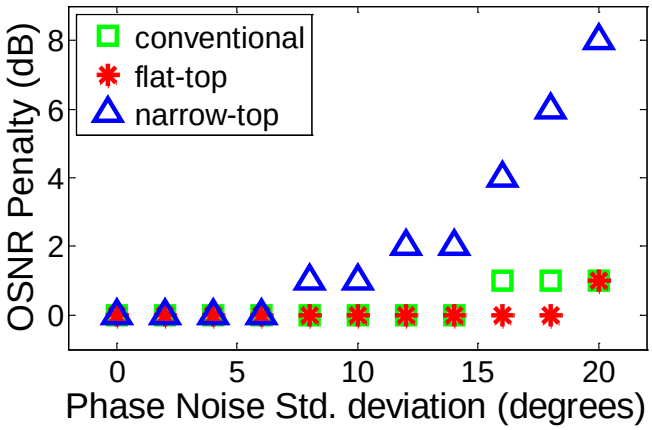

Figure 38 – OSNR penalty as a function of phase noise standard deviation for both narrow-top and flat-top PSAs.

4.3 Summary – flat-top PSA improves phase noise tolerance

In summary, flat-top PSA responses for simultaneous amplitude and phase noise squeezing have been numerically predicted under moderate saturation conditions through proper dispersion engineering. The enhanced phase noise margin of regenerators making use of the proposed PSA responses has also been confirmed, resulting in reduced OSNR penalty over a significantly broader phase noise range than conventional designs.

5 Silicon waveguide based PSA

5.1 Phase sensitive processes in Si-WG

Silicon-on-insulator (SOI) waveguides have been successfully employed to demonstrate a wide range of optical processing functionalities exploiting parametric processes, including amplification and wavelength conversion [56], regeneration [57], as well as Tbit/s signal processing [58]. The waveguide dimensions play a key role in tailoring the nonlinearity, dispersion and surface roughness-induced loss, and therefore in maximizing the conversion efficiency and bandwidth of silicon parametric devices. The strong confinement of SOI nanowires, induced by their high refractive index contrast resulting in sub-μm^2 effective areas, associated with a Kerr nonlinear index two orders of magnitude higher than in silica fibers result in efficient nonlinear interactions over (sub-)mm length scales.

Phase-sensitive parametric processes have recently been the object of a renewed interest, resulting in the demonstration of novel signal processing applications such as phase regeneration [22]. Most applications have been so-far demonstrated using highly nonlinear fibers as the nonlinear medium, where tremendous efforts have been dedicated to the development of stimulated Brillouin scattering mitigation techniques that preserve the phase coherence between the waves involved in the parametric process. Alternatively, phase-sensitive signal processing functionalities have also been demonstrated in semiconductor optical amplifiers [59] and in periodically-poled lithium-niobate waveguides [60]. Being able to realize phase-sensitive processing in SOI waveguides would allow a wealth of new applications on this versatile platform. However, apart from a recent numerical study [61], this option has, to the best of our knowledge, not been explored so far.

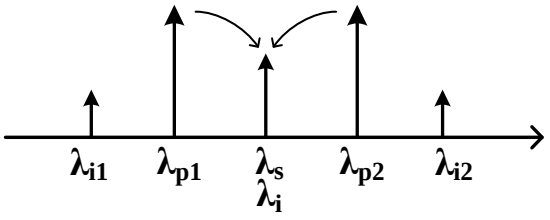

Figure 39 – Wavelength configuration for measuring the phase sensitive processes in a nano-engineered silicon waveguide.

In this chapter, we demonstrate experimentally phase-sensitive parametric processes in a nano-engineered silicon waveguide for the first time. Phase-sensitivity of the signal and higher-order idlers in a dual-pump degenerate-idler scheme is demonstrated. Furthermore, a numerical optimization of the process towards higher peak gain and larger extinction ratio is carried out. Paths towards enhanced phase-sensitive extinction ratio under the presence of both two-photon absorption and the induced free carrier absorption are highlighted.

5.2 Experimental measurement of PS-processes in Si-WG

The experimental setup is shown in Figure 40. Phase coherent waves are generated from a frequency comb obtained by phase modulation of a continuous wave (CW) external cavity laser with a 40 GHz radio frequency signal. A wavelength selective switch (WSS) is then used to select the two pumps and the signal from the frequency comb and to adjust the pump-to-signal power ratio as well as to vary the signal phase. The interacting waves are in the dual-pump degenerate-idler configuration, the signal being located at the center frequency between the pumps. The dual-pumps and phase-shifted signal are then amplified by an erbium-doped fiber amplifier (EDFA). A polarization beam splitter (PBS) is used in combination with polarization controllers (PCs) to align the waves to either the TE or TM mode of the waveguide. The resulting phase-sensitive gain and extinction ratio of the signal and higher-order idlers (at λ_{i1} and λ_{i2}), as shown in Figure 39, are then measured by an optical spectrum analyzer (OSA).

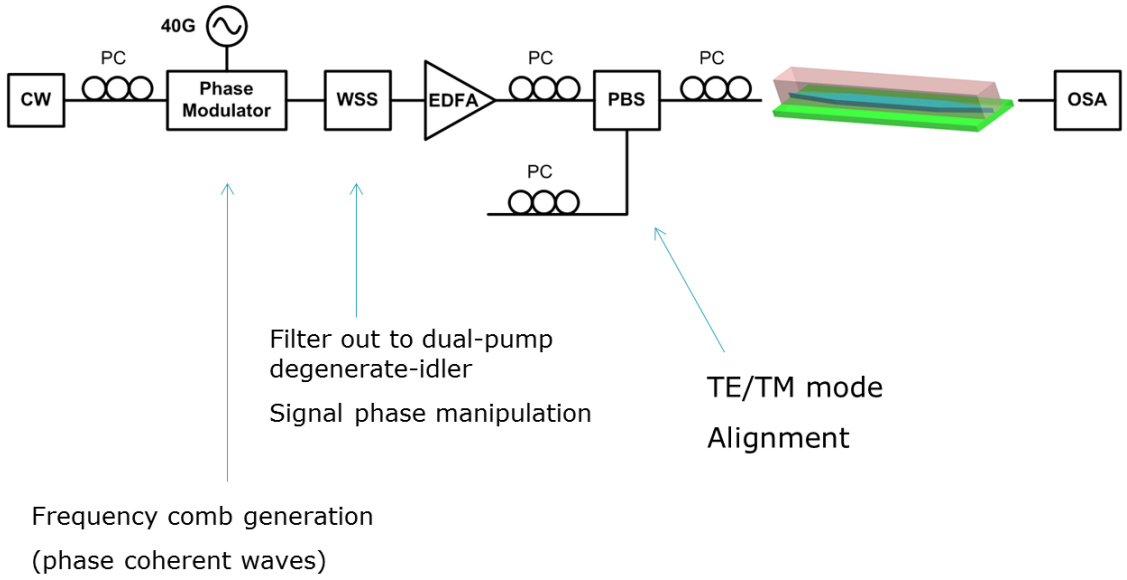

Figure 40 – Experimental setup for measuring the phase sensitive processes in a nano-engineered silicon waveguide.

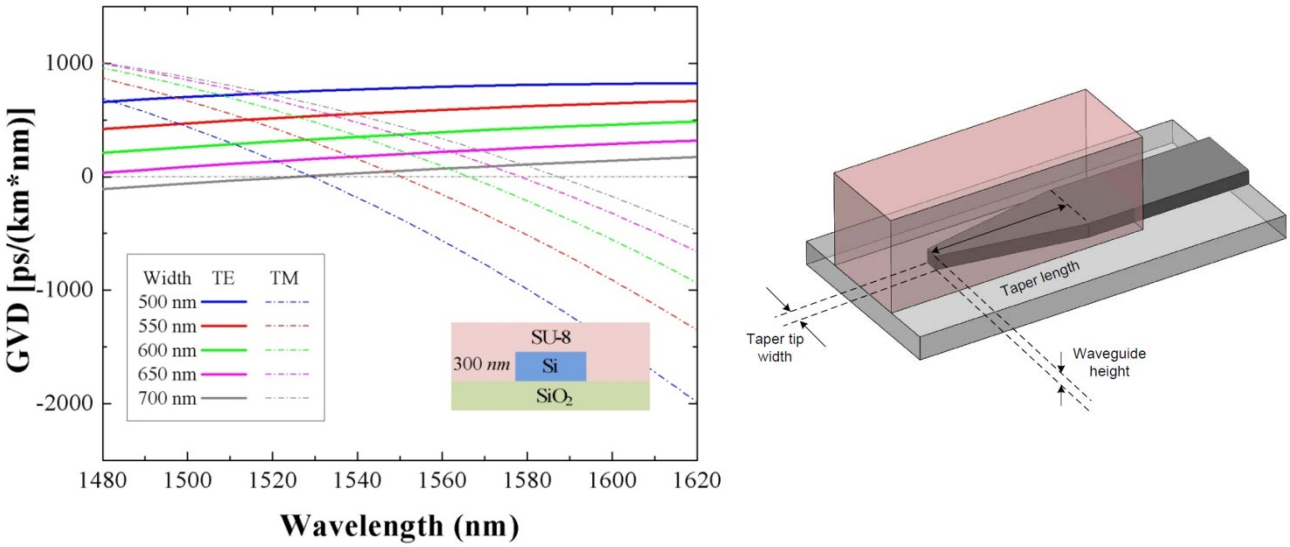

*Figure 41 – (a) Dispersion profile characterized for the TE and TM mode of the silicon nanowires under investigation, and (b) schematic drawing of the inverse taper coupler [*63*].*

The nano-engineered silicon waveguide under test is 16.3 mm long. It is designed to have embedded taper structures on its two output ends (length 300 μm) to minimize coupling loss to tapered fibers to less than 2 dB per facet. The tapered structure is graphically illustrated in Figure 40. The propagation loss of the waveguide is 5.1 dB/cm. The cross section of the waveguide is illustrated and shown as an inset in Figure 41. The height of the waveguide is 300 nm. And the waveguide used in this experiment has a width of 650 nm. Figure 41 shows the dispersion of the TE and TM mode of the waveguides as a function of waveguide width. For the waveguide under test, dispersion of the waveguide is engineered to be equally close to zero at 1560 nm for both the TE and the TM modes. The signal wave is tuned to this wavelength with the dual pump symmetrically surrounding it.

The powers of the signal and the idlers at λ_{i1} and λ_{i2} at the waveguide output are represented as a function of the signal input phase in Figure 42 when the pump-to-signal power ratio at the waveguide input was set to 10 dB with a total input power of 15 dBm injected into the waveguide. A distinctive phase-sensitive power curve can be clearly seen for both signal and idlers. However the signal extinction ratio is limited to about half a dB. In contrast, the extinction ratios of the higher-order idlers reach up to 9 dB. In what follows, the magnitude of this phase sensitivity will be analyzed theoretically and paths to enhance the gain and extinction ratio will be defined.

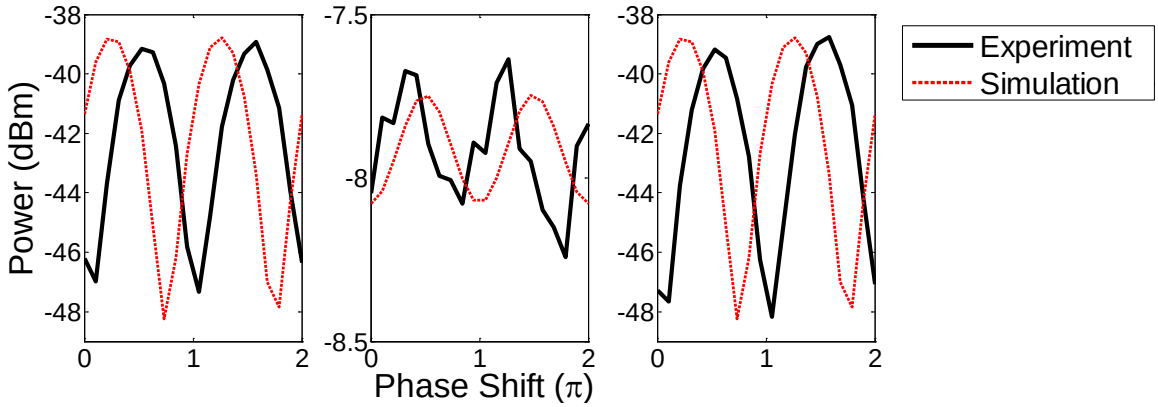

Figure 42 – Experimentally measured phase sensitive curves of a) idler at the shorter wavelength λ_{i1}, b) signal, and c) idler at the longer wavelength λ_{i2}, matched to numerical simulation, with agreement in peak gain level and extinction ratio.

To further estimate how much phase sensitive gain and extinction ratio such a waveguide could ultimately deliver, an extended simulation is carried out using the experimental waveguide parameters.

5.3 Numerical optimization on the impact of TPA and FCA

Wave propagation in the silicon waveguide is simulated by numerically solving the nonlinear Schrödinger equation using the split-step Fourier method. The numerical model includes terms for both two-photon absorption (TPA) and free-carrier generation [62]. The red dashed lines in Figure 42 show the numerical result matched to the experimentally measured curves. With the provided waveguide dimension, the effective area is calculated to be 0.16 μm^2, and the nonlinear parameter γ is found to be 152 $W^{-1}m^{-1}$. The phase sensitive extinction of the idlers is calculated to approximately 9.5 dB, and the signal extinction ratio is found around 0.5 dB, in good agreement with the experiment.

It is obvious that one needs to further enhance the signal extinction ratio to make it possible to utilize such Si-based phase sensitive processes for desired applications such as amplitude and phase regeneration. In Figure 43 we show the simulation optimization result in three cases: 1) with the numerical model including both two-photon and free-carrier absorption (FCA), modeled using two different carrier lifetimes: 10 ns as estimated in our waveguide, as well as reduced down to 1 ns as would be obtained if the generated carriers were swept away, for instance using a PIN junction; 2) with the two-photon absorption effect only, without free-carrier generation term; and 3) an ideal case without either types of nonlinear absorption.

The dynamics behind light-matter interaction in silicon can be briefly described as the following. The optical field propagating through a silicon waveguide can generate free-carriers due to the TPA process, as long as the photon energy is greater than half the bandgap energy of silicon. These free-carriers oscillate with the electric field and contribute to the overall polarization. The free carrier induced polarization contributes to the nonlinear polarization as $\mathrm{P^f}$

$$\mathrm{P_{NL}} = \mathrm{P^{(3)}} + \mathrm{P^f} \qquad \text{Equation 35}$$

$\mathrm{P^f}$ is proportional to the carrier density $N(t)$, and the dynamics of the carrier density is

$$\frac{\partial}{\partial t}N(t) = G(t) - \frac{N(t)}{\tau_0} \qquad \text{Equation 36}$$

where G is the carrier generation rate, and τ_0 is the effective carrier lifetime that includes the effects of recombination, drift and thermal diffusion. Under the presence of TPA induced free carriers, the Kerr and TPA coefficient are defined as

$$n = n_0 + n_2 I, \qquad \alpha = \alpha_0 + \beta_T I \qquad \text{Equation 37}$$

where n and α are the optical intensity dependent refractive index and net absorption, β_T is the TPA parameter (cm/GW) [64]. With the presence of two-photon absorption and free-carrier absorption, the NLSE takes the following form, with linear terms to the left hand side of the equation, and the nonlinear terms to the right:

$$\frac{\partial A}{\partial z} + \frac{i\beta_2}{2}\frac{\partial^2 A}{\partial t^2} - \frac{\beta_3}{6}\frac{\partial^3 \mathrm{A}}{\partial \mathrm{t}^3} + \frac{\alpha}{2}A = i\beta^f A + \frac{1+\rho}{2}\left(\gamma + \frac{i\beta_T}{2A_{eff}}\right)|A|^2 A \qquad \text{Equation 38}$$

Two photon absorption

Nonlinear anisotropy

Free carrier absorption

In the propagation equation, the TPA coefficient contributes as intensity dependent nonlinear loss term.

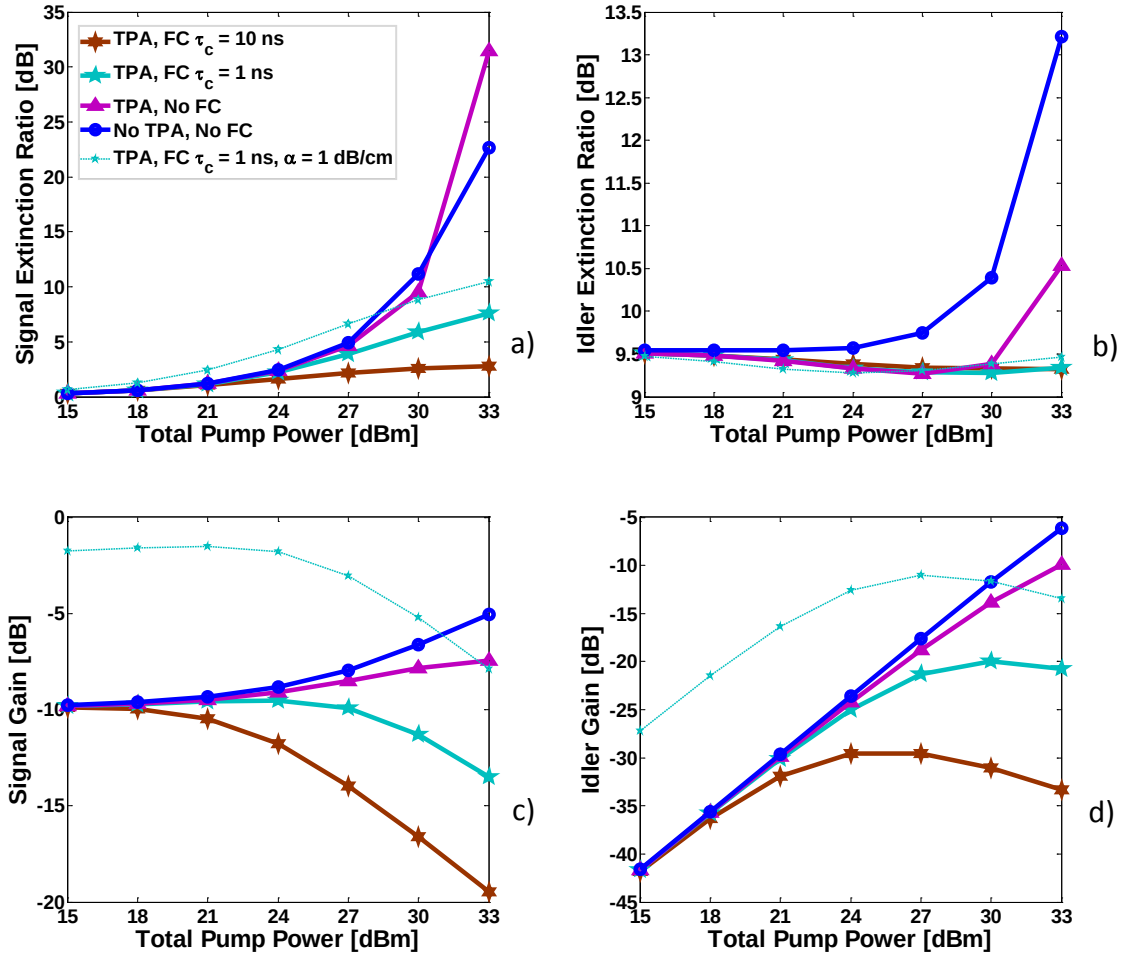

Figure 43 – Phase sensitive gain and extinction ratio optimization of the signal and idlers. Dashed-thin lines correspond to cases when the waveguide propagation loss is reduced from 5.1 dB/cm to 1 dB/cm.

The signal and idler gain and corresponding extinction ratio evolution as a function of total pump power are shown in the graphs of Figure 43. When the two-photon absorption-induced free-carrier absorption has a long carrier lifetime (10 ns), the signal extinction ratio saturates at high pump power level. Due to free-carrier absorption, the signal gain drops drastically with increasing pump power. Using a reduced carrier lifetime equals to 1 ns, the saturation in signal extinction ratio and the drop in gain are relaxed. In this case, a 5 dB higher extinction can be achieved by using 33 dBm total pump power. Another 3 dB improvement in signal extinction ratio can be obtained by reducing the waveguide propagation loss down to a realistic value of 1 dB/cm from the current 5.1 dB/cm.

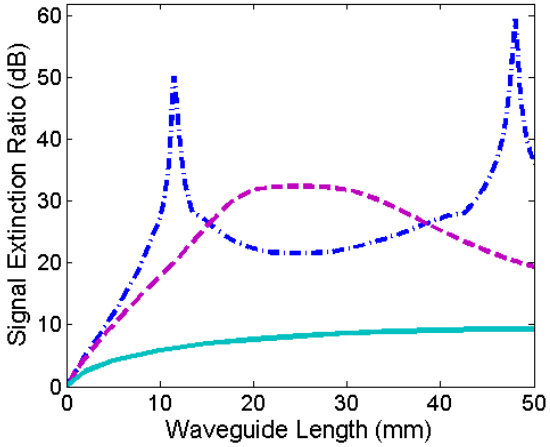

Figure 44 – Phase sensitive signal extinction ratio as a function of silicon waveguide length. Solid-line: TPA and FC lifetime 1 ns; dashed-line: TPA only; dotted-dashed: without TPA and FC. Total pump power is 33 dBm.

Considering the case with two-photon absorption and without free-carrier generation, the signal extinction for this specific waveguide is predicted to be up to 30 dB at 33 dBm total pump power. With the current waveguide length, this value is even ~10 dB higher than in the case where neither two-photon nor free-carrier absorption occur. The origin behind this can be seen from Figure 44, where the signal extinction ratio is plotted as a function of waveguide length, with a total pump power equal to 33 dBm. In the ideal case without either types of nonlinear absorption, a maximum extinction ratio is obtained in a periodic manner. With the presence of two-photon absorption, the signal extinction ratio exceeds the ideal case for a certain range of waveguide lengths at high pump power levels.

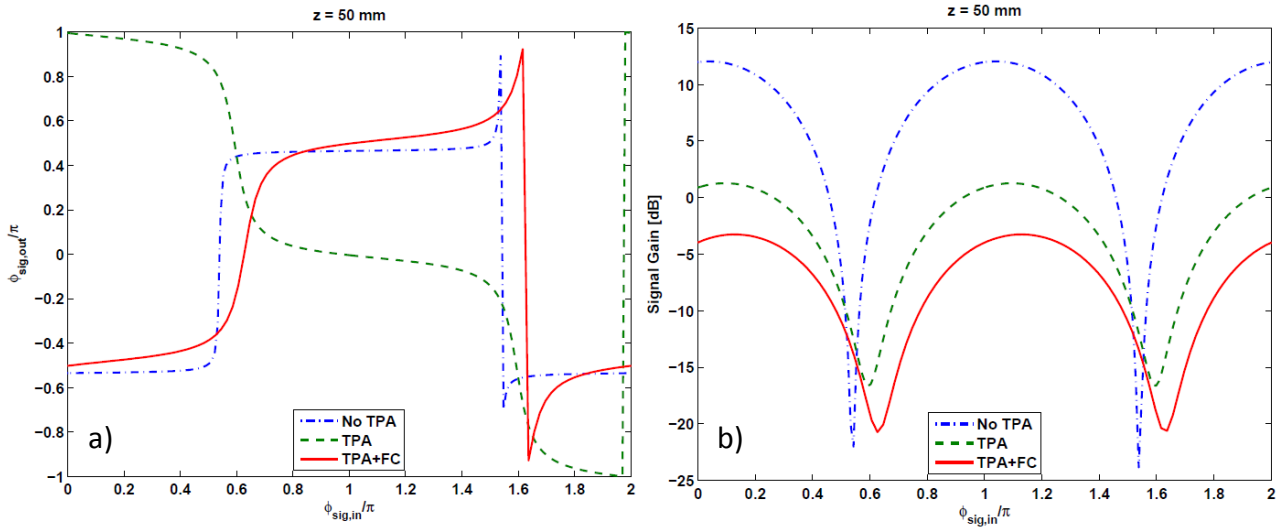

Figure 45 – Impact of TPA and free carriers on (a) the input-output phase relation and (b) the phase sensitive gain [64].

The effect of free carriers does not impact the shape of the signal gain curve, but simply offsets the whole gain profile down with the loss it introduced. However, the sharp step transition of the two level phase response gets smoothened when TPA induced FCA is taking place [64].

5.4 Summary – desired PS-gain and extinction exists in Si-WG

In summary, phase sensitive parametric processes are experimentally measured in a nano-engineered silicon waveguide, and numerically matched. A numerical optimization predicts room for improvement in achieving larger signal phase sensitive extinction ratio for potential applications such as chip-based signal phase and amplitude regeneration. The design of waveguides with reduced propagation loss and reduced carrier lifetime is desired to enable the predicted performance and relevant nonlinear functionalities.

6 Dispersion tolerance of PSAs as inline amplifier

In this investigation, simulations are carried out to study how dual-pump degenerate-idler PSAs work as inline amplifier in a transmission link, where signal is primarily prone to linear transmission impairments such as dispersion. We demonstrate how the phase sensitive gain transfer function varies when the input signal quality is worsened through transmission over certain distance of standard single mode fiber.

Firstly, a simulation is carried out to characterize how the signal quality degrades with respect to the length of a dispersion dominated transmission link. The simulation setup is very simple where we have the binary phase shift keyed signal transmitted over a certain length of single mode fiber, in which the signal is dispersed, combined with dual pump whose phase is coherent to the signal, before being input to a HNLF based phase sensitive amplifier.

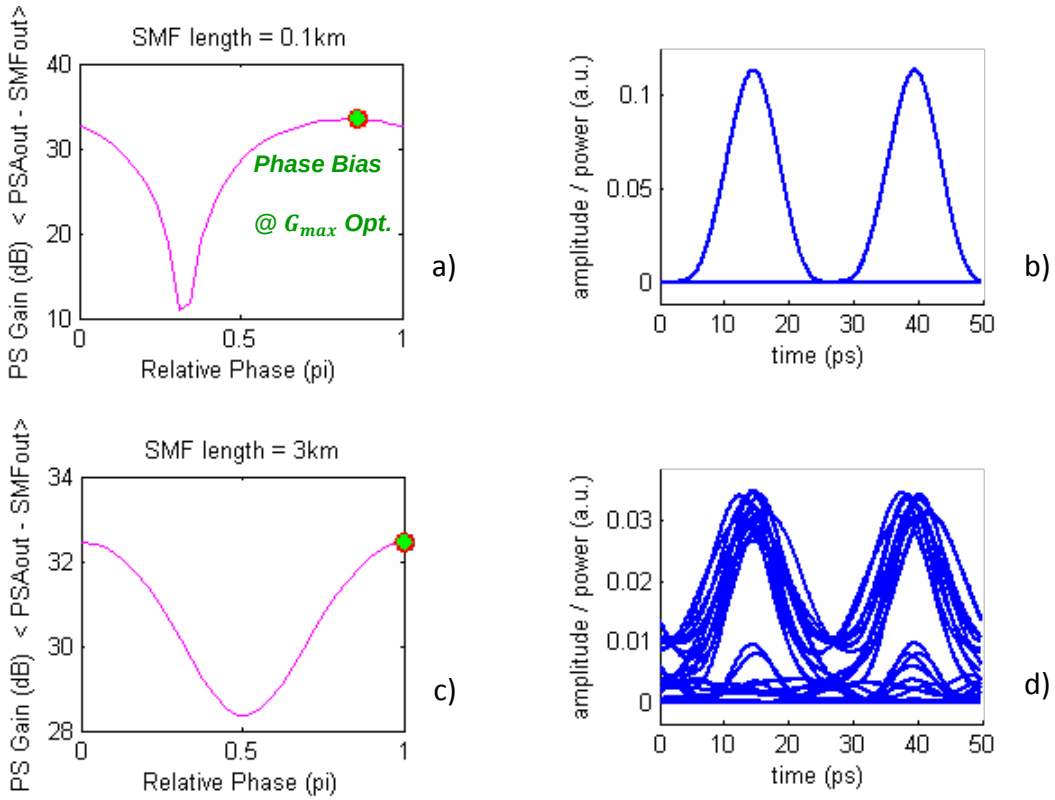

Figure 46 – Phase sensitive gain response and signal eye diagram for single mode fiber length of 100 m (a) and (b); and 3000 m (c) and (d).

Figure 46 shows the simulation results. When the transmission link is very short, composed of single mode fiber of length 100 m, the transfer function of the PSA has a phase extinction ratio greater than 20 dB, while providing up to 33 dB phase sensitive peak gain. The signal at the output acquires no distortion. On the contrary, when the signal is first sent to propagate through a 3000 m long transmission link, the linear impairments acquired along propagation deteriorates the phase sensitivity of a PSA, with the phase sensitive peak gain being retained, while on the other hand, the phase sensitive extinction ratio got reduced to barely 4 dB.

It is seen that the phase sensitive gain profile is affected with respect to the input signal quality. A shift in phase sensitive peak gain is observed in the 3000 m long case compared to the 100 m case, due to higher signal phase noise acquired along longer propagation. Note that the phase sensitive gain profile varies also as a function of pump to signal power ratio. Therefore, when PSAs are used as inline amplifiers, it is very important to bias the input signal phase at the optimum peak gain phase value, or in other words, to align the signal phase to be in phase with the dual-pump before the waves enters the HNLF based PSA. This ensures the signal experience maximum amplification, with good phase sensitive extinction to the out of phase signal quadrature.

The eye opening penalty (EOP) of the signal is then examined as a function of propagation length inside the single mode fiber. This is to find out a maximum transmission length with still a tolerable EOP value, and this length will be set as the inline amplifier repetition length of PSAs, referred to as “span length” in a multi-span transmission link. Figure 47 shows how the EOP varies in the case of signal transmission over SMF alone, over SMF then through PSA, and over SMF through PSA followed by dispersion compensating in a piece of dispersion compensation fiber (DCF).

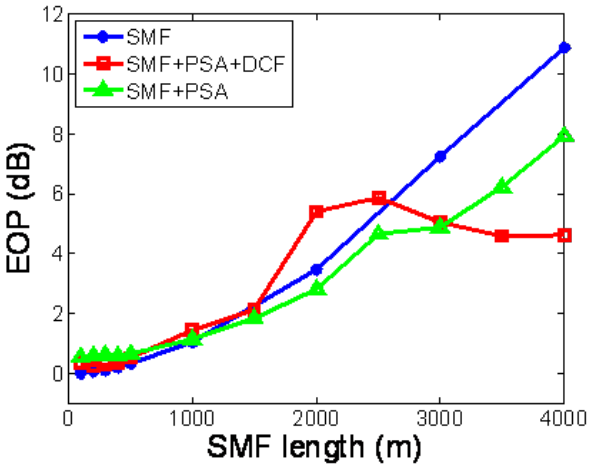

Figure 47 – Signal eye opening penalty as a function of propagation length in single mode fiber.

After signal transmission over each of the examined SMF length, as the signal quality is degraded due to transmission, we made sure that the signal phase is biased at the optimum phase shift value before it enters the PSA, to attain maximum phase sensitive amplification. Comparing the trace labeled SMF with the trace labeled SMF+PSA, a small improvement in EOP is observed. The longer the transmission was prior to a PSA, the more distinct the improvement in EOP value gets. This shows the PSA's ability to restore the optical signal to noise ratio under dispersion dominant linear impairment. When the signal is further dispersion compensated, significant EOP improvement can be seen at longer SMF lengths. The EOP values lie around 4 dB around 4000 m SMF length.

To see for how long a transmission length EOP could remain tolerable, simulations are carried out for longer fiber length, and the resulting curves are plotted in Figure 48 (left). As can be seen, the curve labeled 'SMF+PSA+DCF' has the EOP maintained at a tolerable value of 4 dB over a long distance ranging from 2 to 6 km without worsening.

The following will show how the phase sensitive gain profile evolves with respect to signal quality affected by transmission length. When the transmission length is relatively short, such as 100 m, the PSA gain curve, as shown in Figure 48 (right) has a high gain up to 33 dBm with a large extinction ratio over 20 dB. When the transmission length increases to 2 km, the peak gain of the PSA drops down by 3 dB, and the PS extinction reduces to barely 4 dB. More drop of PS peak gain is observed at 6 km transmission, with a small extinction of 3 to 4 dB. The corresponding eye diagrams at these three distances are shown in Figure 49.

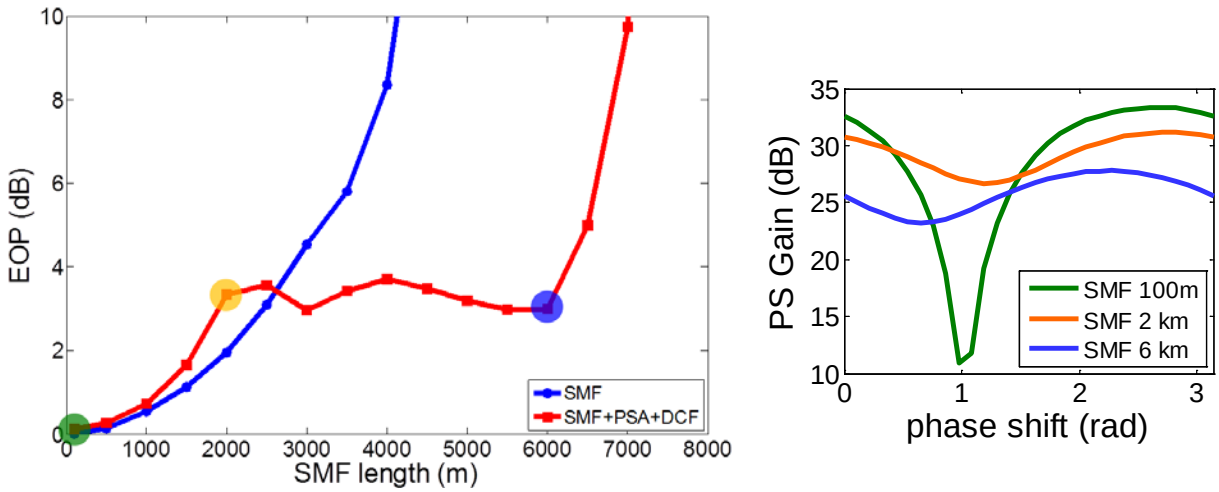

Figure 48 – Signal eye opening penalty as a function of propagation length in single mode fiber (left); Phase sensitive gain curves at 100 m, 2 km and 6 km, respectively (right).

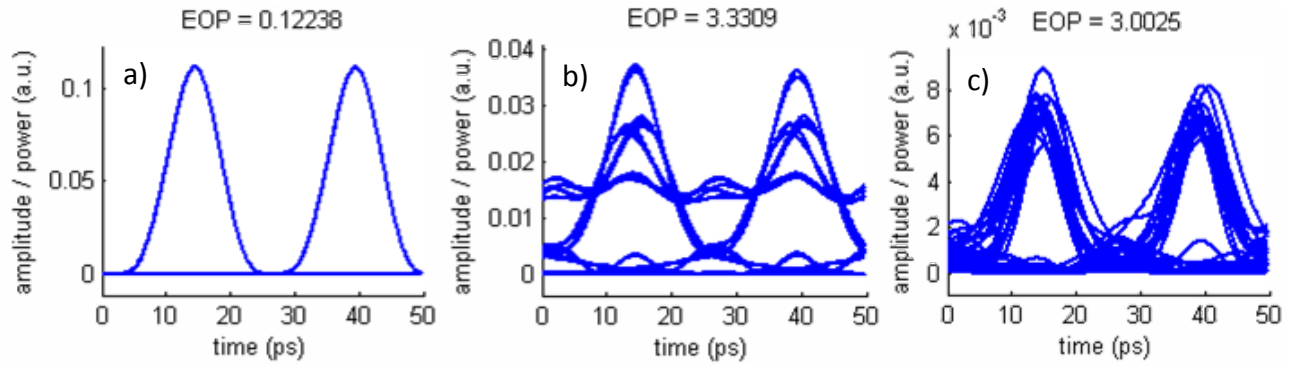

Figure 49 – Eye opening penalty of signal with transmission over a) 100 m b) 2 km and c) 6 km of dispersion compensated single mode fiber link.

The initial input signal power is -10 dBm. At a transmission distance of 100 m, the output signal power through the 'SMF+PSA+DCF' link read from Figure 49 (a) is 100 mW (20 dBm), that leads to a phase sensitive signal gain of 30 dB. At a transmission distance of 2 km, the output signal power is read as 40 mW from Figure 49 (b). At this length, the PSA offers a reduced gain of 26 dB. When the transmission length increased to 6 km, the output power read from Figure 49 (c) is 8 mW, in this case, the gain provided by the PSA is 19 dB.

Under current investigation, in a dispersion compensated single mode fiber link that utilized PSA as inline amplifier, a transmission length of approximately 6 km is a tolerable span length with EOP below 4 dB, and with reasonable gain provided at 19 dB. With proper span length chosen, a multi-span link is then configured and analyzed.

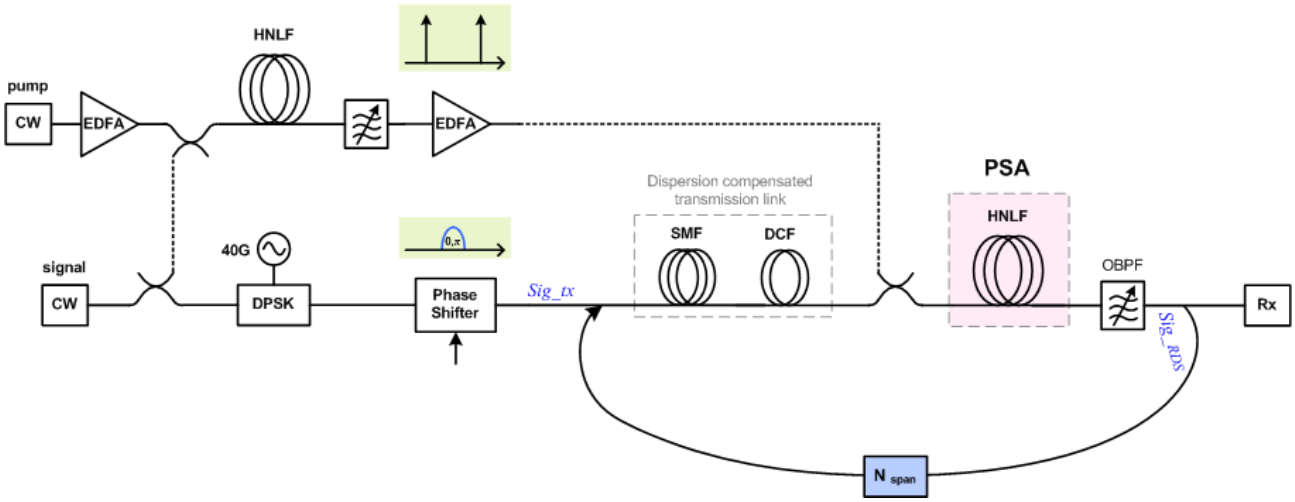

Figure 50 – System setup for PSA used as inline amplifier in a multi-span optical transmission link.

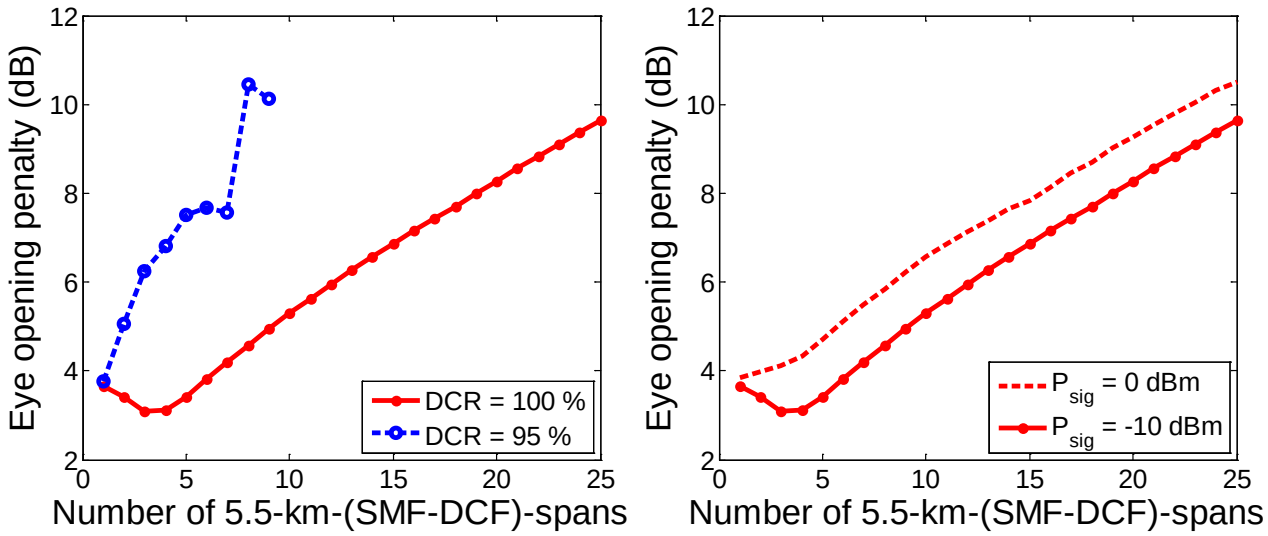

Figure 51 – EOP variation as a function of the number of 5.5-km spans, in terms of: dispersion compensation ratios (left) and input signal power levels (right). Total pump power = 31.5 dBm.

In the multi-span loop simulation, the used span length used was chosen to be 5.5 km, and the span was composed of single mode fiber and dispersion compensating fiber. The signal power is readjusted for each loopback to keep the same pump to signal power ratio in order to keep the PS (peak) gain constant for each span. At each span output, the signal is looped back and used as input for the subsequent span. For each of the spans, the amount of dispersion compensation is defined as the dispersion compensation ratio (DCR), which typically ranges from 90 and 110% for standard single mode fiber based system. In Figure 51 (left), EOP curves are plotted as a function of the number of 5.5 km spans, for two DCR values. For the case of 95% dispersion compensation, the EOP value raises rapidly with the number of spans. This rapid growth in penalty is a result of net accumulation of residual dispersion per span fed back into the subsequent loop. Under 100% dispersion compensation, the EOP values remains relatively low for the first 6 spans, and then increase with increasing number of spans.

Figure 51 (right) then compares the impact of the pump to signal power ratio on the EOP in the case of 100% dispersion compensation. In the small signal regime, where the signal power is equal to -10 dBm, a dip is observed where the EOP experiences reduction in the first 3-4 spans. When the signal power is increased by 10 dB (equals to 0 dBm), the initial reduction of eye opening penalty no longer exists, and the EOP values increase with increasing number of spans. The initial reduction of EOP is an interesting behavior. The two curves in Figure 51 (right), in a way,

resembles the well-known curves of pulse broadening factor versus propagation distance. For the pulse broadening factor, an initial compression (a dip) in the curve is obtained when the chirp parameter (C) has negative sign compared to the chromatic dispersion coefficient (β_2) [45]. If we should understand the two curves in Figure 51 (right) with the same analogy, then the dashed curve is under stronger nonlinear domination, while the dispersion property in both cases remains the same. Interplay between dispersion and nonlinearity-induced phase (chirp) when the waves propagate inside the highly nonlinear fiber based PSA should be the main cause leading to this effect. But more in depth simulations are needed to be carried out to fully understand this behavior.

6.1 Summary – analysis of the eye opening penalty

In summary, we have numerically characterized the dispersion tolerance of PSAs. We have shown that the signal quality at the input of a PSA affects the transfer function of the Std-HNLF based PSA gain profile. Both phase sensitive gain and extinction ratio reduces when the signal quality at the input of the Std-HNLF based PSA degrades. Eye diagrams are measured, and the eye opening penalty is used to characterize the signal degradation. According to the current investigation, 100 % dispersion compensation leads to reduced eye opening penalty. Strong signal power should be avoided to be sent into PSAs as it leads to higher EOP compared to small signal regime. An initial reduction in EOP in the small signal regime is yet to be further investigated.

7 Pulse shaping capabilities of PSA

In this investigation, simulations are carried out to gain brief insights into the pulsed operation of Std-HNLF based dual-pump degenerate-idler phase sensitive amplifiers. Gaussian pulse evolution in a PSA with respect to its signal phase bias value will be shown in the case of chirp-free operation and in the case where signal is pre-chirped before entering the PSA. In the chirped pulse case, it can be shown that when the signal power is high that the pumps have depleted, narrow and square-shaped pulses can be synthesized however with pedestals. The phase sensitive extinction ratio is shown to decrease with increasing chirp parameter values (as defined in Equation 23).

7.1 Characterization of pulsed operation in PSAs

When injecting a Gaussian pulse into a PSA, in the chirp-free case, the signal pulse will experience maximum amplification when it is phase-biased at the peak gain phase value of the PS-gain profile. The signal will experience less gain and even attenuation when its phase deviates from the peak gain phase value of the PSA. The pulse shape in the chirp-free case remains unchanged. This can be seen from Figure 52 in the column to the left. The red dot moving along the PSA curve indicates the actual phase-bias value of the signal pulse.

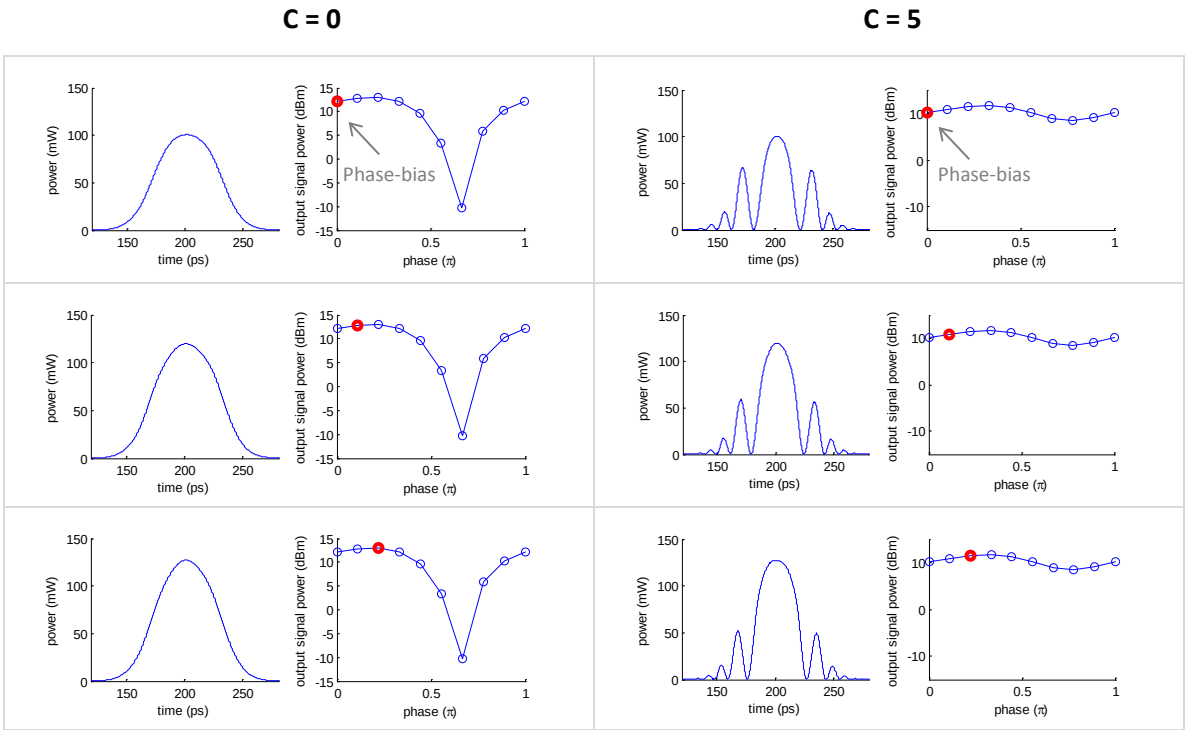

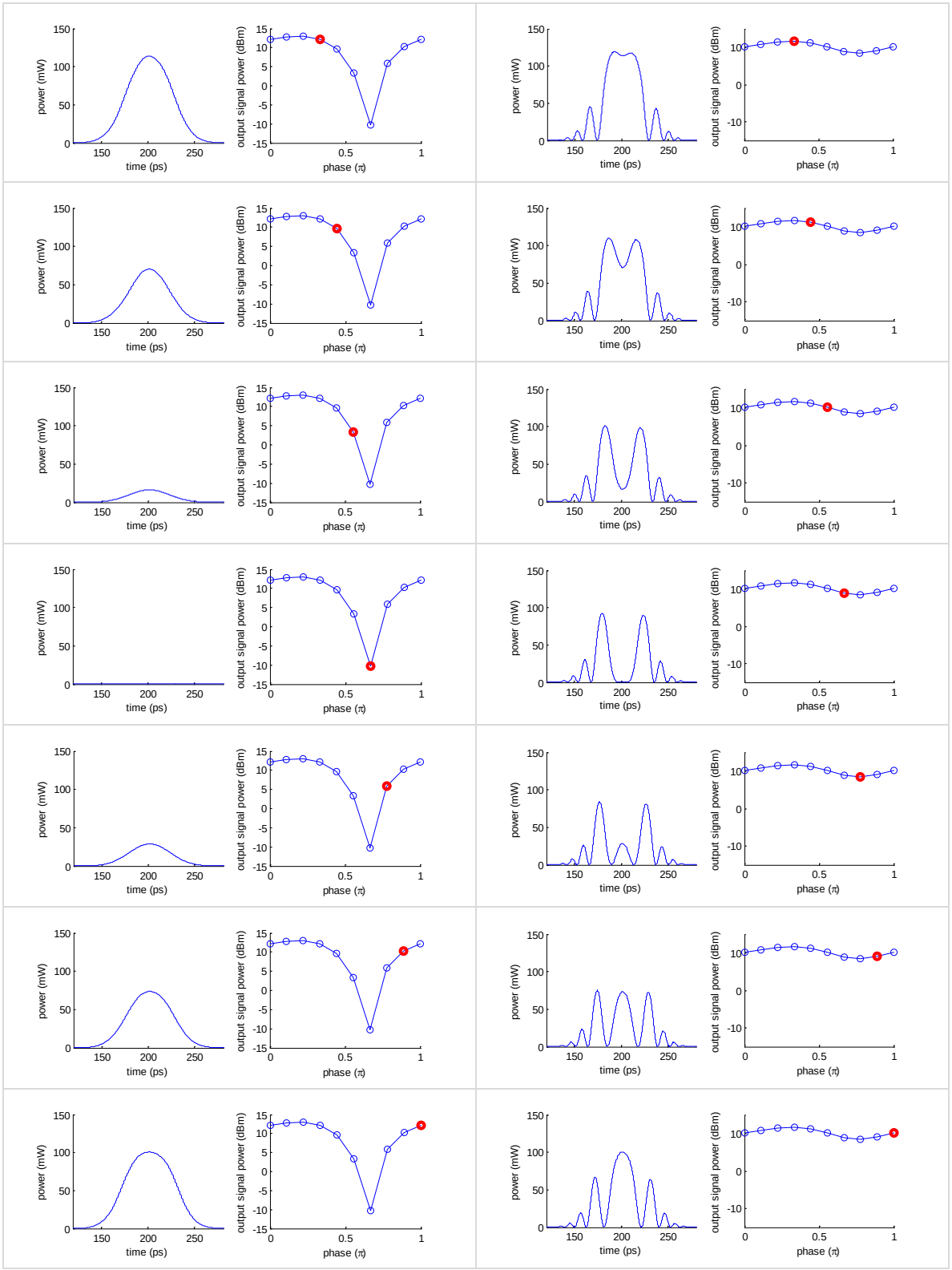

Figure 52 – Gaussian pulse evolution inside a 500 m long Std-HNLF based dual-pump degenerate-idler PSA, with (left) chirp-free case and (right) with the presence of chirp (C = 5) with respect to signal pulse phase-bias value. Total pump power was 31.5 dBm, input signal power was -26 dBm.

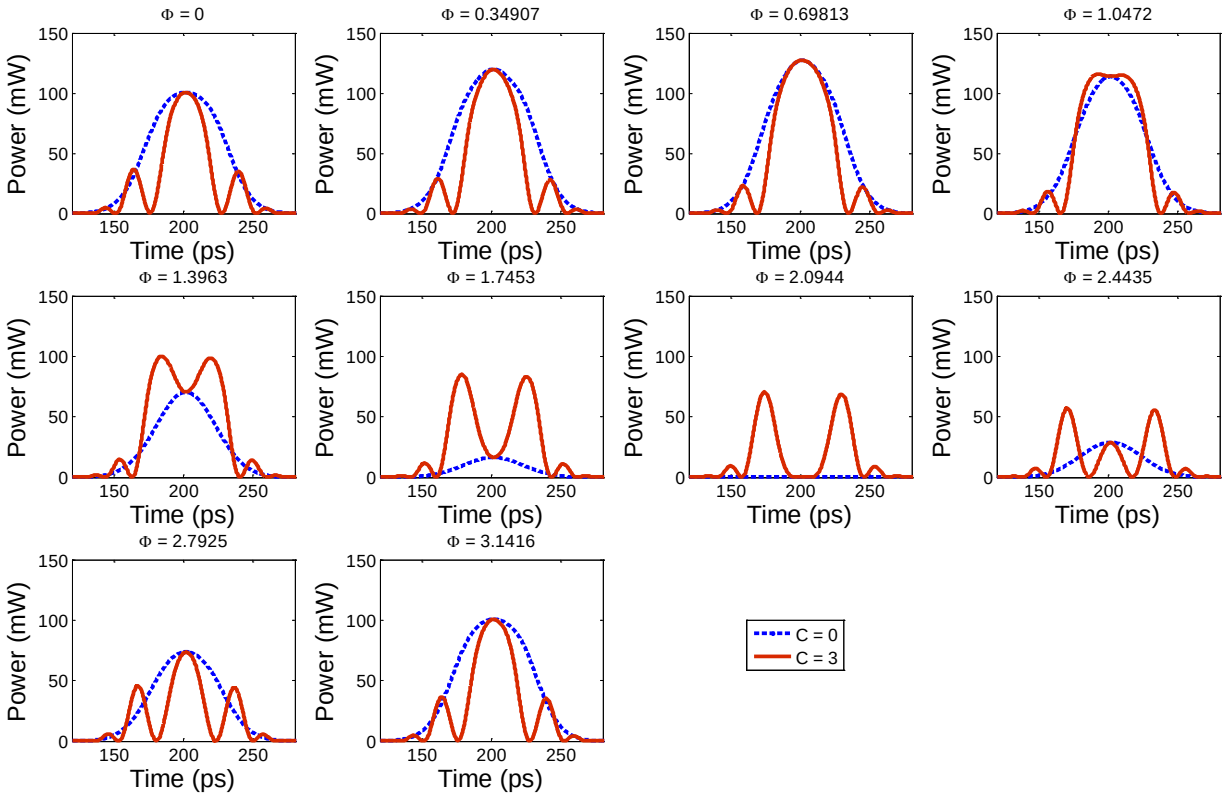

Figure 53 – Gaussian pulse evolution inside of a 500 m long Std-HNLF based dual-pump degenerate-idler PSA, as a function of phase-bias value, for two chirp parameters. Total pump power was 31.5 dBm, signal power was -26 dBm.

When the signal pulse is pre-chirped before entering the PSA, as the results shown in the column to the right of Figure 52, the phase sensitive extinction ratio shrinks to barely 4 dB. The output pulse acquires an oscillatory temporal profile, with a main lobe in the center portion and symmetric side lobes on the two sides (the same temporal profile was experimentally measured when amplifying a short-pulse using a phase sensitive amplifier [65]). The main lobe experiences maximum amplification and attenuation according to its phase-bias value with respect to the PS-gain profile. When the signal is biased out of phase, the central portion experiences attenuation, however the side lobes do not experience attenuation but grow accordingly. The temporal profiles of the Gaussian pulse at different phase-bias values for two chirp parameter values C = 0, and 3, are plotted on top of each other and can be seen from Figure 53.

In the above simulations, for the 500 m long Std-HNLF based dual-pump degenerate-idler PSA, the total pump power used was 31.5 dBm and the signal Gaussian pulse peak power was -26 dBm. The phase sensitive extinction ratio in this case equals 24 dB. When the input power is increased to -11 dBm, the pumps are depleted due to the high input signal power, and the extinction ratio drops to 12 dB. This can be seen from Figure 54, in the chirp-free case.

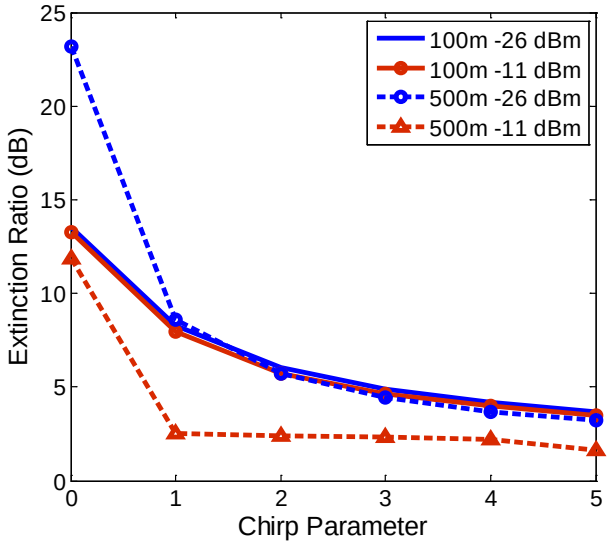

Figure 54 – Extinction ratio degradation as a function of the chirp parameter of the signal pulse, obtained inside of a 100 m long Std-HNLF based dual-pump degenerate-idler PSA.

In Figure 54, the phase sensitive extinction ratio is plotted as a function of Gaussian pulse chirp parameter as defined in Equation 23, for two Std-HNLF fiber lengths at two signal power levels. The extinction ratio decreases with respect to an increasing chirp parameter. When the Std-HNLF length is short such as 100 m, no significant difference in the extinction ratio is observed for the two power levels encountered. When the pulse has evolved over a longer Std-HNLF length such as 500m, the extinction ratio drops significantly when the input signal power is high (Psig = -11 dBm), compared to the small signal case (Psig = -26 dBm). For the input Gaussian pulse with its full-width at half-maximum intensity equals to 50 ps, its output spectral width evolution as a function of the chirp parameter can be calculated as in Equation 24. The resulting curve is shown in Figure 55.

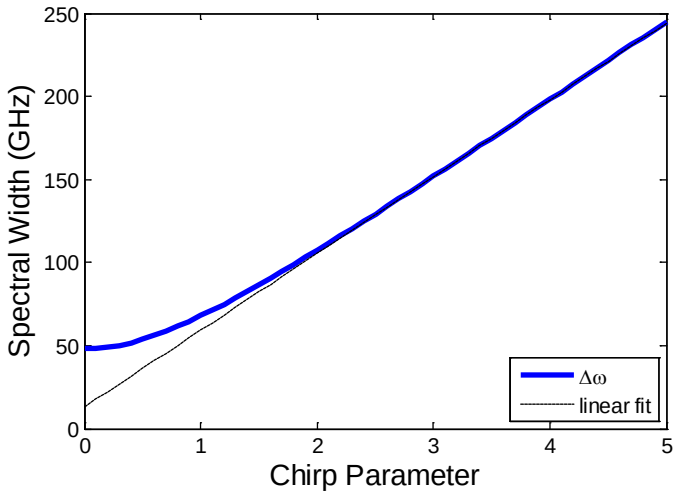

Figure 55 – Gaussian pulse spectral width as a function of chirp parameter.

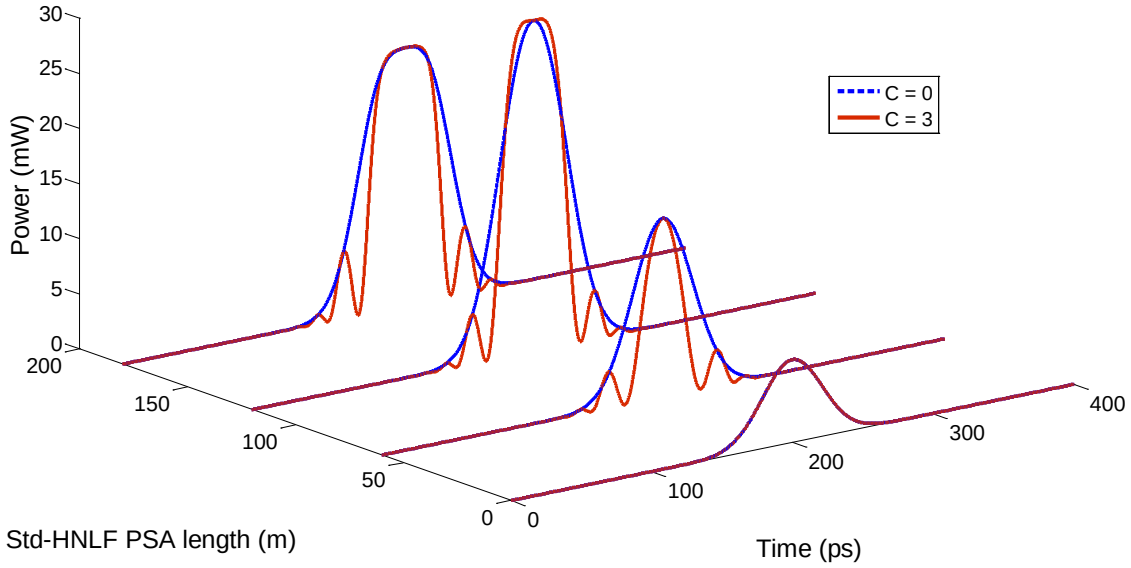

Figure 56 – Pulse shape evolution as a function of Std-HNLF length for a Gaussian pulse, for two different chirp parameter values. Total pump power was 31.5 dBm, signal power was -11 dBm.

In the case where chirp parameter equals to 3, as shown in Figure 56, as the chirped pulse propagates further down the nonlinear fiber, the pulse acquires a narrowed square-shaped temproal profile due to satuation, with pedestals. With proper pedestal removal schemes suggested, a squared shaped pulse can be useful in applications for ultrahigh speed signal processing. Squared shaped pulse generated from PSA can be synthesized with inherent high pulse gain level.

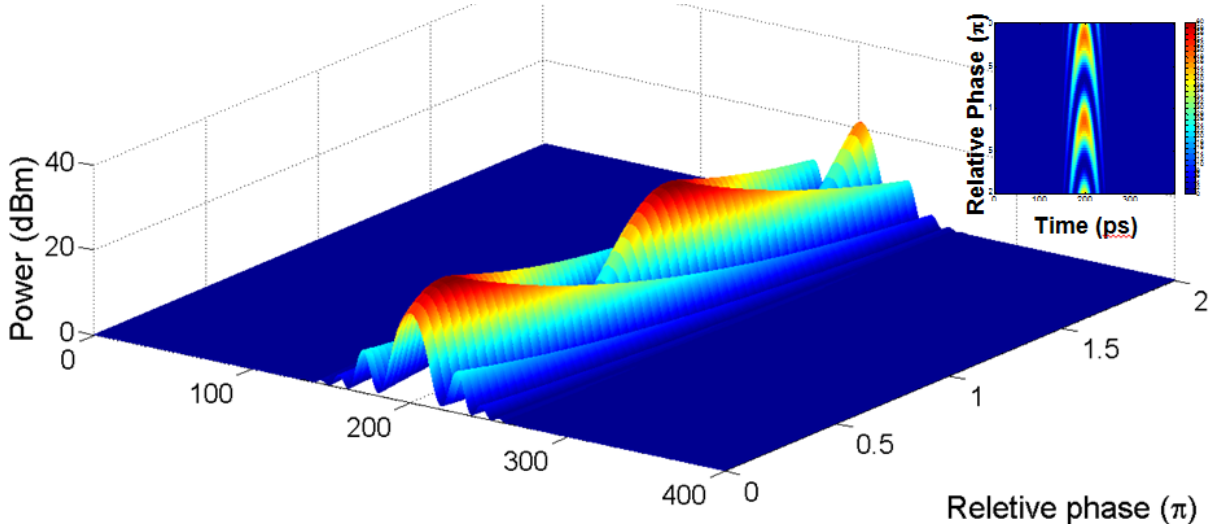

Figure 57 – Pulse shape evolution as a function of phase shift, at a specific fiber length.

Figure 57 shows the chirped Gaussian pulse variation as a function of phase-bias value, plotted over 2π period. The evolution of the pulse shape shows a π periodicity. The maximum peak gain of the pulse is obtained when biased at every multiple of the optimum phase-bias value of the PSA gain profile.

7.2 Summary – PSA pulse shaping via chirp profile designing

In this discussion, Gaussian pulse with linear chirp profile is briefly investigated via numerical simulation. It is shown that the extinction ratio of a phase sensitive amplifier reduces when chirp is introduced. The temporal profile of a Gaussian pulse can be modified in accordance to the pulse chirping profile. With proper parameter settings, narrowed and square-shaped pulse can be synthesized, however with pedestals on the sides. In the future work, nonlinear chirp profiles with i.e. parabolic profile can be designed to explore the capability for supressing the side pedestals.

CHAPTER 8

8 Conclusion

The goal of the project was to demonstrate broadband and high-speed operation of a phase sensitive amplifier based on parametric amplification in optical fibers, and to study its application to the all-optical processing of advanced modulation formats, especially those relying on the phase of the optical signal.

In this thesis, experimental characterizations and numerical investigations on various aspects have been carried out. Stimulated Brillouin scattering (SBS) which limits the power efficiency of any highly nonlinear fiber based optical parametric amplifiers, phase sensitive or not, had been taken into consideration. Effective SBS suppression via single tone pump phase dithering was demonstrated. The reflected power was measured to have been suppressed by 34 dB, and the SBS threshold was shown to be increased from 16 to 30 dBm. The development of novel aluminum-doped high SBS threshold highly nonlinear fiber (Al-HNLF) was briefly reviewed. Their SBS threshold had been characterized both analytically and experimentally.

Wave propagation inside of a fiber is numerically modeled by solving the nonlinear Schrödinger equation numerically using the split-step Fourier method. Pulse propagation under dispersion and nonlinearity dominant regimes has been investigated. Four-wave mixing conversion efficiency and parametric amplification had been characterized numerically. Phase-sensitive amplification (PSAs) was then investigated in a widely adopted two stage 'copier' configuration. PSAs with the dual-pump degenerate-idler configuration have then been further investigated. Optimum operation points for maximum gain and extinction ratio values for such PSAs were found numerically and proven to reside on the power level above the SBS threshold set by commercial Std-HNLF's SBS threshold levels. This claims the necessity for research and development on designing high SBS threshold fiber like the Al-HNLF with higher figure of merit, to counter balance between loss and fiber nonlinearity. The regeneration properties of PSAs with the dual-pump degenerate-idler configuration were investigated consequently. Through optimization, it is shown that phase sensitive gain response with a flat-top gain profile can be designed. The flat-top gain profile is obtained via moderate saturation through proper dispersion engineering. PSAs with a flat-top gain response can provide simultaneous amplitude and phase noise squeezing performance. The phase noise margin of flat-top PSA based regenerators can be significantly enhanced, resulting in

reduced optical signal to noise ratio penalty over a broader phase noise range than conventional designs.

With the aforementioned investigations, implementation of such PSAs in a nano-engineered silicon waveguide was attempted. The experimental measurements show successfully the existence of phase sensitive process in such silicon nanowire. Numerical optimizations brought this discussion further, to find out the achievable phase sensitive extinction ratio values one could expect under the presence of two-photon absorption and free-carriers. The findings show that the extinction ratio of a silicon nanowire based PSA can be significantly improved, if carrier life time is significantly reduced. Hence, the design of silicon nanowires with reduced propagation loss and reduced carrier lifetime are desired to provide the predicted performance, and to fully utilize the potential for chip-based PSA signal processing capabilities.

The PSAs performance was then evaluated in the system context, where the dispersion tolerance of PSAs was studied when used as an inline amplifier in a multi-span transmission link. The phase sensitive extinction ratio is found to reduce with increasing dispersion value acquired along propagation distance inside of a SMF. Ultimately, the phase sensitivity vanishes, and the phase insensitive peak gain reduces from the phase sensitive case by up to 6 dB. In the multi-span test, the eye opening penalty (EOP) was tested for two dispersion compensation ratios. The result shows the necessity to have 100 % dispersion compensation when using PSAs as inline amplifiers to provide low EOPs. EOP is also shown to degrade with stronger signal power presented at the input of a PSA, due to saturation.

Finally, a glimpse is taken at the pulse shaping capabilities of PSA. Pulsed operations of PSAs with chirp-free and pre-chirped Gaussian pulses were investigated. Pulses that are linearly chirped before entering the PSA show oscillatory temporal profile with pedestals at the output of the PSA. The phase sensitive dependence of the pulse temporal profile provides pulse shaping capabilities. With properly designed chirp profiles, pulses can be pre-chirped intentionally, to obtain desired pulse shape at the output of a PSA, with inherent amplification.

Putting PSAs into perspective, the ultra-low noise figure it can provide, together with its versatile and superior amplification and regeneration capabilities help to extend the achievables in signal processing and in optical communications systems.

Ning Kang

Nov. 2012

List of Acronyms

Al-HNLF	aluminium-doped highly nonlinear fiber
BiDF	bismuth-doped fiber
CHF	chalcogenide fiber
CW	continuous wave
DCF	dispersion compensation fiber
DF-HNLF	dispersion flattened highly nonlinear fiber
DPSK	differential phase shift keying
DSF	dispersion shifted fiber
EDFA	erbium doped fiber amplifier
EOP	eye opening penalty
ER	extinction ratio
FCA	free-carrier absorption
FOPA	fiber optical parametric amplifier
FWHM	full width at half maximum
FWM	four-wave mixing

GVD	group-velocity dispersion
HNLF	highly nonlinear fiber
IM	intensity modulation
MSF	micro-structured fiber
NF	noise figure
NLSE	nonlinear Schrödinger equation
NRZ	non return to zero
OBPF	optical bandpass filter
OOK	on-off keying
OPA	optical parametric amplification
OSA	optical spectrum analyser
OSNR	optical signal to noise ratio
PBS	polarization beam splitter
PC	polarization controller
PCF	photonic crystal fiber
PIA	phase insensitive amplifier

PM	phase modulation
PN	phase noise
PS	phase sensitive
PSA	phase sensitive amplifier
PSK	phase shift keying
QPSK	quadrature phase shift keying
RFA	Raman fiber amplifier
RDS	residual dispersion per span
Rx	receiver
RZ	return to zero
SBS	stimulated Brillouin scattering
Si-WG	silicon waveguide
SMF	single mode fiber
SOA	semiconductor optical amplifier
SOI	silicon on insulator
SPM	self-phase modulation

SSFM	split-step Fourier method
Std-HNLF	standard highly nonlinear fiber
TE	transverse electric
TM	transverse magnetic
Tx	Transmitter
TOD	third-order dispersion
TPA	two-photon absorption
WSS	wavelength selective switch
XPM	cross-phase modulation
ZDWL	zero-dispersion wavelength

List of Publications

[A] **N. Kang**, A. Fadil, M. Pu, H. Ji, H. Hu, E. Palushani, D. Vukovic, J. Seoane, H. Ou, K. Rottwitt, and C. Peucheret. "*Experimental demonstration of phase sensitive parametric processes in a nano-engineered silicon waveguide,*" To be submitted to CLEO, 2013.

[B] **N. Kang**, J. Seoane, K. Rottwitt, C. Peucheret. "*Synthesis of flat-top gain response in fiber phase sensitive amplifiers with improved phase noise regeneration tolerance,*" CLEO, CM4N.8, OSA, San Jose, CA , 2012.

[C] Z. Lali-Dastjerdi, O. Ozolins, Y. An, V. Cristofori, F. Da Ros, **N. Kang**, H. Hu, H. C. H. Mulvad, K. Rottwitt, M. Galili, C. Peucheret. "*Demonstration of cascaded in-line single-pump fiber optical parametric amplifiers in recirculating loop transmission,*" ECOC, Mo.2.C.5, OSA, Amsterdam, 2012

[D] Z. Lali-Dastjerdi, T. Lund-Hansen, **N. Kang**, K. Rottwitt, M. Galili, C. Peucheret. "*High-frequency RIN transfer in fibre optic parametric amplifiers,*" CLEO Europe, IEEE, Munich, 2011.

[E] **N. Kang**, T. Lund-Hansen, J. Seoane, K. Rottwitt, C. Peucheret. "*Extinction ratio and gain optimization of dual-pump degenerate-idler phase sensitive amplifiers,*" IEEE Photonics Conference, MM2, Arlington, Virginia, 2011.

[F] C. Peucheret, L. K. Oxenløwe, H. C. H. Mulvad, M. Galili, J. B. Jensen, J. Seoane, E. Palushani, H. Hu, J. Xu, A. Clausen, K. Rottwitt, **N. Kang**, J. Laguardia Areal, H. Ji, B. Zsigri, P. Jeppesen. "*High-speed signal processing using highly nonlinear optical fibres,*" ICOCN, Beijing, China, 2009.

Bibliography

1 M. Marhic and Chung-Ho Hsia. “Optical amplification and squeezed-light generation in fibre interferometers performing degenerate four-wave mixing”, Quantum Opt. 3, pp. 341-358, 1991.

2 A. Bogris and D. Syvridis. “RZ-DPSK signal regeneration based on dual-pump phase-sensitive amplification in fibers”, IEEE Photonics Technology Letters, vol. 18 no. 20, pp. 2144–2146, 2006.

3 D. B. Keck, P.C. Schultz, and F. Zimar. "Attenuation of multimode glass optical waveguides", Applied Physics Letters, vol. 21, no. 5, pp. 215-217, 1972.

4 D.B. Keck, R. D. Maurer, and P. C. Schultz. "On the ultimate lower limit of attenuation in glass optical waveguides", Applied Physics Letters, Vol. 22, no. 7, pp. 307-309, 1973.

5 S. Tomaru, M. Yasu, M. Kawachi, and T. Edahiro. "VAD single mode fibre with 0.2 dB/km loss", Electronics Letters, vol. 17, no. 2, pp. 92-93, 1981.

6 D. J. Richardson. "Filling the Light Pipe", APPLIED PHYSICS, Science, Vol. 330, pp. 327-328, 2010.

7 M. N. Islam. Raman Amplifiers for Telecommunications 2: Sub- Systems and Systems, Springer series in optical sciences, 2004, ISBN 0-387-40656-5.

8 G. Agrawal. "Nonlinear fiber optics: its history and recent progress [Invited] ", J. Opt. Soc. Am. B, Vol. 28, Issue 12, pp. A1-A10, 2011.

9 A. R. Chraplyvy, R. W. Tkach. "Optical fiber nonlinear effects in lightwave communication systems", NLO, IEEE , pp. 302, 1994.

10 R. M. Jopson, C. J. McKinstrie, S. Radic, A. H. Gnauck. "Fiber parametric devices", LEOS, IEEE, ThAA3, pp. 941-942, 2006.

11 J. M. C. Boggio, C. Lundstrom, J. Yang, H. Sunnerud, P. A. Andrekson. "Double-pumped FOPA with 40 dB flat gain over 81 nm bandwidth", ECOC, Tu.3.B.5, pp. 1-2, 2008.

12 A. Demir. "Nonlinear phase noise in optical-fiber-communication systems", J. Lightwave Technol. Vol. 25, Issue 8, pp. 2002-2032, 2007.

13 K. Croussore, C. Kim, and G. Li. "All-optical regeneration of differential phase-shift keying signalsbased on phase-sensitive amplification", Opt. Lett. Vol. 29, Issue 20, pp. 2357-2359, 2004.

14 K. Croussore, I. Kim, Y. Han, C. Kim, G. Li, and S. Radic. "Demonstration of phase-regeneration of DPSK signals based on phase-sensitive amplification", Opt. Express, Vol. 13, Issue 11, pp. 3945-3950, 2005.

15 K. Croussore, G. Li. "Phase regeneration of NRZ-DPSK signals based on symmetric-pump phase-sensitive amplification", Photonics Technology Letters, IEEE , Vol. 19, no. 11, pp. 864-866, 2007.

16 Z. Tong, C. Lundström, E. Tipsuwannakul, M. Karlsson, P. A. Andrekson. "Phase-sensitive amplified DWDM DQPSK signals using free-running Lasers with 6-dB link SNR improvement over EDFA-based systems", ECOC, pp. 1-3, 2010.

17 R. Slavík, F. Parmigiani, J. Kakande, M. Westlund, M. Skold, L. Grüner-Nielsen, R. Phelan, P. Petropoulos, D. J. Richardson. "Robust design of all-optical PSK regenerator based on phase sensitive amplification", OSA, OFC/NFOEC, OMT2, pp.1-3, 2011.

18 R. Slavík, J. Kakande, F. Parmigiani, P. Petropoulos, D. J. Richardson. "All-optical regeneration based on phase sensitive amplification", OSA, CLEO, CWD2, pp. 1-2, 2011.

19 Z. Tong, C. Lundström, P. A. Andrekson, M. Karlsson, A. Bogris. "Ultralow noise, broadband phase-sensitive optical amplifiers, and their applications", Selected Topics in Quantum Electronics, IEEE Journal, Vol. 18, no. 2, pp. 1016-1032, 2012.

20 A. H. Gnauck, P. J. Winzer. "Optical phase-shift-keyed transmission", Lightwave Technology, Journal, Vol. 23, no. 1, pp. 115- 130, 2005.

21 K. Croussore, G. Li. "Phase and amplitude regeneration of differential phase-shift keyed signals using phase-sensitive amplification", Selected Topics in Quantum Electronics, IEEE Journal, Vol. 14, no. 3, pp. 648-658, 2008.

22 R. Slavík, F. Parmigiani, J. Kakande, C. Lundström, M. Sjödin, P. A. Andrekson, R. Weerasuriya, S. Sygletos, A. D. Ellis, L. Grüner-Nielsen, D. Jakobsen, S. Herstrøm, R. Phelan, J. O'Gorman, A. Bogris, D. Syvridis, S. Dasgupta, P. Petropoulos, and D. J. Richardson. “All-optical phase and amplitude regenerator for next-generation telecommunications systems”, Nature Photonics, Vol. 4, pp. 690-695, 2010.

23 F. Parmigiani, R. Slavík, J. Kakande, C. Lundstrom, M. Sjodin, P. A. Andrekson, R. Weerasuriya, S. Sygletos, A. D. Ellis, L. Grüner-Nielsen, D. Jakobsen, S. Herstrm, R. Phelan, J. O'Gorman, A. Bogris, D. Syvridis, S. Dasgupta, P. Petropoulos, D. J. Richardson. "All-optical phase regeneration of 40 Gbit/s DPSK signals in a black-box phase sensitive amplifier", OFC/NFOEC, PDPC3, pp. 1-3, 2010.

24 J. Kakande, F. Parmigiani, R. Slavík, P. Petropoulos, D. J. Richardson. "Phase sensitive amplifiers for regeneration of phase encoded optical signal formats", ICTON, Tu.A1.6, pp.1-4, 2011.

25 F. Parmigiani, J. Kakande, R. Slavík, P. Petropoulos, and D. Richardson. "Potential and practical implementations of phase sensitive amplifiers for all-optical signal regeneration", CLEO/EQEC, OSA, 2011.

26 R. Stolen, J. Bjorkholm. "Parametric amplification and frequency conversion in optical fibers", Quantum Electronics, IEEE Journal, Vol. 18, no. 7, pp. 1062- 1072, 1982.

27 J. Hansryd, P. A. Andrekson. "Broad-band continuous-wave-pumped fiber optical parametric amplifier with 49-dB gain and wavelength-conversion efficiency", Photonics Technology Letters, IEEE , Vol. 13, no. 3, pp. 194-196, 2001.

28 J. Li, J. Hansryd, P. O. Hedekvist, P. A. Andrekson, S. N. Knudsen. "300-Gb/s eye-diagram measurement by optical sampling using fiber-based parametric amplification", Photonics Technology Letters, IEEE , Vol. 13, no. 9, pp. 987-989, 2001.

29 P. A. Andrekson. "High resolution optical waveform sampling", IEEE/LEOS Winter Topicals Meeting Series, pp. 187-188, 2009.

30 S. Radic, C. J. McKinstrie, R. M. Jopson, J. C. Centanni, A. R. Chraplyvy. "All-optical regeneration in one- and two-pump parametric amplifiers using highly nonlinear optical fiber", Photonics Technology Letters, IEEE , Vol. 15, no. 7, pp. 957-959, 2003.

31 Peucheret, C.; Lorenzen, M.; Seoane, J.; Noordegraaf, D.; Nielsen, C.V.; Grüner-Nielsen, L.; Rottwitt, K.; , "Amplitude regeneration of RZ-DPSK signals in single-pump fiber-optic parametric amplifiers," Photonics Technology Letters, IEEE , vol.21, no.13, pp.872-874, July1, 2009

32 J. Wang, H. Ji, H. Hu, H. C. H. Mulvad, M. Galili, E. Palushani, J. Yu, P. Jeppesen, and L. K. Oxenløwe. "Simultaneous Regeneration of Two 160 Gbit/s WDM Channels in a Single Highly Nonlinear Fiber", ECOC, OSA, Tu.1.A.1, 2012.

33 A. Kobyakov, M. Sauer, and D. Chowdhury. "Stimulated Brillouin scattering in optical fibers", Adv. Opt. Photon. Vol. 2, Issue 1, pp. 1-59, 2010.

34 M. Takahashi, M. Tadakuma, R. Sugizaki, T. Yagi. "SBS suppression techniques in highly nonlinear fibers", Photonics Society Summer Topical Meeting Series, 2010 IEEE , TuC3.1, pp. 149-150, 2010.

35 J. Coles, B. Kuo, N. Alic, S. Moro, C. Bres, J. Boggio, P. A. Andrekson, M. Karlsson, and S. Radic. "Bandwidth-efficient phase modulation techniques for Stimulated Brillouin Scattering suppression in fiber optic parametric amplifiers", Opt. Express, Vol. 18, Issue 17, pp. 18138-18150, 2010.

36 Y. Liu, Z. Lv, Y. Dong, and Q. Li. "Research on stimulated Brillouin scattering suppression based on multi-frequency phase modulation", Chin. Opt. Lett. Vol. 7, Issue 1, pp. 29-31, 2009.

37 F. Yaman, Q. Lin, S. Radic, G. P. Agrawal. "Impact of pump-phase modulation on dual-pump fiber-optic parametric amplifiers and wavelength converters", Photonics Technology Letters, IEEE, Vol. 17, no. 10, pp. 2053- 2055, 2005.

38 J. D. Marconi, J. M. C. Boggio, F. A. Callegari, A. Guimaraes, R. Arradi, H. L. Fragnito. "Double pumped parametric amplifier with SBS suppression by applying a strain distribution to the fiber", LEOS, IEEE, Vol.2, pp. 701- 702, 2004.

39 M. Lorenzen, D. Noordegraaf, C. V. Nielsen, O. Odgaard, L. Grüner-Nielsen, K. Rottwitt. "Brillouin suppression in a fiber optical parametric amplifier by combining temperature distribution and phase modulation", OFC/NFOEC, pp.1-3, 2008.

40 D. J. Richardson, X. Feng, F. Poletti, S. Dasgupta, A. Camerlingo, F. Parmigiani, P. Petropoulos, W. H. Loh, S. Herstrøm, L. Grüner-Nielsen. "Recent advances in highly nonlinear fibres", ECOC, pp. 1-3, 2010.

41 L. Grüner-Nielsen, S. Dasgupta, M. D. Mermelstein, D. Jakobsen, S. Herstrom, M. E. V. Pedersen, E. L. Lim, S. Alam, F. Parmigiani, D. Richardson, B. Palsdottir. "A silica based highly nonlinear fibre with improved threshold for stimulated brillouin scattering", ECOC, Tu.4.D.3 pp. 1-3, 2010.

42 F. Parmigiani, R. Slavík, A. Camerlingo, L. Grüner-Nielsen, D. Jakobsen, S. Herstrom, R. Phelan, J. O'Gorman, S. Dasgupta, J. Kakande, S. Sygletos, A. Ellis, P. Petropoulos, and D. Richardson. "Generation of high repetition rate (>100 GHz) ultrastable pulse trains from a coherent optical beat-signal through non-linear compression using a high SBS-threshold fiber," Nonlinear Photonics, OSA Technical Digest, NThA5, 2010.

43 L. Grüner-Nielsen, D. Jakobsen, S. Herstrøm, B. Pálsdóttir, S. Dasgupta, D. Richardson, C. Lundström, S. Olsson, and P. A. Andrekson. "Brillouin suppressed highly nonlinear fibers", ECOC, OSA, We.1.F.1, 2012.

44 B. Zhang, K. Guo, J. Tian, Y. Song. "Numerical analysis of femtosecond pulse propagation and supercontinuum generation in tapered fiber", Proc. SPIE 6839, Nonlinear Optics, 68390Z, 2008.

45 G. P. Agrawal, Nonlinear fiber optics, 3rd edition, Academic press, 2001, ISBN 0-12-045143-3.

46 M. E. Marhic, Fiber Optical parametric amplifiers, oscillators and related devices, 1st edition, Cambridge university press, 2008, ISBN 978-0-521-86102-1.

47 C. G. Joergensen, T. Veng, L. Grüner-Nielsen, and M. Yan. "Dispersion flattened highly non-linear fiber", ECOC, 2003.

48 Z. Tong, C. Lundström, E. Tipsuwannakul, M. Karlsson, P. A. Andrekson. "Phase-sensitive amplified DWDM DQPSK signals using free-running Lasers with 6-dB link SNR improvement over EDFA-based systems", ECOC, pp.1-3, 2010.

49 Z. Tong, C. Lundstrom, A. Bogris, M. Karlsson, P. A. Andrekson, D. Syvridis. "Measurement of sub-1dB noise figure in a non-degenerate cascaded phase-sensitive fibre parametric amplifier", ECOC, Paper 1.1.2, pp. 1-2, 2009.

50 Z. Tong, C. Lundström, P. A. Andrekson, C. J. McKinstrie, M. Karlsson, D. J. Blessing, E. Tipsuwannakul, B. J. Puttnam, H. Toda, and L. Grüner-Nielsen. "Towards ultrasensitive optical links enabled by low-noise phase-sensitive amplifiers", Nature Photonics, Vol. 5, pp. 430-436, 2011.

51 P. A. Andrekson, C. Lundström, Z. Tong. "Phase-sensitive fiber-optic parametric amplifiers and their applications", ECOC, We.6.E.1, pp. 1-6, 2010.

52 P. A. Andrekson. "Phase sensitive fiber optic parametric amplifiers", ECOC, Th.11.LeCervin.1, pp.1-3, 2011.

53 M. D. Mermelstein, “SBS threshold measurements and acoustic beam propagation modeling in guiding and anti-guiding single mode optical fibers,” Opt. Express, vol. 17, pp. 16225-16237, 2009.

54 K. Croussore, I. Kim, C. Kim, Y. Han, and G. Li. “Phase-and-amplitude regeneration of differential phase-shift keyed signals using a phase-sensitive amplifier,” Opt. Express 14, 2085-2094, 2006.

55 J. Kakande, F. Parmigiani, R. Slavík, L. Grüner-Nielsen, D. Jakobsen, S. Herstrøm, P. Petropoulos, D. J. Richardson. “Saturation effects in degenerate phase sensitive fiber optic parametric amplifiers,” ECOC, Th.10.C.2, 2010.

56 M. A. Foster, A. C. Turner, J. E. Sharping, B. S. Schmidt, M. Lipson, and A. L. Gaeta. “Broad-band optical parametric gain on a silicon photonic chip,” Nature 441, 960-963, 2006.

57 R. Salem, M. A. Foster, A. C. Turner, D. F. Geraghty, M. Lipson, and A. L. Gaeta. “Signal regeneration using low-power four-wave mixing on silicon chip,” Nature Photon. 2, 35-38, 2008.

58 L. K. Oxenløwe, H. Ji, M. Galili, M. Pu, H. Hu, H. C. H. Mulvad, K. Yvind, J. M. Hvam, A. T. Clausen, and P. Jeppesen. “Silicon photonics for signal processing of Tbit/s serial data signals,” IEEE J. Selected Topics Quantum Electron. Vol. 18, no. 2, pp. 996-1005, 2012.

59 R. P. Webb, J. M. Dailey, R. J. Manning, and A. D. Ellis. “Phase discrimination and simultaneous frequency conversion of the orthogonal components of an optical signal by four-wave mixing in an SOA,” Opt. Express, Vol. 19, Issue 21, 20015–20022, 2011.

60 B. J. Puttnam, D. Mazroa, S. Shinada, and N. Wada. “Phase-squeezing properties of non-degenerate PSAs using PPLN waveguides,” Opt. Express, Vol. 19, Issue 26, B131-B139, 2011.

61 W. Li and X. Sang, “Phase-sensitive parametric amplifiers in silicon waveguides,” J. Mod. Optics, Vol. 58, Issue 14, pp. 1246-1251, 2011.

62 Q. Lin, O. J. Painter, and G. P. Agrawal. “Nonlinear optical phenomena in silicon waveguides: modelling and applications,” Opt. Express, Vol. 15, Issue 25, pp. 16604-16644, 2007.

63 M. Pu. “Silicon Nano-photonics devices“, A thesis submitted in partial fulfilment for the degree of Doctor of Philosophy, Department of Photonics Engineering, Technical University of Denmark, 2010.

64 A. Fadil. “Parametric processes in silicon nanowires and applications“, Master Thesis, Department of Photonics Engineering, Technical University of Denmark, 2011.

65 C. Lundström, B. Corcoran, S. Olsson, Z. Tong, M. Karlsson, and P. Andrekson. "Short-Pulse Amplification in a Phase-Sensitive Amplifier", OFC/NFOEC, OSA Technical Digest, paper OTh1C.1, 2012.